Multiple Timescales in the Fitzhugh-Nagumo Model

by

Erik Bergland

B.Sc., Rensselaer Polytechnic Institute; Troy, NY, 2018

M.Sc., Brown University; Providence, RI, 2021

A dissertation submitted in partial fulfillment of the

requirements for the degree of Doctor of Philosophy

in The Division of Applied Mathematics at Brown University

PROVIDENCE, RHODE ISLAND

October 2024

This dissertation by Erik Bergland is accepted in its present form
by The Division of Applied Mathematics as satisfying the
dissertation requirement for the degree of Doctor of Philosophy.

Date________________ ____

Björn Sandstede, Ph.D., Advisor

Recommended to the Graduate Council

Date________________ ____

Govind Menon, Ph.D., Reader

Date________________ ____

Paul Carter, Ph.D., Reader

Approved by the Graduate Council

Date________________ ____

Thomas A. Lewis, Dean of the Graduate School

Vita

Education

Brown University, Providence, RI — AUGUST 2024
Ph.D. in Applied Mathematics
Adviser: Dr. Björn Sandstede

Rensselaer Polytechnic Institute, Troy, NY — MAY 2018
Bachelor Science (Applied Mathematics)(Summa Cum Laude)
Bill and Nancy Siegmann Applied Mathematical Modeling Prize

Research

JUNE 2021- DEC. 2022 **Brown University**
Temporal pulse replication in the Fitzhugh-Nagumo model. Investigated the temporal transition from single-pulse to double-pulse profiles of solutions to the Fitzhugh-Nagumo model, and their connections to the bifurcation structure of stationary solutions.

DEC. 2022- *present* **Brown University**
Stability of ODE dynamics in fast-slow reaction-diffusion systems. Proved deviations from solutions to the underlying kinetic equations of the Fitzhugh-Nagumo model decay algebraically as the kinetic solutions drift near the slow manifold by combining geometric singular perturbation theory with pointwise estimates. Also analyzed the behavior near a fold point and along fast jumps.

JAN. 2024- *present* **Brown University**
Locally synchronized patterns in weakly coupled bistable oscillators. Proved the existence of snaking patterns in the bifurcation diagrams of a finite set of weakly-coupled oscillators with in-phase coupling.

Feb. 2019- May 2019	**Rensselaer Polytechnic Institute** *An integro-differential model of language competition*. Developed a model for competing languages taking into account government efforts, spatial distribution of speakers, and immigration. Used the model to analyze long-term trends for common languages spoken in various regions.

Papers

Gaspard, M., Craig, P., & **Bergland, E.**. (2019). "An Integro-Differential Model of Language Competition". *SIAM Journal of Undergraduate Research Online*, 12.

Papers in Preparation

Bergland, E., Bramburger, J., & Sandstede, B. "Localized Synchronous Patterns in Weakly Coupled Bistable Oscillators".

Teaching, Mentoring and Training

SUMMER 2022	**Co-instructor** for Brown University's pre-college session for STEM 910: The Frontier of Knowledge.
FALL 2020- SPRING 2021	**Teaching Assistant** for Brown University Gave recitations and graded homework and exams for APMA 350: Introduction to Applied Ordinary Differential Equations and APMA 360: Introduction to Applied Partial Differential Equations.
SUMMER 2024	**REU Mentor** Mentored undergraduates working with Dr. Björn Sandstede.
FALL 2021- FALL 2023	**Mentor** for the Applied Math Directed Reading Program Developed project on modeling language competition with dynamical systems techniques; mentored five undergraduates on this topic and worked with four after the program's official end due to additional interest.

Honors and Awards

Bill and Nancy Siegmann Applied Mathematical Modeling Prize	MAY 2019
Dean's Honor List	MAY 2018
Dean's Honor List	DEC 2017
Dean's Honor List	MAY 2017
Dean's Honor List	DEC 2016
Dean's Honor List	MAY 2016
Dean's Honor List	DEC 2015

Presentations

Bergland, E., & Sandstede, B. "Multiple-Timescale Dynamics in the Fitzhugh-Nagumo Equation". **Boston University Dynamics Seminar**, March 13, 2023.

Bergland, E., & Sandstede, B. "Exploring Temporal Pulse Replication in the Fitzhugh-Nagumo Equation". **BIRS Workshop - 22w5057**, November, 2022.

Service

Graduate Faculty Liaison for the Division of Applied Math	SUMMER 2022 - SPRING 2024
Representative, Brown Graduate Student Council	FALL 2022 - SPRING 2024
Grader, Brown Mathematical Competition for Modelling	FALL 2021 - FALL 2023
Organizer, Applied Math Graduate Student Retreat	Fall 2022

Professional Organizations

Society for Industrial and Applied Mathematics

Graduate Course Work

Semigroup Theory
Group Theory
Recent Applications of Probability and Statistics
Algebraic Topology
Differential Geometry
Partial Differential Equations
Nonlinear Dynamical Systems
Theory of Probability
Complex Analysis
Real and Functional Analysis

Dedication

To Teressa Chambers, my fixed point. That we met during this time of our lives truly is providence.

Acknowledgments

It would be truly impossible to list all the people who made this thesis a reality. First and foremost, I must thank my advisor Björn. Guiding a graduate student is a challenge in the best of times, and in the midst of a global pandemic is anything but the best of times. His kindness, understanding, and drive to uncover the truth gave me the strength to develop into the mathematician I always hoped I could be.

I also wish to thank Govind Menon and Paul Carter for serving on my thesis committee. To Paul, I owe an additional debt of gratitude for the conversations that helped me develop my approach to the computations at the end of the third chapter. You never failed to offer a useful direction, and the good humor you showed when we discussed thorny computational issues always raised my spirits.

I also could not have made it to this point without the support of others in my cohort and research group. Tim, Moyi, Katie, Wenjun, Kevin, June, and many others besides, whether it was math help or camaraderie, you were always there for me.

I cannot thank my wife Teressa, my sister Kelly, my parents Rob and Lori, and all my friends and family enough. With your love, no problem is unsolvable. Finally, a special thanks to my grandfather Jerry. Poppi, who knew sabermetrics would take me this far?

Contents

List of Tables

List of Figures

Chapter One

Introduction

1.1 Motivation: Fitzhugh–Nagumo and GSPT

The Fitzhugh–Nagumo (FHN) model of neuron activity is a simplification of the Hodgkin-Huxley model. While the original model proposed in Fitzhugh (1961) was simply a system of ODEs, we shall concern ourselves here with the form given in Nagumo et al. (1962)

$$\begin{aligned}\frac{\partial u}{\partial t} &= \frac{\partial^2 u}{\partial x^2} + f(u) - w \\ \frac{\partial w}{\partial t} &= \epsilon(u - \gamma w)\end{aligned} \tag{1.1}$$

where $f(u) = u(u-a)(1-u)$ is an S-shaped nonlinearity with γ positive and $\epsilon > 0$ is a small positive parameter. Frequently, w is referred to as the recovery variable. We note that its dynamics are governed by an ODE. Meanwhile u, which originally represented the neuron's membrane voltage, obeys a PDE of reaction-diffusion type.

The Fitzhugh–Nagumo model has long been a laboratory for singularly perturbed systems in the context of PDEs. Its primary importance to this thesis, however, begins with the paper Carter and Sandstede (2018). Here, the authors unfolded what they referred to as the **homoclinic banana**. Using techniques from the field of **geometric singular perturbation theory**, they were able to describe an isola of traveling wave solutions, organized by canard dynamics at the origin. In this family of solutions, one-pulses evolved into two-pulses by exciting their oscillatory tail. We henceforth refer to this phenomenon as **parametric pulse replication**. Example solutions are depicted in Figure 1.1.

The homoclinic banana continued to play a crucial role in the follow-up paper Carter et al. (2021). The authors reported that in addition to describing the mechanism for parametric pulse replication, the banana also seemed to be an attractor

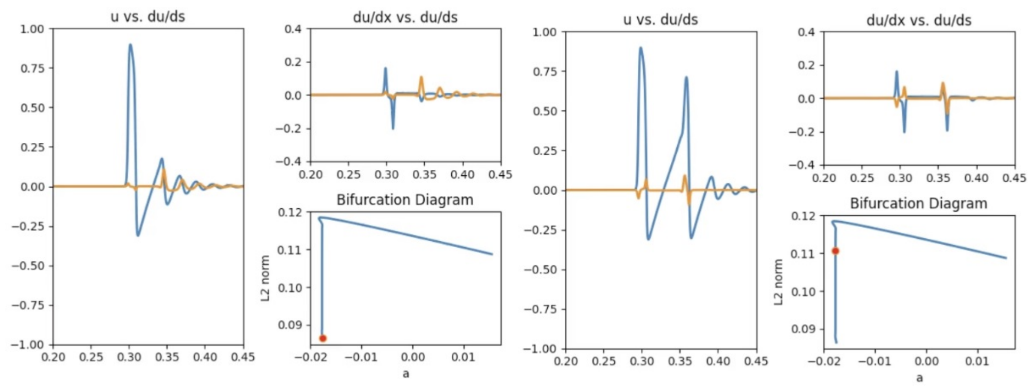

(a) 1-pulse near the bottom (b) 2-pulse near the top

Figure 1.1: AUTO computation of the homoclinic banana. The nearly vertical portion of the diagram where the transition occurs is exponentially thin due to canard dynamics. Solutions are shown in blue, and derivatives with respect to arclength are shown in orange.

for the Fitzhugh–Nagumo model. Beginning with an initial condition resembling the one-pulses of the isola, the authors observed that the solution excited its tail and became a two-pulse. The authors dubbed the process, depicted in Figure 1.2, **temporal pulse replication**, and also observed that the resulting solutions seemed to slowly drift up the nearly vertical portion of the homoclinic banana organized by the canard dynamics, analogous to the motion along an invariant slow manifold in geometric singular perturbation theory. They set out to study the linear stability of this portion of the banana, as a first step towards putting this observation on a rigorous footing.

Surprisingly, the authors discovered that the intermediate solutions between the one and two-pulses were massively unstable at the linear level. More specifically, the linearization about each pulse had $\mathcal{O}(1/\epsilon)$-many eigenvalues in the right-half plane, with the excursion being $\mathcal{O}(1)$ with respect to ϵ. The authors were able to prove that these eigenvalues accumulated on the absolute spectrum of a portion of the critical manifold used to construct the pulses. A diagram from their paper depicting this behavior is shown in Figure 1.3. Nevertheless, the numerics seemed to indicate that

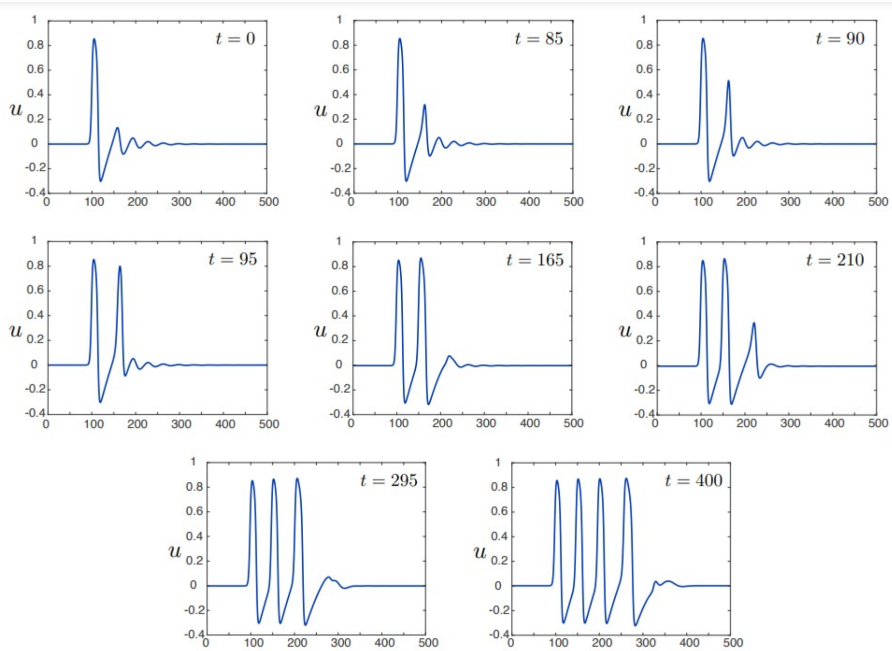

Figure 1.2: Numerics from Carter et al. (2021), reproduced with permission. The oscillatory tail of a pulse grows into a new excursion in time. The process then repeats, allowing n-pulses to become $n+1$-pulses.

this repulsion was somehow overcome.

It is known that systems exhibiting multiple-timescale behavior can undergo a **delayed loss of stability**, see e.g. Schecter (1985). Thus, it is possible for solutions to remain near a manifold even when that manifold is linearly unstable. However, while such analysis has been carried out in great detail in the case of some ODE systems, comparatively fewer works are available in the PDE setting. Therefore, a key motivation in this thesis is to extend results from the ODE case to the PDE setting. We briefly review multiple-timescales theory for ODEs in the next section.

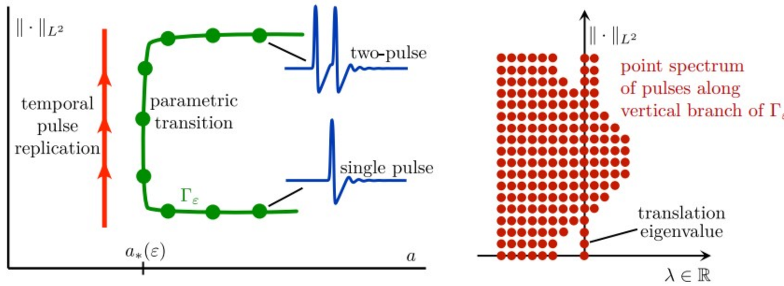

Figure 1.3: A figure from Carter et al. (2021), reproduced with permission. As one travels up the homoclinic banana, the absolute spectrum where eigenvalues accumulate reaches into the right half-plane.

1.2 Multiple timescales: a review

The field of multiple-timescale dynamics concerns itself with the analysis of systems where the constituent variables evolve at vastly different rates. While more general problem statements are possible (for a recent overview, see Wechselberger (2020)), in the case of systems of ODEs these often take the form

$$\begin{aligned} \frac{dx}{dt} &= f(x, y, \epsilon) \\ \frac{dy}{dt} &= \epsilon g(x, y, \epsilon) \end{aligned} \tag{1.2}$$

where $0 < \epsilon \ll 1$ is a small parameter, $x \in \mathbb{R}^m$, and $y \in \mathbb{R}^n$. Keeping with the standard parlance, we refer to x as a **fast variable** and y as a **slow variable**. This terminology stems from the presence of ϵ on the right-hand side of the second ODE, which causes the time derivative of y to be much smaller than that of x.

Such problems have a long history in the field of dynamical systems. They have been analyzed with many techniques, including nonstandard analysis (Cartier (1981)) and asymptotic analysis (e.g. Kramers (1926)). The most crucial of these methods for the purposes of this thesis is geometric singular perturbation theory, as laid out in Fenichel (1979) and henceforth abbreviated as GSPT.

The picture that ultimately emerges from GSPT is that (1.2) does not give a full description of what can occur in a system with multiple timescales by itself. The behavior of the system can be broken down into three parts: slowly drifting along the slow manifold, entering a neighborhood of a nonhyperbolic point, and making a fast jump to a new portion of the critical manifold. We discuss each behavior in turn.

1.2.1 Drifting along the slow manifold

If we define the **slow time** $\tau = \epsilon t$, our system becomes

$$\begin{aligned} \epsilon \frac{dx}{d\tau} &= f(x, y, \epsilon) \\ \frac{dy}{d\tau} &= g(x, y, \epsilon) \end{aligned} \tag{1.3}$$

Taking the formal limit as $\epsilon \to 0^+$, we arrive at

$$\begin{aligned} 0 &= f(x, y, 0) \\ \frac{dy}{d\tau} &= g(x, y, 0) \end{aligned} \tag{1.4}$$

Our system has now fundamentally changed its character: rather than considering two variables evolving at different rates, we instead find ourselves in the realm of constrained dynamical systems. We refer to the set $C_0 = \{(x, y) |\ 0 = f(x, y, 0)\}$ as the **critical manifold**. We note that this set is composed entirely of fixed points of (1.2) when $\varepsilon = 0$.

Equation (1.4) is subject to the following interpretation: the system is constrained to lie along the critical manifold. Within this constraint, the variable y changes on the slow timescale τ. In other words, our system is confined to a slow drift along a particular manifold determined by the equilibria of the fast vector field f. As y evolves, x instantaneously changes such that $f(x, y, 0) = 0$.

In Fenichel (1979), Neil Fenichel proved that this basic picture extends to the case when ϵ is small but nonzero as long as one considers a portion of the critical manifold that is **normally hyperbolic**.

Definition 1.2.1. We say that a point (x, y) on the critical manifold is **normally hyperbolic** if

$$\sigma\big(D_x f(x, y, 0)\big) \cap i\mathbb{R} = \varnothing$$

where $\sigma(A)$ refers to the spectrum of the matrix A. If $\sigma\big(D_x f(x, y, 0)\big)$ is contained entirely in the left half-plane, we say the point is **normally attractive**. Likewise, if it is entirely contained in the right half-plane we say it is **normally repelling**. If every point of a subset of the critical manifold is normally hyperbolic, we refer to that subset as normally hyperbolic. The terminology of normal attraction or repulsion is extended similarly.

As an example, take the system

$$\begin{aligned} \frac{dx}{dt} &= -y - x^2 \\ \frac{dy}{dt} &= -\varepsilon(1 + x^2). \end{aligned}$$

We see that the critical manifold for this system is $y = -x^2$. For $x < 0$ the critical manifold is normally repelling: $\frac{\partial f}{\partial x}(x, x^2, 0) = -2x < 0$. Similarly, for $x > 0$ the critical manifold is normally attracting. In a neighborhood away from $x = 0$, one can prove that the critical manifold is perturbed to a nearby locally invariant **slow manifold**.

Remark 1. Fenichel's result does not guarantee the uniqueness of the slow manifold,

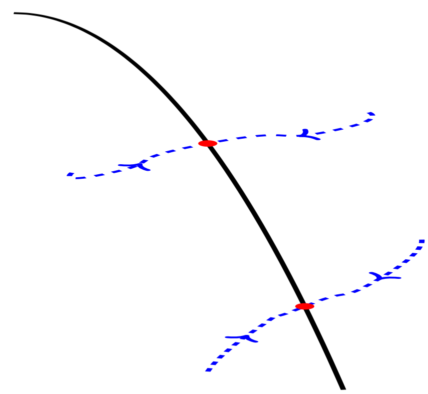

Figure 1.4: A fast-slow system near the slow manifold, shown with a solid line. Examples of stable fibers are shown with dashed lines, with their corresponding basepoint in red.

and there are in fact infinitely many such manifolds. However, all of them lie within a neighborhood of size $\mathcal{O}(e^{-\frac{1}{\varepsilon}})$. Therefore, we will simply leave the choice of a manifold implicit and refer to "the" slow manifold throughout this thesis.

On the slow manifold, the dynamics are governed by (1.4) to lowest order. In our example, this means that

$$\frac{dy}{d\tau} = -1 - y + \mathcal{O}(\varepsilon).$$

One can go even further. In addition to proving the existence of the slow manifold, Fenichel demonstrated that one can foliate a suitable neighborhood of this manifold into stable and unstable fibers with a basepoint on the slow manifold. In a normally attracting region, this simplifies further, since there are no unstable directions. This situation is depicted in Figure 1.4. Solutions that are initialized away from the slow manifold are attracted to it on the fast timescale.

We shall go into more explicit detail in future sections, as we will make use of this decomposition in order to perform certain computations. For now, the main take-away is that in the vicinity of the slow manifold, the behavior of the system is split into two essentially orthogonal parts: the basepoint drifts along the slow manifold, and any offsets from the basepoint decay exponentially. Even more importantly, this decay occurs on the fast timescale. Therefore, understanding the shape of the slow manifold and the speed of the drift along it essentially gives a complete picture of the dynamics in a region that is normally hyperbolic.

1.2.2 Passing near a fold

In the previous section, we saw that the point $(0, 0)$ on our example critical manifold was not normally hyperbolic. As such, we cannot use Fenichel's results in a neighborhood of this point and must resort to alternative methods of analysis.

In the seminal paper Krupa and Szmolyan (2001), the authors regain hyperbolicity by essentially magnifying the dynamics occuring at the origin. To accomplish this goal, the authors apply the blowup transformation

$$x = \hat{r}\hat{x}, \quad y = \hat{r}^2\hat{y}, \quad \varepsilon = \hat{r}^3\hat{\varepsilon}$$

where $(\hat{x}, \hat{y}, \hat{\varepsilon}) \in S^2$ and $\hat{r} \in [0, \rho]$, for some suitably small $\rho > 0$. One can immediately observe that $\hat{r} = 0$ corresponds to the origin with $\varepsilon = 0$, regardless of the values of $(\hat{x}, \hat{y}, \hat{\varepsilon})$. Therefore, the origin has been "blown up" to a degenerate sphere. One might then hope to understand the dynamics on this singular sphere and translate the results back to our original system.

To that end, the authors define three regions D_1, D_2, and D_3, which use the coordinate charts K_1, K_2, and K_3 respectively. In the first, we take $\hat{y} = 1$. In the second, we take $\hat{\varepsilon} = 1$, and in the final chart we choose $\hat{x} = 1$. In each chart, one obtains a transformed system. Let us take the example of K_2. Following the conventions of Krupa and Szmolyan, we denote the variables in K_i with the subscript i and drop the hat from our notation. Our transformation is then

$$x = r_2 x_2, \quad y = r_2^2 y_2, \quad \varepsilon = r_2^3.$$

Applying this transformation, our equations become

$$\begin{aligned} \frac{dx_2}{dt} &= r_2(-y_2 + x_2^2) \\ \frac{dy_2}{dt} &= -r_2(1 + r_2^2 x_2^2) \\ \frac{dr_2}{dt} &= 0. \end{aligned} \tag{1.5}$$

At this point, we recall that we are ultimately interested in understanding the behavior of this system near $r_2 = 0$, which corresponds to the point $(x, y, \varepsilon) = (0, 0, 0)$. Therefore, we rescale our time coordinate and define $t_2 = r_2 t$. We then obtain

$$\begin{aligned} \frac{dx_2}{dt_2} &= -y_2 + x_2^2 \\ \frac{dy_2}{dt_2} &= -1 + \mathcal{O}(r_2) \\ \frac{dr_2}{dt_2} &= 0. \end{aligned} \tag{1.6}$$

For any positive r_2, this transformation is well-defined. Furthermore, by rescaling time we have only changed the rate at which dynamics occur. The phase portraits of (1.5) and (1.6) are identical. Therefore, we can carry out our analysis using the latter. This is referred to as **desingularizing** the system.

Remark 2. The exponents of $\hat{r}$ in our original coordinate transformations are chosen to facilitate this desingularization. It is known (see Dumortier (1977)) that for planar systems, one can achieve desingularization with finitely many blowups under mild

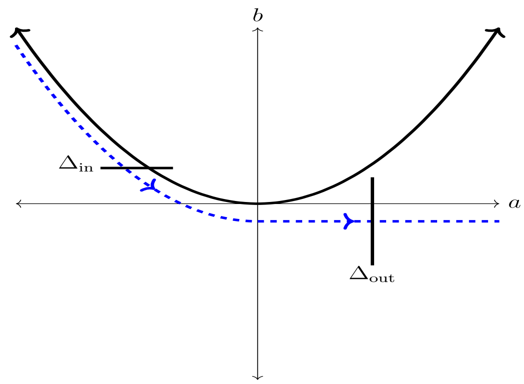

Figure 1.5: An example solution near a fold point. The solution transitions from drifting close to the critical manifold (solid black) to a fast jump, spending $\mathcal{O}(\varepsilon^{-\frac{1}{3}})$-time in the transition region.

conditions. However, this result is not constructive.

It remains only to carry out similar blowups in the other two charts and carefully match the results. Effectively, the charts K_1 and K_3 allow for the matching of solutions on the slow manifold and on the fast jump ("exterior" to the fold) with "inner" solutions in a neighborhood of the fold. One possible solution is shown in Figure 1.5. The solution transitions from drifting along the slow manifold to a fast jump, while taking $\mathcal{O}(\varepsilon^{-\frac{1}{3}})$-time near the fold to do so.

1.2.3 A fast jump

After passing through a region near the fold point, the dynamics of the system are characterized by the formal limit $\varepsilon \to 0^+$ in (1.2) to lowest order. To see this, we suppose that we are given initial data (x_0, y_0) to (1.2) such that $f(x_0, y_0, 0) \neq 0$, and that we wish to analyze the system on the interval $t \in [0, \bar{T}]$ for some $\bar{T} > 0$. Assuming our functions f and g are as smooth as needed, we attempt to find a regular series expansion for both x and y, i.e.

$$x(t) = x^0(t) + \varepsilon x^1(t) + \mathcal{O}(\varepsilon^2)$$
$$y(t) = y^0(t) + \varepsilon y^1(t) + \mathcal{O}(\varepsilon^2)$$

To lowest order, our system becomes

$$\frac{dx^0}{dt} = f(x^0, y^0, 0)$$
$$\frac{dy^0}{dt} = 0$$

Therefore, we have that $y^0 = y_0$ for $t \in [0, \bar{T}]$. For values of $\bar{T}$ that are $\mathcal{O}(1)$ with respect to ε, this expansion is consistent.

Eventually, when the fast jump travels horizontally in the x-direction of the phase plane, one approaches another piece of the critical manifold. If that piece is normally hyperbolic, then the fast jump solution can intersect one of the stable fibers of the slow manifold. The system will then be described by the slow flow once more.

1.3 Overview of thesis

This thesis begins by attempting to grapple with the problem posed in Carter et al. (2021). Namely, how does a set of solutions with strong repulsion at the linear level seemingly serve as an attractor for the dynamics? To that end, we proposed a toy model that attempted to make use of the fact that temporal pulse replication appears to be a multiple-timescales phenomenon. However, we ultimately prove that this model is insufficient to capture the observed behavior in the full Fitzhugh–Nagumo system, and offer observations on why no finite-dimensional model may suffice.

In an effort to better understand the nature of multiple-timescale behavior in PDEs, we consider a simpler problem: the persistence of fast-slow dynamics in the chemical kinetics of a reaction-diffusion system. We recall that in (1.1), ignoring the diffusion term in the first equation yields a system of fast-slow ODEs. One can then analyze these ODEs via Fenichel theory and geometric blowup. The solutions to this system drift along portions of a normally stable slow manifold for long periods of time, before passing near fold points and making quick jumps to another portion of the slow manifold.

These solutions to the underlying system of ODEs are in fact genuine solutions to the full Fitzhugh–Nagumo model, given that one begins with spatially homogeneous initial data. A natural question then arises: does the picture given by the system of ODEs persist when one begins with initial data that is only mildly non-homogeneous in space? This question is the focus of the second chapter. The problem of determining whether the ODE solution serves as an attractor to the PDE dynamics has several useful features compared to the problem studied in Chapter 1. First and foremost, the potential attractor is not infinite-dimensional, since it is spatially homogeneous. Second, the linear instability of the potential attractor is confined to a relatively small interval of time while the solutions to the ODE make a fast jump.

We proceed to analyze the stability of our ODE attractor in three different regimes: drifting near the slow manifold, during a fast jump, and in the vicinity of a fold. The main theoretical tool used to carry out the analysis of each region is pointwise estimates. In the first regime, we find that given constraints on our initial data related to the underlying geometry of the fast-slow system, we can prove an algebraic decay of offsets from the underlying ODE solutions. In the absence of these geometric constraints, we achieve only boundedness of offsets.

In the second of these regimes, we find that although the underlying critical manifold is no longer attractive, and thus leads to linear instability, we can nonetheless make use of the fact that solutions to the kinetic ODEs spend only a short period of time exhibiting this behavior to establish the boundedness of offsets. With the decay obtained in the first regime, one can still hope to remain close to the underlying ODE solutions.

Finally, we elucidate the challenges found when attempting to extend these methods of analysis to a region near the fold, where solutions transition from a slow drift to a quick jump. Solutions to the kinetic ODEs spend time near a fold on the order of $\mathcal{O}(\epsilon^{-\frac{1}{3}})$, and a significant fraction of this time is spent in a region where the underlying critical manifold is linearly unstable. We prove bounds on key quantities, making extensive use of the geometric blowup coordinates found in Krupa and Szmolyan (2001) near the fold point.

In the final chapter of this thesis, we return to the analysis of a bifurcation diagram and analyze the behavior of weakly coupled oscillators. We make use of core-far-field decomposition to demonstrate snaking behavior.

Chapter Two

Temporal Pulse Replication

2.1 Parametric pulse replication

We turn now to a more detailed review of the phenomenon of parametric pulse replication, in order to motivate the existence of temporal pulse replication. To begin, we shall search for traveling wave solutions to the Fitzhugh–Nagumo equations. Switching to the co-moving frame variable $\xi = x + ct$, our system becomes

$$\begin{aligned} \frac{\partial u}{\partial t} &= \frac{\partial^2 u}{\partial \xi^2} - c\frac{\partial u}{\partial \xi} + f(u) - w \\ \frac{\partial w}{\partial t} &= -\frac{\partial u}{\partial \xi} + \epsilon(u - \gamma w) \end{aligned} \tag{2.1}$$

If we search for solutions that are stationary in the co-moving frame, we may set the time derivatives to zero and rewrite this as a system of ODEs

$$\begin{aligned} u_\xi &= v \\ v_\xi &= cv - f(u) + w \\ w_\xi &= \frac{\epsilon}{c}(u - \gamma w) \end{aligned} \tag{2.2}$$

where we have defined $v := \frac{\partial u}{\partial \xi}$. In the parlance of multiple timescale dynamics, we have obtained a $(2, 1)$-fast-slow system. One can immediately determine the critical manifold for this system: $v = 0$ and $w = f(u)$. The manifold is depicted in Figure 2.1

Our critical manifold contains 3 non-hyperbolic points: two fold points at the local extrema of the cubic, and a canard point at the origin. Carter *et al.* were able to show that the transition from single to double pulses is organized by the canard. One-pulses make one excursion around the circuit formed by the stable left and right branches of the critical manifold, using the fold points to jump between them. They then spend only a short time near the unstable center portion of the

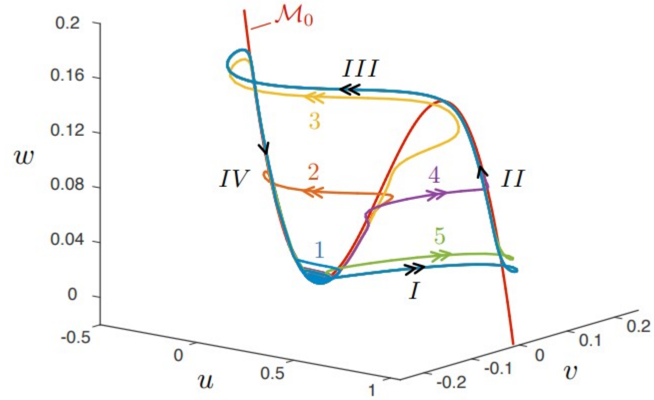

Figure 2.1: Figure from Carter et al. (2021), reproduced with permission. The critical manifold is shown in red. The number of peaks in a pulse solution is determined by the number of excursions made from left to right and back again on the manifold.

critical manifold before returning to the origin. The oscillatory tail of the transition grows by spending more time near the unstable section of the critical manifold, and the two-pulses result from jumping away from the unstable center section in the direction of the right branch, instead of towards the left and the origin.

Due to the presence of the canard point, the parameter regime in which parametric pulse replication takes place is exponentially thin. Ultimately, it is this fact which motivates the desire to prove that an invariant manifold lies near this portion of the homoclinic banana, since the parameter values for each of these solutions are equal up to exponentially small errors.

2.2 Projections and toy models

In order to provide a more formal motivation for believing the hypothesized explanation for temporal pulse replication, and as a first step towards a toy model, we shall take a step back and consider the Fitzhugh-Nagumo model in a more abstract setting.

We suppose that we have chosen a suitable Hilbert space X, such that we may pose the Fitzhugh-Nagumo model as an initial-value problem in this space:

$$\begin{aligned} \dot{\bar{u}} &= f(\bar{u}, \mu) \\ \bar{u}(0) &= \bar{u}_0 \end{aligned} \tag{2.3}$$

where $\bar{u} = (u, w)$ and $\mu = (a, c)$. We suppose that there exists a family of stationary solutions $(\Gamma(s), \tilde{\mu}(s))$ for $s \in I$, where I is some interval in $\mathbb{R}$ and represents a bifurcation parameter. In other words, we stipulate that $f(\Gamma(s), \tilde{\mu}(s)) = 0$. With these definitions in hand, we now search for solutions of the form $\bar{u}(t) = \Gamma(s(t)) + v(t)$ for fixed parameter values μ. Substituting into our ODE, we find that

$$\Gamma'(s(t))\dot{s} + \dot{v} = f_{\bar{u}}(\Gamma(s(t)), \tilde{\mu}(s(t)))v + f_{\mu}(\Gamma(s(t)), \tilde{\mu}(s(t)))[\mu - \tilde{\mu}(s(t))] + h(t) \tag{2.4}$$

where $h(t)$ collects the errors in approximating our system by its linear behavior,

$$h(t) = f(\Gamma(s(t)) + v(t), \mu) - f_{\bar{u}}(\Gamma(s(t)), \tilde{\mu}(s(t)))v - f_{\mu}(\Gamma(s(t)), \tilde{\mu}(s(t)))[\mu - \tilde{\mu}(s(t))],$$

and the prime denotes differentiation with respect to s. We have made use of the fact that $(\Gamma(s), \tilde{\mu}(s))$ are stationary solutions of (2.3). We now suppose that $z \in X$, and take the projection of both sides of our equation onto z. This yields

$$\dot{s}\langle \Gamma', z\rangle + \langle \dot{v}, z\rangle = \langle f_{\bar{u}} v, z\rangle + \langle f_{\mu}[\mu - \tilde{\mu}(s(t))], z\rangle + \langle h, z\rangle \tag{2.5}$$

where we have suppressed the dependence of functions on their arguments where possible to simplify the presentation.

2.2.1 Desired properties of projectors

In order to prove that temporal pulse replication is in some sense caused by parametric pulse replication, we wish to show that $v(t)$ is small in the norm of our underlying Hilbert space X as long as $v(0)$ is sufficiently small in the same norm.

Furthermore, in order to show that our solutions slowly drift along the family of transitional pulses found in the homoclinic banana, we must determine $s(t)$. More specifically, we wish to show that $\dot{s}$ is small, indicating that our solutions change slowly.

To answer the latter question, we suppose that we have found a projection z_0 such that $\langle \dot{v}, z_0 \rangle = \langle f_{\bar{u}} v, z_0 \rangle = 0$. Our equation becomes

$$\dot{s}\langle \Gamma', z_0 \rangle = \langle f_\mu[\mu - \tilde{\mu}(s(t))], z_0 \rangle + \langle h(t), z_0 \rangle. \tag{2.6}$$

If we have succeeded in proving that v is small, the last term is small as well. Therefore, we find that $\dot{s}$ is roughly proportional to the difference between μ and $\tilde{\mu}(s(t))$. We recall that the latter is constant up to exponential errors. Thus, the difference between the parameter values and the center of the region containing $\tilde{\mu}(s(t))$ would serve as a small parameter governing the drift along our proposed invariant manifold.

Before returning to the question of the magnitude of $v(t)$, let us rewrite (2.5) slightly. We assume that z is a function of $s(t)$. This yields

$$\dot{s}\Big(\langle \Gamma', z \rangle - \langle v, z' \rangle\Big) + \frac{d}{dt}\langle v, z \rangle = \langle f_{\bar{u}} v, z \rangle + \langle f_\mu[\mu - \tilde{\mu}(s(t))], z \rangle + \langle h(t), z \rangle, \tag{2.7}$$

where we have made use of the product rule on the left-hand side of our equation. Let us now suppose that we can find a family of projections $(z_n)_{n=1}^{\infty}$ that span the Hilbert space X and satisfy the requirement above. We define functions $c_n^i(s(t))$ via

$$f_{\bar{u}}^*\Big(\Gamma(s(t)), \tilde{\mu}(s(t)))z_n(s(t)\Big) := \sum_{i=1}^{\infty} c_n^i(s(t))z_i(s(t)) \tag{2.8}$$

where we have included all functional dependencies to emphasize the dependence on $s(t)$, and $f_{\bar{u}}^*$ is the adjoint of $f_{\bar{u}}$. Applying each of our projections in turn, we obtain

$$\frac{d}{dt}\langle v, z_n\rangle = \sum_{i=1}^{\infty} c_n^i\langle v, z_i\rangle - \dot{s}\Big(\langle\Gamma', z_n\rangle - \langle v, z_n'\rangle\Big) + \langle f_\mu[\mu - \tilde{\mu}(s(t))], z_n\rangle + \langle h(t), z_n\rangle. \tag{2.9}$$

Thus, we have arrived at an infinite-dimensional system of ODEs. If it were possible to make use of this system to prove $\langle v, z_n\rangle$ were small for all n, we could answer the first of our questions. This goal would be simpler if one could find an appropriate projection to show that $\dot{s}$ was small, since then the second term on the right-hand side of this equation would have a similar magnitude to the the third term. If the difference between $\mu - \tilde{\mu}(s(t))$ were sufficiently small, these terms may have a negligible impact on the magnitude of $\langle v, z_n\rangle$.

2.2.2 A lack of candidate projectors

Let us consider the projector z_0 first. We note that $\langle f_{\bar{u}}v, z_0\rangle = 0$ is equivalent to requiring that $\langle v, f_{\bar{u}}^* z_0\rangle = 0$, implying that z_0 lies in the null space of the adjoint of $f_{\bar{u}}$. This is in turn equivalent to saying that z_0 lies in the closure of the range of $f_{\bar{u}}$. This range spans the space of vectors orthogonal to the manifold, and thus we would automatically find that $\langle g', z_0\rangle = 0$ for any function g. This would mean that $\langle\Gamma', z_0\rangle = 0$, so we would not be able to solve for $\dot{s}$. One could attempt to drop the condition $0 = \langle v, f_{\tilde{u}}^* z_0 \rangle$. However, one would then preserve the term depending linearly on the magnitude of v on the right-hand side of the equation for $\dot{s}$. One would then need to prove v is small to recover our original strategy, and in fact our strategy for proving v is small depended in part on the smallness of $\dot{s}$. A more sophisticated bootstrapping argument would be required in this case.

Furthermore, we must confront the lack of candidates for the projectors $(z_n)_{n=1}^{\infty}$. The most natural choice would be to make use of spectral projection. However, we do not have any prior knowledge of the behavior of the eigenfunctions of the adjoint of our linearization about the transitional pulses, nor its accompanying spectrum.

In fact, the main source of information about our system is the fact that $f(\Gamma(s), \tilde{\mu}(s)) = 0$, and the related fact that

$$f_{\bar{u}}(\Gamma(s), \tilde{\mu}(s))\Gamma'(s) + f_{\mu}(\Gamma(s), \tilde{\mu}(s))\tilde{\mu}'(s) = 0$$

Since $\tilde{\mu}(s)$ changes very little as s varies, the latter term in this equation is small, which demonstrates that $\Gamma'(s)$ is approximately a null eigenvector of our linearization. However, this does not provide information about the adjoint.

2.3 A simplified model

Due to the difficulty of finding a toy model from first principles using suitable projections, we shall instead examine a model that arises directly from considering an idealized version of our problem when restricted to finite dimensions.

We recall that $O(\epsilon^{-1})$ eigenvalues of the transitional pulses cross the imaginary axis as we travel up the homoclinic banana, and then cross back until only one eigenvalue remains in the right half-plane. We attempt to distill the key characteristics of this scenario into a 2-dimensional model

$$\begin{aligned} \dot{m} &= f_1(m, v, a) \\ \dot{v} &= f_2(m, v, a) \end{aligned} \tag{2.10}$$

where a is a small parameter, and $m \in [0, 1]$.

Remark 3. We use a as our small parameter instead of the more traditional ε since the latter denotes the small parameter in the spatial-dynamical system used to construct the banana. Furthermore, we are interested in small changes in the other parameters of this system, one of which is a.

To begin, we suppose that we have a vertical critical manifold, corresponding to the exponentially thin region of the homoclinic banana. Therefore, we require that $f_1(m, v, 0) = 0$ and $f_2(m, 0, 0) = 0$. Taylor-expanding the right-hand side of our system, we find that

$$\begin{aligned} \dot{m} &= a\frac{\partial f_1(m, v, 0)}{\partial a} + ... \\ \dot{v} &= a\frac{\partial f_2(m, 0, 0)}{\partial a} + v\frac{\partial f_2(m, 0, 0)}{\partial v} + ... \end{aligned}$$

or

$$\begin{aligned} \dot{m} &= a\Big[\frac{\partial f_1(m, 0, 0)}{\partial a} + v\frac{\partial f_1(m, 0, 0)}{\partial a}\Big] + ... \\ \dot{v} &= a\frac{\partial f_2(m, 0, 0)}{\partial a} + v\frac{\partial f_2(m, 0, 0)}{\partial v} + ... \end{aligned}$$

If we ignore higher-order terms and define $g(m) := \frac{\partial f_1(m,0,0)}{\partial a}$, $g_2(m) := \frac{\partial f_1(m,0,0)}{\partial a}$, $\lambda(m) := \frac{\partial f_2(m,0,0)}{\partial v}$, and $g_3(m) := \frac{\partial f_2(m,0,0)}{\partial a}$, we see that the simplest toy model that

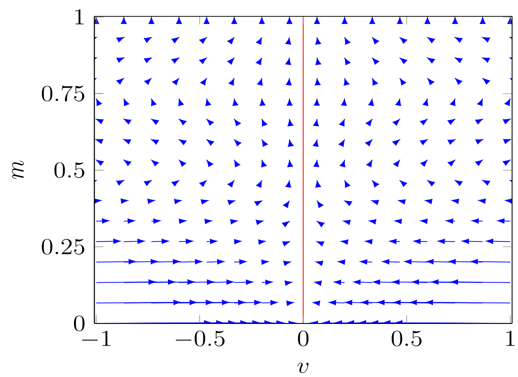

Figure 2.2: Vector field for the model when $g_2 = g_3 := 0$

obeys our prerequisites is

$$\begin{aligned} \dot{m} &= a\big[g(m) + g_2(m)v\big] \\ \dot{v} &= \lambda(m)v + ag_3(m) \end{aligned} \tag{2.11}$$

In addition to the conditions given so far, we also suppose that $\lambda(m)$ is initially negative, before "crossing the imaginary axis" and becoming positive, and then crossing back to become negative once more. This behavior simulates the crossing of eigenvalues into the right half-plane in our original model.

Our goal is to prove that $|v(t)|$ remains small when $|v(0)|$ is sufficiently small, for all t such that $m \in [0, 1]$. To that end, we notice that when $v \approx 0$, our first equation decouples, and we can rewrite the system with m serving as the dependent variable. With that motivation in mind, we define $m = m_0 + u$, where $\dot{m}_0 = ag(m_0)$. Our system becomes

$$\begin{aligned} \dot{m}_0 &= ag(m_0) \\ \dot{u} &= a\big[g'(m_0)u + F_1(m_0, u) + g_2(m_0 + u)v\big] \\ \dot{v} &= \lambda(m_0)v + F_2(m_0, u, v) + ag_3(m_0 + u) \end{aligned} \tag{2.12}$$

where $F_1(m_0, u) := g(m_0 + u) - g'(m_0)u$ and $F_2(m_0, u, v) := \lambda(m_0 + u)v - \lambda(m_0)v$.

Dividing the latter two equations by $\dot{m}_0$ yields

$$\begin{aligned}\frac{du}{dm_0} &= \frac{g'(m_0)}{g(m_0)}u + \frac{F_1(m_0,u)}{g(m_0)} + \frac{g_2(m_0+u)}{g(m_0)}v \\ \frac{dv}{dm_0} &= \frac{1}{a}\frac{\lambda(m_0)}{g(m_0)}v + \frac{1}{a}\frac{F_2(m_0,u,v)}{g(m_0)} + \frac{g_3(m_0+u)}{g(m_0)}\end{aligned}$$

For the purposes of our analysis here, we will assume that there exists positive constants d_1, d_2 such that $d_1 \leq g(m_0) \leq d_2$ for all $m_0 \in [0,1]$. By redefining functions as necessary, our system of interest becomes

$$\begin{aligned}\frac{du}{dm_0} &= \frac{g'(m_0)}{g(m_0)}u + F_1(m_0,u) + g_2(m_0+u)v \\ \frac{dv}{dm_0} &= \frac{1}{a}\lambda(m_0)v + \frac{1}{a}F_2(m_0,u,v) + g_3(m_0+u)\end{aligned} \tag{2.13}$$

where $|F_1(m_0,u)| \leq C_1|u|^2$, $|F_2(m_0,u,v)| \leq C_2|u||v|$, and $|g_i(m_0+u)| \leq c_i$ for $i = 2,3$ for all $m_0 \in [0,1]$.

2.3.1 Solving the toy model

We begin by solving (2.13) by variation of parameters, with initial data $(u(0),v(0)) = (0,v_0)$. The condition on $u(0)$ reflects the fact that m and m_0 are equal at the beginning of a trajectory. We obtain

$$\begin{aligned}u(m_0) &= \int_0^{m_0} \left[F_1(\sigma,u(\sigma)) + g_2(\sigma+u(\sigma))v(\sigma)\right]\frac{g(m_0)}{g(\sigma)}\mathrm{d}\sigma \\ v(m_0) &= v_0 \exp\left(\frac{1}{a}\int_0^{m_0}\lambda(s)\mathrm{d}s\right) \\ &\quad + \int_0^{m_0}\left[\frac{1}{a}F_2(\sigma,u(\sigma),v(\sigma)) + g_3(\sigma+u(\sigma))\right]\exp\left(\frac{1}{a}\int_0^{\sigma}\lambda(s)\mathrm{d}s\right)\mathrm{d}\sigma\end{aligned} \tag{2.14}$$

Let us consider the first equation of (2.14). We define $||f||_T := \sup_{m_0\in[0,T]}|f(m_0)|$, and observe that

$$|u(m_0)| \leq \frac{d_2}{d_1}(C_1||u||_T^2 + c_2||v||_T)$$

Taking the supremum of both sides and rearranging, we find that

$$(1 - \frac{C_1 d_2}{d_1}||u||_T)||u||_T \leq \frac{c_2 d_2}{d_1}||v||_T$$

If we select the maximal $T > 0$ such that $||u||_T \leq \frac{d_1}{2C_1 d_2}$, we establish the stronger estimate

$$||u||_T \leq \frac{2c_2 d_2}{d_1}||v||_T \tag{2.15}$$

2.3.2 Impossibility of small v for generic solutions

Ultimately, we aim to prove that $||v||_1$ is small. Let us suppose that in fact, we have proved that for all $|v_0|$ sufficiently small, there exist constants $K > 0$ and $p > \frac{1}{2}$ such that $||v||_1 \leq Ka^p$. It then immediately follows that $||u||_1 \leq \frac{2c_2 d_2 K}{d_1}a^p$, since for $a < (\frac{d_1}{2C_1 d_2})^{1/p}\frac{Kd_1}{2c_2 d_2}$, we have that $||u||_1 \leq \frac{d_1}{2C_1 d_2}$, justifying the bootstrap estimate in the previous section.

With these estimates in hand, we observe that

$$\left|\frac{1}{a}F_2(\sigma, u(\sigma), v(\sigma))\right| \leq \frac{2K^2 C_2 c_2 d_2}{d_1}a^{2p-1}$$

Thus, we see that

$$v(m_0) = v_0 \exp\Big(\frac{1}{a}\int_0^{m_0}\lambda(s)\mathrm{d}s\Big) + \int_0^{m_0}[g_3(\sigma + O(a^p)) + O(a^{2p-1})]\exp\Big(\frac{1}{a}\int_0^{\sigma}\lambda(s)\mathrm{d}s\Big)\mathrm{d}\sigma \tag{2.16}$$

Therefore, we see that for a sufficiently small, in order for the magnitude of $v(m_0)$ to be uniformly small, we must have cancellation between these terms. This holds since g_3 is non-negligible, and the integral of $\exp\left(\frac{1}{a}\int_0^\sigma \lambda(s)\mathrm{d}s\right)$ is not uniformly small. However, such cancellation is not at all generic, and would imply other inconsistencies. Thus, we conclude that this toy model does not adequately reproduce the dynamics found in temporal pulse replication.

2.4 Discussion

We have made two attempts at finding a finite-dimensional toy model for the phenomenon of temporal pulse replication in the Fitzhugh-Nagumo model. The first involves casting the model as an ODE in a suitable Hilbert space and taking projections. The second involves attempting to prescribe similar spectral behavior in a finite-dimensional ODE model as was observed in Carter et al. (2021). The first approach relies more on reasoning from first principles, and suffers from a lack of candidate projections. The second is more computationally manageable, but ultimately fails to replicate the expected behavior.

The failure of the second approach hints at a potential pitfall for future work to find a toy model. We see that while solutions to our model can remain close to the critical manifold in regions that are normally attractive, they are still pushed exponentially far away from the critical manifold by the presence of normally repelling regions.

The initial motivation for pursuing the approach discussed here was simply that the normally attractive regions would swamp the exponential growth of solutions coming from the repelling regions. If true, this cancellation would provide a possible explanation for the apparent irrelevance of the linear instability of the transitional pulses of the homoclinic banana. However, (2.16) demonstrates that for $g_3 \neq 0$, this cancellation generically does not occur.

This difficulty suggests that the infinite dimensional nature of the original problem may be crucial to observing temporal pulse replication. If one cannot expect normally attractive regions to counterbalance normally repelling ones, then solutions to the Fitzhugh-Nagumo model must be able to evolve in modes that are not currently unstable. However, the number of unstable modes is $O(\frac{1}{\epsilon})$. Thus, for any finite-dimensional toy model of dimension N, the number of unstable directions will exceed N for small enough ϵ, and there will be no way for solutions to the toy model to avoid growing exponentially large for at least a short time.

In the chapter to come, we study a simplified situation which simultaneously removes both the infinite-dimensional nature of the attractor and the long times spent near linearly unstable solutions.

Chapter Three

Multiple Timescales and Stability of ODE Solutions

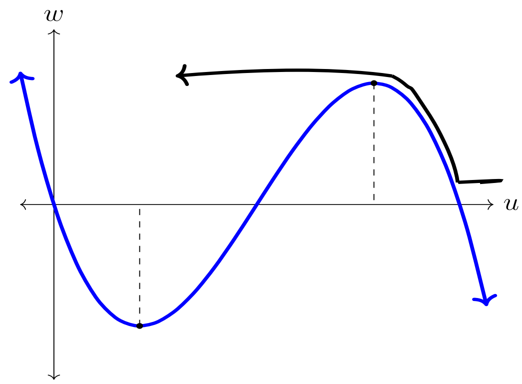

Figure 3.1: Example solution to (3.1). The critical manifold is shown in blue, and the fold points lie at the extrema of the curve.

3.1 Spatial homogeneity and Fitzhugh–Nagumo

Let us consider the Fitzhugh–Nagumo model as an initial value problem, and suppose that we take spatially-homogeneous initial data: $u(x, 0) = u_0$, $w(x, 0) = w_0$. It is clear that the solution to this problem will also be spatially-homogeneous, with the solution at each value of x satisfying

$$\begin{aligned} \frac{du}{dt} &= f(u) - w \\ \frac{dw}{dt} &= \epsilon(u - \gamma w) \end{aligned} \tag{3.1}$$

with initial data $u(0) = u_0$ and $w(0) = w_0$. A brief examination of this system reveals it to be a fast-slow system of order $(1, 1)$, with an S-shaped critical manifold $w = f(u)$. Standard techniques for fast-slow systems from Fenichel (1979) and Krupa and Szmolyan (2001) suffice to demonstrate the behavior of solutions to this system. Solutions are attracted to the rightmost or leftmost branch of the nonlinearity on the fast timescale. They then drift along it on the slow timescale, before reaching a fold point found at an extrema of the cubic. There, they transition back to the fast timescale and make a jump to the other side of the cubic. An example solution is shown in Figure 3.1.

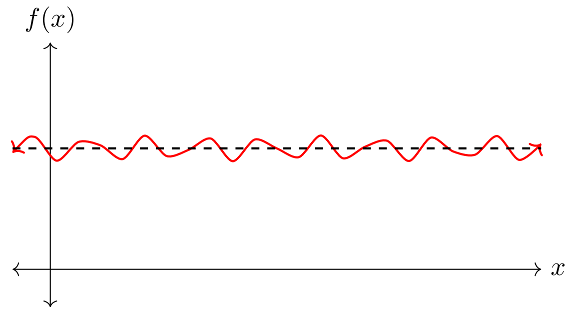

Figure 3.2: A function with only a small amount of spatial variation (red), centered around a constant function (dashed black).

While the behavior of solutions in this case follows from the underlying theory of fast-slow systems of ODEs, the situation is much less clear when our data is *nearly* spatially-homogeneous. We shall make this notion more precise in the section to follow, but for now the reader should have in mind functions like those shown in Figure 3.2

We note that the fold points of the critical manifold separate it into three pieces. We shall refer to these as the left, center, and right branches respectively. Along the left and right branches, our critical manifold is normally attractive. One might aim to show that, as in the ODE case, the part of the solution which does not lie on the nearby slow manifold decays over time.

Along the fast jump, we have that $f'(u) > 0$. Examining the variational equation of (3.1), one would expect to see solutions growing exponentially. However, solutions spend comparatively little time making a fast jump, and one might hope to prove that they do not blow up as $\varepsilon \to 0^+$.

In a neighborhood of the fold point, the situation is more complicated. Solutions remain in this neighborhood for long periods of time. Examining the work of Krupa and Szmolyan (2001) in more detail, we see that solutions spend on the order of $\mathcal{O}(\varepsilon^{-\frac{1}{3}})$ time in a region where $f'(u) > 0$. Thus, as in the case of the theory of fast-slow ODEs, the analysis near a fold point is more challenging than either of the other two regimes.

This chapter is organized as follows. First, we shall define a spatially-dependent family of solutions to (3.1), which will serve as an ansatz of the solution to our full problem with nearly spatially-homogeneous initial data near a normally attractive branch. We shall then carry out computations in a simplified setting, aided by the Fenichel normal form for the underlying ODE system, to argue that the control of the PDE solutions via the ODE solutions must be much weaker than the exponential convergence to the slow manifold found in the case of a pure fast-slow system. We shall then introduce the technique of pointwise estimates, which has been used to great effect in e.g. Beck (2006), Beck et al. (2011), Kappitula (1992), and many other works. We discuss the necessity of using these techniques, as opposed to the well-known machinery of semigroups.

We then compute estimates for the deviation of solutions to the full Fitzhugh–Nagumo model from our ODE ansatz near the slow manifold and along a fast jump. Finally, we compute the key quantities that allow us to gain control over the solutions in these two regions near the fold, and discuss the inadequacies of these results.

3.2 Spatially-inhomogeneous kinetic solutions

We have seen that in the case of spatially-homogeneous initial data, the solutions to the Fitzhugh–Nagumo model can be found from the fast-slow system of ODEs (3.1). In the case of inhomogeneous initial data, we make the following definition.

Definition 3.2.1. For initial data $(u_0, w_0)(x)$, we define $(u_\epsilon^{\mathrm{ODE}}, w_\epsilon^{\mathrm{ODE}})(t; x)$ to be the solution to the initial value problem

$$\begin{aligned} \frac{du}{dt} &= f(u) - w \\ \frac{dw}{dt} &= \epsilon(u - \gamma w) \\ u(0) = u_0(x),&\ w(0) = w_0(x) \end{aligned} \tag{3.2}$$

In this definition, we make use of parametric notation for the argument x to emphasize the secondary role it plays. In essence, the spatial variable simply parametrizes the initial condition of our problem. The dynamics take place solely in the variable t, which acts to evolve our initial data forward in time. We refer to the system of ODEs in the definition as the **kinetic system**, and their solutions as the **kinetic solutions**.

To clarify the idea behind the definition above, consider a simpler problem. We suppose that we wish to solve $u_t = u_{xx} - u$ with initial data $u(0; x) = \sin(x)$. The corresponding kinetic system is $u_t = -u$. Figure 3.3 plots our comparison ansatz in this case.

The goal of this work is to determine to what extent, if any, these spatially-inhomogeneous solutions to the kinetic system determine the behavior of the solutions to the full Fitzhugh–Nagumo model.

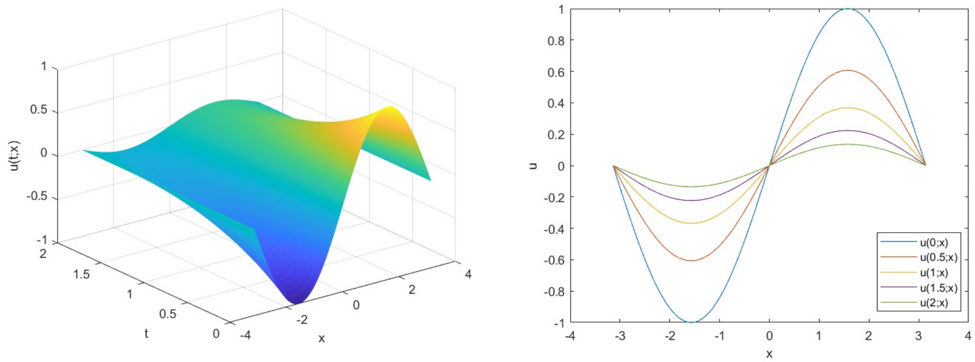

(a) Surface plot of our ansatz. (b) A plot of the ansatz at selected times.

Figure 3.3: A numerical solution of the kinetic equation $u_t = -u$, with spatially-varying initial data.

3.3 Building intuition: Fenichel normal form

3.3.1 Exponential convergence along fibers

In addition to proving the existence of a slow manifold, the work of Fenichel (1979) provides more information about the behavior of solutions near the manifold. For a fast-slow system of the form (1.2), there exists a smooth coordinate transformation such that the resulting solutions are in **Fenichel normal form**. If we label the new dynamical variables a, b, and c, then our transformed system takes the form

$$\begin{aligned} \frac{da}{dt} &= -\lambda^s(a,b,c,\varepsilon)a \\ \frac{db}{dt} &= \lambda^u(a,b,c,\varepsilon)b \\ \frac{dc}{dt} &= \varepsilon(h(c,\varepsilon) + H(a,b,c,\varepsilon)ab) \end{aligned} \tag{3.3}$$

where $\lambda^s(a,b,c,\varepsilon) > \lambda_0^s$ and $\lambda^u(a,b,c,\varepsilon) > \lambda_0^u$ uniformly in ε for some λ_0^s, λ_0^u positive. The interpretation for this system is as follows: a decays exponentially on the fast timescale, b grows exponentially, and c captures the movement along the slow manifold. We have thus foliated our space along the slow manifold, with the variables a

and b representing the position on the stable and unstable fibers and c representing the basepoint of the fiber.

If the critical manifold of the original problem is normally attractive, then $b \equiv 0$, and modulo additional coordinate transformations our problem becomes

$$\begin{aligned}\frac{da}{dt} &= -\lambda^s(a, c, \varepsilon)a \\ \frac{dc}{dt} &= \varepsilon h(c, \varepsilon).\end{aligned} \tag{3.4}$$

Our problem falls into this category along the left and right branches of the critical manifold, and thus these equations describe the underlying behavior of solutions to the kinetic equations. Let us suppose that we had two solutions to the kinetic equations with constant initial data. To first order, the difference in magnitude of these solutions would be controlled by the variational equation of (3.1). In Appendix A, we prove the following lemma.

Lemma 3.3.1. *Let us suppose that we are given a system of ODEs $\dot{u} = f(u)$, $f : \mathbb{R}^n \to \mathbb{R}^n$ and a diffeomorphism $g : \mathbb{R}^n \to \mathbb{R}^n$ with inverse $h : \mathbb{R}^n \to \mathbb{R}^n$. If $\tilde{u}$ solves*

$$\dot{\tilde{u}} = \nabla_{\tilde{u}} f(u(t)) + z(t)$$

then $g_u(u)\tilde{u}$ satisfies

$$\dot{\tilde{v}} = \nabla_{\tilde{v}} F(v(t)) + g_u(h(v))z(t)$$

In the case where $z(t) \equiv 0$, this means that if the solutions to two systems of ODEs are related via a coordinate transformation, then the solutions to their variational equations are related by the pushforward of the transformation. Ultimately, we need only study the variational equation of one system to understand the solutions to the other. Thus, we can get a handle on the divergence of solutions to (3.1) by studying the variational equation of the system in Fenichel normal form. If one were to linearize about a solution (a, c), this equation would take the form

$$\frac{d\bar{a}}{dt} = -\lambda^s(a,c,\varepsilon)\bar{a} - \lambda^s_a(a,c,\varepsilon)a\bar{a} - \lambda^s_c(a,c,\varepsilon)a\bar{c}$$
$$\frac{dc}{dt} = \varepsilon h_c(c,\varepsilon)\bar{c}.$$

Let us consider initial data of the form $(\bar{a}, \bar{c}) = (\bar{a}_0, 0)$. Geometrically, such initial data corresponds to two nearby solutions beginning on the same stable fiber. The second equation tells us that this situation is invariant under the flow: $\bar{c}(t) \equiv 0$, and thus two solutions starting on the same fiber remain on the same fiber. Solving the first equation by variation of parameters, we find that

$$\begin{aligned} \bar{a}(t) &= \exp\Big(-\int_0^t \lambda^s(a(u), c(u), \varepsilon)\mathrm{d}u\Big)\bar{a}_0 \\ &\quad - \int_0^t \exp\Big(-\int_v^t \lambda^s(a(u), c(u), \varepsilon)\mathrm{d}u\Big)\lambda^s_a(a(v), c(v), \varepsilon)a(v)\bar{a}(v)\mathrm{dv}. \end{aligned} \tag{3.5}$$

We now observe that the following bounds hold:

$$\exp\Big(-\int_v^t \lambda^s(a(u), c(u), \varepsilon)\mathrm{d}u\Big) \leq e^{-\lambda^s_0(t-v)} \tag{3.6}$$

and

$$|a(v)| \leq |a(0)|e^{-\lambda^s_0 v}. \tag{3.7}$$

Let us define a new norm via

$$||\bar{a}|| := \sup_{t\in\mathbb{R}} e^{\lambda^s_0 t}|\bar{a}(t)|. \tag{3.8}$$

Using the bounds from above, we can show that

$$\begin{aligned} e^{\lambda_0^s t}|\bar{a}(t)| &\leq |\bar{a}_0| + |a(0)| \cdot ||a|| \int_0^t e^{-\lambda_0^s v} \mathrm{dv} \\ &\leq |\bar{a}_0| + \frac{|a(0)|}{\lambda_0^s} |||\bar{a}||. \end{aligned}$$

Finally, taking the supremum on both sides and rearranging, we find that

$$||\bar{a}|| \leq \frac{|\bar{a}_0|\lambda_0^s}{\lambda_0^s - |a(0)|}$$

What we have demonstrated is that when two solutions begin close together on the same stable fiber, they draw exponentially closer together over time at the linear level. We note that one could conclude this fact more immediately, since all solutions lying along the stable fiber approach the basepoint, and thus each other, exponentially quickly. However, we now seek to generalize this analysis in the situation where the effects of diffusion are present.

3.3.2 Effects of diffusion

Let us suppose that we linearize the Fitzhugh–Nagumo equation around a solution to the kinetic equations. We suppose that there is a point (u_0, w_0) such that the initial data for this solution lies on the stable fiber corresponding to (u_0, w_0). The resulting variational equation is

$$\begin{aligned} \frac{\partial \bar{u}_\varepsilon}{\partial t} &= \frac{\partial^2 \bar{u}_\varepsilon}{\partial x^2} + \frac{\partial^2 u_\varepsilon^{\mathrm{ODE}}}{\partial x^2} + f'(u_\varepsilon^{\mathrm{ODE}})\bar{u}_\varepsilon - \bar{w}_\varepsilon \\ \frac{\partial \bar{w}_\varepsilon}{\partial t} &= \varepsilon(\bar{u}_\varepsilon - \gamma \bar{w}_\varepsilon). \end{aligned} \tag{3.9}$$

We note that with the exception of the color-coded terms in the first equation, this is precisely the variational equation whose dynamics we analyzed in the previous section. Let us now take an additional step towards the full problem: we neglect only the term $\frac{\partial^2 \bar{u}_\varepsilon}{\partial x^2}$. The resulting equation is equal to the variational equation of the kinetic equations, plus an inhomogeneous source term.

$$\begin{aligned} \frac{\partial \bar{u}_\varepsilon}{\partial t} &= f'(u_\varepsilon^{\mathrm{ODE}})\bar{u}_\varepsilon - \bar{w}_\varepsilon + \frac{\partial^2 u_\varepsilon^{\mathrm{ODE}}}{\partial x^2} \\ \frac{\partial \bar{w}_\varepsilon}{\partial t} &= \varepsilon(\bar{u}_\varepsilon - \gamma \bar{w}_\varepsilon). \end{aligned} \tag{3.10}$$

Let us suppose that we may obtain the bound

$$\left| \frac{\partial^2 u_\varepsilon^{\mathrm{ODE}}}{\partial x^2} \right| \leq C e^{-\alpha t} \tag{3.11}$$

uniformly in x. If we assume that the derivatives of λ^s and h are bounded, we can in fact prove this assumption in a similar manner to the analysis in the previous section. Lemma 3.3.1 then says that in order to control the magnitude of solutions to (3.10), it is enough to understand the behavior of solutions to

$$\begin{aligned} \frac{d\bar{a}}{dt} &= -\lambda^s(a,c,\varepsilon)\bar{a} - \lambda^s_a(a,c,\varepsilon)a\bar{a} - \lambda^s_c(a,c,\varepsilon)a\bar{c} + g_1(t;x) \\ \frac{d\bar{c}}{dt} &= \varepsilon h_c(c,\varepsilon)\bar{c} + g_2(t;x), \end{aligned} \tag{3.12}$$

where $|g_i(t;x)| \leq C_i e^{-\alpha t}$ uniformly in x. This inequality is an immediate consequence of (3.11) and the smoothness of our coordinate transformation. Solving (3.12) via variation of parameters, we obtain

$$\begin{aligned}
\bar{a}(t) &= \exp\Big(-\int_0^t \lambda^s(a(u),c(u),\varepsilon)\mathrm{d}u\Big)\bar{a}_0 \\
&\quad - \int_0^t \exp\Big(-\int_v^t \lambda^s(a(u),c(u),\varepsilon)\mathrm{d}u\Big)\lambda^s_a(a(v),c(v),\varepsilon)a(v)\bar{a}(v)\mathrm{d}v \\
&\quad - \int_0^t \exp\Big(-\int_v^t \lambda^s(a(u),c(u),\varepsilon)\mathrm{d}u\Big)\lambda^s_c(a(v),c(v),\varepsilon)a(v)\bar{c}(v)\mathrm{d}v \qquad (3.13) \\
&\quad + \int_0^t \exp\Big(-\int_v^t \lambda^s(a(u),c(u),\varepsilon)\mathrm{d}u\Big)g_1(v;x)\mathrm{d}v \\
\bar{c}(t) &= \int_0^t \exp\Big(\varepsilon\int_v^t h_c(c(u),\varepsilon)\mathrm{d}u\Big)g_2(v;x)\mathrm{d}v.
\end{aligned}$$

Examining the second of these equations, we see immediately that even if two solutions begin on the same stable fiber (i.e. $\bar{c}(0) = 0$), the perturbation from the spatial variation will generically disrupt this state of affairs. Furthermore, if h_c is bounded below by a positive number, then we cannot even expect $\bar{c}$ to decay with time. We would in fact expect to see exponential growth, with a growth constant that is $\mathcal{O}(\varepsilon)$.

To avoid making assumptions on the sign of h_c, let us restrict ourselves to the time interval $t \in [0, \frac{1}{\varepsilon}]$. This restriction is motivated by the fact that in our original dynamical system we only expect to remain near the slow manifold for $\mathcal{O}(\frac{1}{\varepsilon})$-time before making a fast jump. With this assumption in hand, we can prove that our perturbation in $\bar{c}$ remains bounded as follows

$$|\bar{c}(t)| \leq C_2 \exp\Big(\sup_{t\in[0,\frac{1}{\varepsilon}]}|h_c(c(t),\varepsilon)|\Big)\int_0^t e^{-\alpha v}\mathrm{d}v = \frac{C_2}{\alpha}\exp\Big(sup_{t\in[0,\frac{1}{\varepsilon}]}|h_c(c(t),\varepsilon)|\Big).$$

However, this result suggests that we can only prove that the perturbations along the stable fiber $\bar{a}$ are bounded at the linear level. Attempting to use the same argument that we applied to (3.5) would fail without decay in $\bar{c}$. This analysis provides evidence for the claim that we should not expect to see exponential decay of solutions to the slow manifold like in the case of fast-slow systems of ODEs.

Up until now, we have examined a truncated form of the system, and proved only boundedness in finite time. In the next section, we will return to the full problem and examine the remaining effects of diffusion. Utilizing pointwise estimates, we will show that we can recover some form of decay.

3.4 Behavior near the slow manifold

Let us suppose once again that we have a solution to the kinetic equations. If $(u_\varepsilon, w_\varepsilon)(x,t)$ is the solution to the Fitzhugh–Nagumo equations with initial data $(u_0, w_0)(x)$, then we define the **offset** by

$$\begin{aligned}\bar{u}_\varepsilon &:= u_\varepsilon - u_\varepsilon^{\text{ODE}}\\ \bar{w}_\varepsilon &:= w_\varepsilon - w_\varepsilon^{\text{ODE}}.\end{aligned}$$

The offsets then satisfy the system of equations

$$\begin{aligned}\frac{\partial \bar{u}_\varepsilon}{\partial t} &= \frac{\partial^2 \bar{u}_\varepsilon}{\partial x^2} + \frac{\partial^2 u_\varepsilon^{\text{ODE}}}{\partial x^2} + f'(u_\varepsilon^{\text{ODE}})\bar{u}_\varepsilon - \bar{w}_\varepsilon + N(\bar{u}_\varepsilon, u_\varepsilon^{\text{ODE}})\\ \frac{\partial \bar{w}_\varepsilon}{\partial t} &= \varepsilon(\bar{u}_\varepsilon - \gamma \bar{w}_\varepsilon).\end{aligned} \tag{3.14}$$

where $N(\bar{u}_\varepsilon, u_\varepsilon^{\text{ODE}})$ is quadratic-order in the first argument. We also observe that $\bar{u}_\varepsilon(x,0) = \bar{w}_\varepsilon(x,0) = 0$, since the solutions to both the kinetic equations and the Fitzhugh–Nagumo equations have the same initial data.

Ideally, we would like to be able solve (3.14) in a manner similar to the variational equations in the previous section. Such a solution is the topic of the next section.

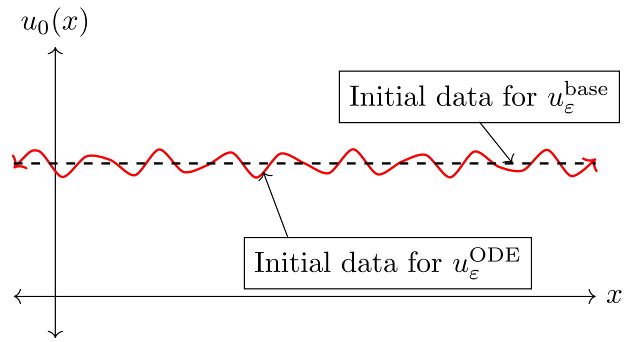

Figure 3.4: The base solution has spatially homogeneous initial data. The initial data for the kinetic solutions are "centered" around this constant value.

3.4.1 Variation of parameters

We begin by rewriting (3.14). We suppose that $(u_\varepsilon^{\text{base}}, w_\varepsilon^{\text{base}})(t)$ is a spatially-homogeneous solution to the kinetic equations given by choosing initial data $(u_\varepsilon^{\text{base},0}, w_\varepsilon^{\text{base},0})$. The relationship between $u_\varepsilon^{\text{ODE}}$ and u^{base} is shown in Figure 3.4. Our equations become

$$\begin{aligned}
\frac{\partial \bar{u}_\varepsilon}{\partial t} &= \frac{\partial^2 \bar{u}_\varepsilon}{\partial x^2} + f'(u_\varepsilon^{\text{base}})\bar{u}_\varepsilon - \bar{w}_\varepsilon + \frac{\partial^2 [u_\varepsilon^{\text{ODE}} - u_\varepsilon^{\text{base}}]}{\partial x^2} + [f'(u_\varepsilon^{\text{ODE}}) - f'(u_\varepsilon^{\text{base}})]\bar{u}_\varepsilon + N(\bar{u}_\varepsilon, u_\varepsilon^{\text{ODE}}) \\
\frac{\partial \bar{w}_\varepsilon}{\partial t} &= -\varepsilon\gamma\bar{w}_\varepsilon + \varepsilon\bar{u}_\varepsilon.
\end{aligned} \tag{3.15}$$

We can write this equation in operator form. We define $\bar{v}_\varepsilon = (\bar{u}_\varepsilon, \bar{w}_\varepsilon)^T$ and obtain

$$\frac{\partial \bar{v}_\varepsilon}{\partial t} = A(t)\bar{v}_\varepsilon + g(x,t) \tag{3.16}$$

where

$$A(t) = \begin{pmatrix} \partial_x^2 + f'(u^{\text{base}}(t)) & -1 \\ 0 & -\varepsilon\gamma \end{pmatrix}$$

and

$$g(x,t) = \begin{pmatrix} \frac{\partial^2[u_\varepsilon^{\mathrm{ODE}} - u_\varepsilon^{\mathrm{base}}]}{\partial x^2} + [f'(u_\varepsilon^{\mathrm{ODE}}) - f'(u_\varepsilon^{\mathrm{base}})]\bar{u}_\varepsilon + N(\bar{u}_\varepsilon, u_\varepsilon^{\mathrm{ODE}}) \\ \varepsilon \bar{u}_\varepsilon \end{pmatrix}.$$

If we can solve the homogeneous problem associated with (3.16), then we can solve our full problem via variation of parameters. This fact motivates the form of our decomposition: we have chosen $A(t)$ to be upper triangular, and in such a manner that the two terms in the $(1,1)$ entry commute with each other.

Remark 4. The latter condition is a familiar one in the context of semigroup theory: if two operators commute with each other, then the semigroup generated by their sum can be factored into the semigroup generated by the first acting on the semigroup generated by the second, or vice-versa.

We turn now to the task of solving the homogeneous problem. We see that this problem could be decomposed in turn. Denoting the solution to the homogeneous problem by $\hat{v}_\varepsilon$, we have that

$$\frac{\partial \hat{v}_\varepsilon}{\partial t} = \hat{A}(t)\hat{v}_\varepsilon + \hat{g}(x,t) \tag{3.17}$$

where

$$\hat{A}(t) = \begin{pmatrix} \partial_x^2 + f'(u^{\mathrm{base}}(t)) & 0 \\ 0 & -\varepsilon\gamma \end{pmatrix}$$

and

$$\hat{g}(x,t) = \begin{pmatrix} -\hat{w}_\varepsilon \\ 0 \end{pmatrix}.$$

We can immediately solve (3.17) via variation of parameters. We find that

$$\hat{u}_\varepsilon(x,t) = E_\varepsilon(t,0)\big[\mathscr{N}(\cdot,t) * \hat{u}_\varepsilon(\cdot,0)\big] - \int_0^t E_\varepsilon(t,s)e^{-\varepsilon\gamma s}\big[\mathscr{N}(\cdot,t-s) * \hat{w}_\varepsilon(\cdot,0)\big]\mathrm{d}s$$
$$\hat{w}_\varepsilon(x,t) = e^{-\varepsilon\gamma t}\hat{w}_\varepsilon(x,0) \tag{3.18}$$

where

$$\mathscr{N}(x,t) = \frac{1}{\sqrt{4\pi t}}e^{-x^2/4t}$$

is the fundamental solution to the heat equation and

$$E_\varepsilon(t,s) = \exp\Big(\int_s^t f'(u_\varepsilon^{\text{base}}(\tau))\mathrm{d}\tau\Big). \tag{3.19}$$

With this result in hand, the solution to our full problem is

$$\begin{aligned}
\bar{u}_\varepsilon(t) = &\int_0^t E_\varepsilon(t,\tau)\big[\mathscr{N}(\cdot,t-\tau) * (u_\varepsilon^{\text{ODE}}(\tau) - u_\varepsilon^{\text{base}}(\tau))_{xx}\big]\mathrm{d}\tau \\
&+ \int_0^t E_\varepsilon(t,\tau)[\mathscr{N}(\cdot,t-\tau) * (f'(u_\varepsilon^{\text{ODE}}(\tau)) - f_\varepsilon'(u^{\text{base}}(\tau)))\bar{u}_\varepsilon(\tau)]\mathrm{d}\tau \\
&- \varepsilon\int_0^t\int_0^\tau E_\varepsilon(t,\tau)e^{-\varepsilon\gamma(\tau-s)}\big[\mathscr{N}(\cdot,t-\tau) * \bar{u}_\varepsilon(s)\big]\mathrm{d}s\mathrm{d}\tau \\
&+ \int_0^t E_\varepsilon(t,\tau)[\mathscr{N}(\cdot,t-\tau) * N(\bar{u}_\varepsilon, u_\varepsilon^{\text{ODE}})(\cdot,\tau)]\mathrm{d}\tau \\
\bar{w}_\varepsilon(t) = &\ \varepsilon\int_0^t e^{-\varepsilon\gamma(t-\tau)}\bar{u}_\varepsilon(\tau)\mathrm{d}\tau
\end{aligned} \tag{3.20}$$

where we have used the fact that $\bar{u}_\varepsilon(x,0) = \bar{w}_\varepsilon(x,0) \equiv 0$. Examining the structure of (3.20), we see that the first equation has been decoupled. Thus, we can search for bounds on $\bar{u}_\varepsilon$, and then use the second of our equations to control $\bar{w}_\varepsilon$.

3.4.2 Key results

In this section, we shall state our three main results. The first of these pertains to the case we have discussed thus far, in which the initial data for our problem lies along the stable fiber of a point on the slow manifold of the kinetic system.

Theorem 3.4.1. *Choose $p < 1$. There exists a $\gamma_0 > 0$, $C > 0$, $C_{\text{quad}} > 0$ $r_1 > 0$, $\tau_{\max} > 0$ and $\delta > 0$ such that for all $\gamma > \gamma_0$ the following is true for all $\varepsilon > 0$ sufficiently small. Select a basepoint $(u_\varepsilon^{\text{base},0}, u_\varepsilon^{\text{base},0})$ on a strong stable fiber of the slow manifold of (3.2). Furthermore, suppose $u_\varepsilon^0(x) \in C_b^2(\mathbb{R}) \cap \left(u_\varepsilon^{\text{base},0} + L^1(\mathbb{R})\right)$ and $w_\varepsilon^0(x) \in C_b^2(\mathbb{R}) \cap \left(w_\varepsilon^{\text{base},0} + L^1(\mathbb{R})\right)$, and that $(u_\varepsilon^0, w_\varepsilon^0)(x)$ lie along the strong stable fiber of the slow manifold determined by $(u_\varepsilon^{\text{base},0}, u_\varepsilon^{\text{base},0})$. Let $(u_\varepsilon^{\text{base}}, w_\varepsilon^{\text{base}})$, $(u_\varepsilon^{\text{ODE}}, w_\varepsilon^{\text{ODE}})$, and $(\bar{u}_\varepsilon, \bar{w}_\varepsilon)$ be defined as in the derivation of (3.20). If the following conditions hold:*

1. $f'(u_\varepsilon^{\text{base}}(t)) \leq -r_1 < 0$ *uniformly for* $t \leq T_{\max} = \frac{\tau_{\max}}{\varepsilon}$.
2. $||u_\varepsilon^0(\cdot) - u^{\text{base}}(0)||_\infty + ||w_\varepsilon^0(\cdot) - w^{\text{base}}(0)||_\infty < \delta$

then for all $t \leq \frac{\tau_{\max}}{\varepsilon}$

1. $||u_\varepsilon^{\text{ODE}}(t;\cdot) - u^{\text{base}}(t)||_\infty + ||w_\varepsilon^{\text{ODE}}(t;\cdot) - w^{\text{base}}(t)||_\infty < \delta e^{-r_2 t}$
2. $||\bar{u}_\varepsilon(t)||_\infty + ||\bar{w}_\varepsilon(t)||_\infty \leq C\delta(1+t)^{-p}$

As alluded to earlier, the decay rate in the second conclusion is algebraic. However, we see that the first condition holds for $t \leq \frac{\tau_{\max}}{\varepsilon}$. Therefore, we expect that the magnitude of our offsets will shrink to size $\mathcal{O}(\delta\varepsilon^p)$.

The second of our results establishes a bound when we weaken the assumption that our initial data lies on a single stable fiber.

Theorem 3.4.2. *There exists a $\gamma_0 > 0$, $C > 0$, $C_{\text{quad}} > 0$ $r_1 > 0$, $\tau_{\max} > 0$ and $\delta > 0$ such that for all $\gamma > \gamma_0$ the following is true for all $\varepsilon > 0$ sufficiently small. Select a basepoint $(u_\varepsilon^{\text{base},0}, u_\varepsilon^{\text{base},0})$. Furthermore, suppose $u_\varepsilon^0(x) \in C_b^2(\mathbb{R}) \cap \left(u_\varepsilon^{\text{base},0} + L^1(\mathbb{R})\right)$ and $w_\varepsilon^0(x) \in C_b^2(\mathbb{R}) \cap \left(w_\varepsilon^{\text{base},0} + L^1(\mathbb{R})\right)$, and that $||u_\varepsilon^0 - u^{\text{base},0}||_\infty + ||w_\varepsilon^0 - w^{\text{base},0}||_\infty < \delta$ for $\delta > 0$ sufficiently small, uniformly in ε. Let $(u_\varepsilon^{\text{base}}, w_\varepsilon^{\text{base}})$, $(u_\varepsilon^{\text{ODE}}, w_\varepsilon^{\text{ODE}})$, and $(\bar{u}_\varepsilon, \bar{w}_\varepsilon)$ be defined as in the derivation of (3.20). If the following condition holds:*

1. *$f'(u_\varepsilon^{\text{base}}(t)) \leq -r_1 < 0$ uniformly for $t \leq T_{\max} = \frac{\tau_{\max}}{\varepsilon}$.*

then for all $t \leq \frac{\tau_{\max}}{\varepsilon}$

1. *$||\bar{u}_\varepsilon||_\infty + ||\bar{w}_\varepsilon||_\infty \leq C\delta$*

We have already observed that treating diffusion solely from a semigroups perspective means that one cannot take advantage of the algebraic decay of solutions to the heat equation. The result is boundedness, at best. Here we likewise see that the geometric structure of our initial data is crucially important. Without it, we cannot expect $u_\varepsilon^{\text{ODE}}$ to decay exponentially to $u_\varepsilon^{\text{base}}$.

These two theorems tell us that it is the combined effect of the exponential decay of solutions to the kinetic equations to their basepoint and the algebraic decay from the diffusion terms that enforce an algebraic decay on the offsets. Effectively, the diffusion terms introduce an inhomogeneity, $\frac{\partial^2 u_\varepsilon^{\text{ODE}}}{\partial x^2}$, to our equations which breaks the decomposition of the system into a slowly drifting basepoint with exponentially

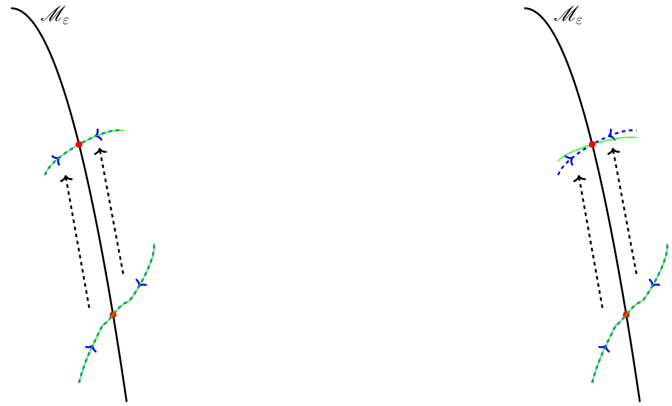

(a) Kinetic system (b) Full system

Figure 3.5: In the kinetic system, initial data (green) that is initially arranged along a stable fiber (dashed blue) of the slow manifold (black) evolves to lie along another stable fiber, while contracting to the basepoint. In the full system, the fibers are not invariant and the initial data is forced off, while still contracting at a much slower rate.

contracting fibers. However, the diffusion also provides the means to salvage algebraic decay on the fast timescale, when combined with the exponential decay of the diffusion-free kinetic system. The situation is depicted in Figure 3.5.

Our final result concerns the stability of the fixed point $(0,0)$. We include it here since this point lies on the critical manifold.

Theorem 3.4.3. *Choose $p < 1$. There exists a $\gamma_0 > 0$, $C > 0$, $C_{\text{quad}} > 0$ $\tau_{\max} > 0$ and $\delta_0 > 0$ such that for all $\gamma > \gamma_0$ the following is true for all $\varepsilon > 0$ sufficiently small. Let $(u_\varepsilon^{\text{ODE}}, w_\varepsilon^{\text{ODE}})$ and $(\bar{u}_\varepsilon, \bar{w}_\varepsilon)$ be defined as before. We suppose that $||u_\varepsilon^0||_\infty + ||w_\varepsilon^0||_\infty < \delta\varepsilon$ for $\delta > 0$ sufficiently small, uniformly in ε. Then for all $t \geq 0$ we have that*

$$||\bar{u}_\varepsilon||_\infty + ||\bar{w}_\varepsilon||_\infty \leq C\delta(1+t)^{-p}$$

This theorem tells us that if our solutions enter a sufficiently close neighborhood of the origin, our offsets will decay to zero algebraically. Since our spatial ansatz will decay exponentially to the origin, albeit at an ε-dependent rate, we expect the solutions to the full Fitzhugh–Nagumo system (1.1) will decay as well.

Remark 5. In Bates and Jones (1989), the authors obtain exponential decay of the semigroup generated by linearizing the Fitzhugh–Nagumo model about the origin. However, the rate of decay is bounded above by $\varepsilon\gamma$, and is therefore not uniform as one decreases ε. In the limit as $\varepsilon \to 0^+$, one should expect only boundedness when using methods based purely on semigroups.

3.4.3 Limits of semigroups

In Remark 5, we alluded to the notion of semigroups. Linear semigroups have proven to be an extremely fruitful method for stability analysis in a number of contexts, including PDES (e.g. Bates and Jones (1989)), and delay differential equations (for an example, see Bátkai and Piazzera (2002)). As such, it is natural to wonder why one would not make use of them in this case. As an example, we could rewrite the second term in (3.20) as

$$\begin{aligned}&\int_0^t E_\varepsilon(t,\tau)[\mathscr{N}(\cdot, t-\tau) * (f'(u_\varepsilon^{\mathrm{ODE}}(\tau)) - f_\varepsilon'(u^{\mathrm{base}}(\tau)))\bar{u}_\varepsilon(\tau)]\mathrm{d}\tau \\ &= \int_0^t E_\varepsilon(t,\tau)e^{(t-\tau)\partial_x^2}(f'(u_\varepsilon^{\mathrm{ODE}}(\tau)) - f_\varepsilon'(u^{\mathrm{base}}(\tau)))\bar{u}_\varepsilon(\tau)]\mathrm{d}\tau.\end{aligned}$$

In semigroup theory, if one can obtain good control of the spectrum of the **generator**, in our case ∂_x^2 defined on some suitable function space, then one can often infer bounds on the semigroup. Examples of such results can be found in e.g. Engel and Nagel (1999).

In general, any semigroup $T(t)$ with generator A densely defined on a Banach space X has a **growth bound** ω_0, defined by

$$\omega_0 := \inf\{w \in \mathbb{R} : \ \exists M_w \geq 1 \ \forall t \geq 0 \ ||T(t)|| \leq M_w e^{wt}\}$$

where $||\cdot||$ is the operator norm of linear maps from X to X. In the finite dimensional case where the generator A is a matrix, the growth bound always coincides with the maximal real part of the eigenvalues of A. In other words, if we define the **spectral bound** $s(A)$ via

$$s(A) := \sup\{\lambda \in \sigma(A) : \ \text{Re}\ \lambda\}$$

then $\omega_0 = s(A)$. A generator on an infinite-dimensional Banach space must satisfy additional criteria for equality to hold. However, one can demonstrate fairly simply that $\omega_0 \geq s(A)$.

This lower bound already has crucial implications for the question under consideration in this chapter, because the Laplacian ∂_x^2 defined on the Hilbert space $H^2(\mathbb{R})$ has no spectral gap: the essential spectrum of this operator intersects the imaginary axis of the complex plane (Figure 3.6). Thus we see that $s(\partial_x^2) = 0$, so our semigroup does not exhibit exponential decay. If one were to consider the operator solely from the perspective of semigroups, the best result one could obtain is that solutions to the heat equations remain bounded.

While it is true that the diffusion terms are not the only ones in (3.14) that promote stability, we have already seen in §3.3.2 that ignoring the effects of the Laplacian only allows one to prove boundedness in finite time. Therefore, we conclude that treating the diffusion from a semigroups perspective is not sufficient.

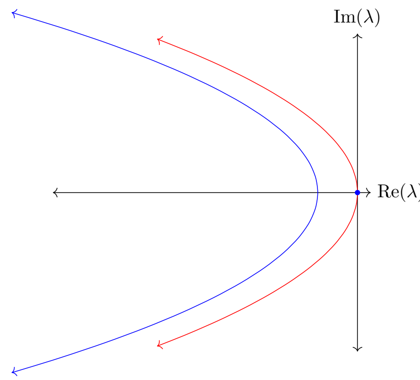

Figure 3.6: The essential spectrum of a shifted parabolic operator $\partial_x^2 - 1$ (blue) and ∂_x^2 (red).

3.4.4 Benefits of pointwise estimates

In the previous section, we have established that semigroups are not up to the task of proving that solutions to (3.14) decay in time. Intuitively, this is because semigroups, which are defined in a manner analogous to the exponential function, are essentially only able to "see" exponential decay. Since none is forthcoming from solutions to the heat equation, one can prove only that solutions do not grow exponentially either.

Fortunately, the Laplacian can also be easily treated using the method of pointwise estimates. Many examples of this technique can be found in the literature, either explicitly using the name as in Beck et al. (2010) or Beck et al. (2011), or earlier papers such as Kappitula (1992) which use similar techniques. To explain the method, let us suppose that we have a problem of the following form

$$u_t = Au + N(u) \tag{3.21}$$

where $u \in X$, X is a Banach space, $A : X \to X$ is a densely-defined linear operator analogous to our generator above, and $N(u)$ is a pointwise-defined quadratic-order nonlinearity such that $N(0) = 0$. As we did above, we can first find a solution to the homogeneous linear problem $u_t = Au$, and solve (3.21) via variation of parameters. If the nonlinearity is sufficiently well-behaved, we can then extend any stability results from the linear level to the nonlinear level.

The key operational difference between semigroup methods and pointwise estimates is that we control solutions to the linear problem by either explicitly computing or obtaining estimates on the Green's function for the operator A. In this setting, one can frequently obtain algebraic decay even for operators with spectrum on the imaginary axis. Therefore, we have chosen to write the solution to (3.14) using the fundamental solution to the heat equation, which is directly related to the Green's function.

We shall now make use of (3.20) to establish that our offsets decay in time as solutions to the kinetic system drift near the slow manifold. Per the discussion above, we expect an algebraic rate of decay. While this is a far cry from the exponential decay to the slow manifold in the kinetic system, we will see that this still takes place on the fast timescale. Therefore, we can accumulate significant decay while our ansatz $(u_\varepsilon^{\mathrm{ODE}}, w_\varepsilon^{\mathrm{ODE}})$ evolves in this regime.

3.4.5 Estimates of important quantities

In order to establish the theorems discussed in §3.4.2, we must first derive a few estimates. The first of these is a result on the L^p norms of derivatives of the heat kernel $\mathscr{N}(x,t)$. Similar bounds can be found in many textbooks, but we include a proof here for completeness.

Lemma 3.4.4. *Let $k \geq 0$, $1 \leq p \leq \infty$. Then*

$$||\partial_x^k \mathscr{N}(\cdot,t)||_{L^p(\mathbb{R})} \leq C_{k,p} t^{\frac{1}{2}(\frac{1}{p}-1-k)}$$

Proof. We define the similarity variable $y = \frac{x}{\sqrt{t}}$. We may rewrite $\mathscr{N}$ as

$$\mathscr{N}(x,t) = (4\pi t)^{-\frac{1}{2}} f(y)$$

where $f(y) = e^{-\frac{y^2}{4}}$. We also observe that $\partial_x^k = t^{-\frac{k}{2}}\partial_y^k$. Therefore, for $p < \infty$, we find that

$$\begin{aligned}
||\partial_x^k \mathscr{N}(\cdot,t)||_{L^p(\mathbb{R})}^p &= \int_{\mathbb{R}} |\partial_x^k \mathscr{N}(x,t)|^p \mathrm{d}x \\
&= (4\pi t)^{-\frac{p}{2}} t^{\frac{1}{2}} t^{-\frac{pk}{2}} \int_{\mathbb{R}} |\partial_y^k f(y)|^p \mathrm{d}y \\
&= (4\pi t)^{-\frac{p}{2}} t^{\frac{1}{2}} t^{-\frac{pk}{2}} \int_{\mathbb{R}} |Q_k(y) f(y)|^p \mathrm{d}y \\
&= C_{k,p}^p t^{\frac{1}{2}(1-p-kp)}
\end{aligned}$$

where the second line follows via a change of variables. The third line follows since for each k, $\partial_y^k f(y) = Q_k(y) f(y)$ where $Q_k(y)$ is a polynomial function of y of order k. These derivatives are integrable due to the decay of $f(y)$, and the result is a constant depending on p and k. Taking the p-th root on both sides completes the proof for finite p. For $p = \infty$, we may similarly observe that

$$\begin{aligned}
|\partial_x^k \mathscr{N}(x,t)| &= (4\pi t)^{-\frac{1}{2}} t^{-\frac{k}{2}} |Q_k(y) f(y)| \\
&\leq C_{k,\infty} t^{-\frac{1}{2}(1+k)}
\end{aligned}$$

since a polynomial function multiplied by $e^{-\frac{y^2}{4}}$ is uniformly bounded. This completes the proof. $\square$

The second lemma is a bound for an elementary integral that comes up repeatedly in the proofs of our theorems. The proof technique is essentially a slight modification of the computations used to demonstrate Lemma 3.2 of Kappitula (1991), which is concerned with very similar integrals.

Lemma 3.4.5. *Let $p < 1$, $r > 0$. Then*

$$\int_0^t \frac{e^{-r\tau}}{[1+(t-\tau)]^p}\mathrm{d}\tau \leq \frac{C_p}{r}(1+t)^{-p}$$

Proof. Making the u-substitution $\tau \mapsto t-\tau$ followed by $\tau \mapsto \tau+1$ and using the Taylor series for the exponential function, we find that

$$\begin{aligned}
\int_0^t \frac{e^{-r\tau}}{[1+(t-\tau)]^p}\mathrm{d}\tau &= e^{-r(1+t)}\int_0^t \frac{e^{r(1+\tau)}}{(1+\tau)^p}\mathrm{d}\tau \\
&= e^{-r(1+t)}\int_1^{1+t} \frac{e^{r\tau}}{\tau^p}\mathrm{d}\tau \\
&= e^{-r(1+t)}\int_1^{1+t} \sum_{n=0}^{\infty} \frac{r^n\tau^{n-p}}{n!}\mathrm{d}\tau \\
&= e^{-r(1+t)}\Big[\int_1^{1+t} \tau^{-p}\mathrm{d}\tau + \sum_{n=1}^{\infty}\int_1^{1+t}\frac{r^n\tau^{n-p}}{n!}\mathrm{d}\tau\Big] \\
&\leq e^{-rt}\Big[\frac{(1+t)^{1-p}}{1-p} + \sum_{n=1}^{\infty}\frac{r^n(1+t)^{n+1-p}}{(n+1)!}\frac{n+1}{n+1-p}\Big]
\end{aligned}$$

where we have exchanged integration and summation via the absolute convergence of the Taylor series of the exponential function. Rearranging, we have that

$$\begin{aligned}
\int_1^{1+t} \frac{e^{-r\tau}}{[1+(t-\tau)]^p} \mathrm{d}\tau &\le e^{-r(1+t)} \Big[\frac{(1+t)^{1-p}}{1-p} + \sum_{n=1}^{\infty} \frac{r^n (1+t)^{n+1-p}}{(n+1)!} \frac{n+1}{n+1-p} \Big] \\
&= e^{-r(1+t)} \Big[\frac{1+t}{1-p} + \frac{1}{r} \sum_{n=1}^{\infty} \frac{r^{n+1}(1+t)^{n+1}}{(n+1)!} \frac{n+1}{n+1-p} \Big] (1+t)^{-p} \\
&\le e^{-r(1+t)} \Big[\frac{1+t}{1-p} + \frac{2}{r} \sum_{n=1}^{\infty} \frac{r^{n+1}(1+t)^{n+1}}{(n+1)!} \Big] (1+t)^{-p} \\
&\le \Big[\frac{(1+t)e^{-r(1+t)}}{1-p} + \frac{2}{r} \Big] (1+t)^{-p} \\
&\le \Big[\frac{2}{r} + \frac{1}{1-p} \cdot \max\{e^{-r}, \frac{1}{re}\} \Big] (1+t)^{-p} \\
&\le \Big[2 + \frac{1}{e(1-p)} \Big] \frac{(1+t)^{-p}}{r}.
\end{aligned}$$

The second-to-last line follows by explicit computation of the global maximum of $(1+t)e^{-r(1+t)}$ for $t \ge 0$. The last line follows since a similar computation shows that $\frac{e^{-r}}{(re)^{-1}}$ is bounded above by 1 for positive r, and thus $\max\{e^{-r}, \frac{1}{re}\} = \frac{1}{re}$. □

Remark 6. We prove this result with $(1+(t-\tau))^p$ in the denominator instead of $(t-\tau)^p$ because in the proof of our key theorems, we must deal with the pathological case $p = 1$. Since $(1+(t-\tau))^{-1} \le (1+(t-\tau))^{-p}$, we can eliminate this difficulty.

Remark 7. This result can be thought of as a generalization of the fact that

$$\int_0^t e^{-r_1(t-\tau)} e^{-r_2\tau} \mathrm{d}\tau \le \frac{1}{|r_1 - r_2|} e^{-\min\{r_1, r_2\}t}.$$

In other words, when we compute the convolution in time of two exponential functions, the "worst" rate bounds the result. Similarly, when computing the convolution in time between an algebraically decaying function and an exponentially decaying one, the algebraic rate survives.

In the next section, we will make use of these lemmas to prove a theorem which will immediately allow us to derive bounds on the offsets, whether those offsets are initialized near a stable fiber, in a generic neighborhood of the slow manifold, or near the origin.

3.4.6 Bootstrap theorem

We reproduce (3.20) below for convenience.

$$\begin{aligned}
\bar{u}_\varepsilon(t) = &\int_0^t E_\varepsilon(t,\tau)\big[\mathscr{N}(\cdot, t-\tau) * (u_\varepsilon^{\mathrm{ODE}}(\tau) - u_\varepsilon^{\mathrm{base}}(\tau))_{xx}\big]\mathrm{d}\tau \\
&+ \int_0^t E_\varepsilon(t,\tau)[\mathscr{N}(\cdot, t-\tau) * (f'(u_\varepsilon^{\mathrm{ODE}}(\tau)) - f_\varepsilon'(u^{\mathrm{base}}(\tau)))\bar{u}_\varepsilon(\tau)]\mathrm{d}\tau \\
&- \varepsilon \int_0^t \int_0^\tau E_\varepsilon(t,\tau) e^{-\varepsilon\gamma(\tau - s)}\big[\mathscr{N}(\cdot, t-\tau) * \bar{u}_\varepsilon(s)\big]\mathrm{d}s\mathrm{d}\tau \\
&+ \int_0^t E_\varepsilon(t,\tau)[\mathscr{N}(\cdot, t-\tau) * N(\bar{u}_\varepsilon, u_\varepsilon^{\mathrm{ODE}})(\cdot,\tau)]\mathrm{d}\tau \\
\bar{w}_\varepsilon(t) = &\ \varepsilon \int_0^t e^{-\varepsilon\gamma(t-\tau)}\bar{u}_\varepsilon(\tau)\mathrm{d}\tau.
\end{aligned}$$

We make the following observations. The first two terms of the first equation of (3.20) depend on the difference between $u_\varepsilon^{\mathrm{ODE}}$ and $u_\varepsilon^{\mathrm{base}}$. In each of our theorems, we make assumptions about the magnitude of this difference, either implicitly or explicitly. The remaining terms depend only on $\bar{u}_\varepsilon$. Therefore, if the magnitude of the first two terms can be controlled in some way, it may be possible to extend that control to the remaining terms to prove an estimate via bootstrapping. With this done, we can use the second equation to control $\bar{w}_\varepsilon$ in terms of $\bar{u}_\varepsilon$. We shall now prove a theorem in exactly this manner, and use it to establish our offset estimates near the slow manifold.

Theorem 3.4.6. *Choose $p \in [0, 1)$. There exists a $\gamma_0 > 0$, $\delta_0 > 0$, $C > 0$, $C_{\mathrm{quad}} > 0$, $r > 0$, and $\tau_{\max} > 0$ such that for all $\gamma > \gamma_0$ the following is true for all $\varepsilon > 0$ suf-*

ficiently small. Given initial data (u_0, w_0), *let* $(u_\varepsilon^{\mathrm{ODE}}, w_\varepsilon^{\mathrm{ODE}})$ *be defined as previously and suppose that* $(u_\varepsilon^{\mathrm{base}}, w_\varepsilon^{\mathrm{base}})$ *is a spatially-homogeneous solution to the kinetic system. If* $(\bar{u}_\varepsilon, \bar{w}_\varepsilon)$ *satisfies (3.20) and the following conditions hold for all* $t \leq \frac{\tau_{\max}}{\varepsilon}$ *and a* $\delta \leq \delta_0$*:*

1. $E_\varepsilon(t,\tau) \leq e^{-r(t-\tau)}$, *where* $E_\varepsilon(t,\tau) := \exp\Big(\int_\tau^t f'(u_\varepsilon^{\mathrm{base}}(s))ds\Big)$
2. $\int_0^t E_\varepsilon(t,\tau)||\mathscr{N}(\cdot, t-\tau) * (u_\varepsilon^{\mathrm{ODE}}(\tau) - u_\varepsilon^{\mathrm{base}}(\tau))_{xx}||_\infty \mathrm{d}\tau \leq C\delta(1+t)^{-p}$
3. $\int_0^t \frac{E_\varepsilon(t,\tau)}{(1+\tau)^p}||f'(u_\varepsilon^{\mathrm{ODE}}(\tau)) - f'(u_\varepsilon^{\mathrm{base}}(\tau))||_\infty \mathrm{d}\tau \leq C\delta(1+t)^{-p}$
4. $||N(u, u_\varepsilon^{\mathrm{ODE}})||_\infty \leq C_{\mathrm{quad}}||u||_\infty^2$

then we conclude that there exists a $\tilde{C} > 0$ *such that for all* $t \leq \frac{\tau_{\max}}{\varepsilon}$

$$||\bar{u}_\varepsilon(t)||_\infty + ||\bar{w}_\varepsilon(t)||_\infty \leq \tilde{C}\delta(1+t)^{-p}.$$

Proof. Let us take the L^∞-norm of both sides of the first equation of (3.20). We obtain

$$\begin{aligned} ||\bar{u}_\varepsilon(t)||_\infty \leq & \int_0^t E_\varepsilon(t,\tau)||[\mathscr{N}(\cdot,(t-\tau)) * (u_\varepsilon^{\mathrm{ODE}} - u_\varepsilon^{\mathrm{base}})_{xx}]||_\infty \mathrm{d}\tau \\ & + \int_0^t E_\varepsilon(t,\tau)||(f'(u_\varepsilon^{\mathrm{ODE}}(\tau)) - f'(u_\varepsilon^{\mathrm{base}}(\tau)))\bar{u}_\varepsilon(\tau)||_\infty \mathrm{d}\tau \\ & + \varepsilon \int_0^t \int_0^\tau E_\varepsilon(t,\tau)e^{-\varepsilon\gamma(\tau-s)}||\bar{u}_\varepsilon(s)||_\infty \mathrm{d}s\mathrm{d}\tau + \int_0^t E_\varepsilon(t,\tau)||N(\bar{u}_\varepsilon, u_\varepsilon^{\mathrm{ODE}})||_\infty \mathrm{d}\tau. \end{aligned} \tag{3.22}$$

We define the T-dependent norm

$$|||u|||_T := \sup_{t\leq T}(1+t)^p||u(t)||_\infty$$

for any $T \leq \frac{\tau_{\max}}{\varepsilon}$. We shall choose T at a later point. For now, we always suppose that $t \leq T$. We now rewrite (3.22) using our first and third conditions and the definition of our new norm. We find that

$$\begin{aligned}||\bar{u}_\varepsilon(t)||_\infty \leq C\delta(1+t)^{-p} + |||\bar{u}_\varepsilon|||_T \int_0^t \frac{E_\varepsilon(t,\tau)}{(1+\tau)^p} ||f'(u_\varepsilon^{\mathrm{ODE}}(\tau)) - f'(u_\varepsilon^{\mathrm{base}}(\tau))||_\infty \mathrm{d}\tau \\ + \varepsilon |||\bar{u}_\varepsilon|||_T \int_0^t \int_0^\tau E_\varepsilon(t,\tau) e^{-\varepsilon\gamma(\tau-s)}(1+s)^{-p} \mathrm{d}s\mathrm{d}\tau \\ + C_{\mathrm{quad}} |||\bar{u}_\varepsilon|||_T^2 \int_0^t E_\varepsilon(t,\tau)(1+t)^{-p}\mathrm{d}\tau.\end{aligned}$$

We may further refine the estimate above by applying our second condition, yielding

$$\begin{aligned}||\bar{u}_\varepsilon(t)||_\infty \leq C\delta(1+t)^{-p} + C\delta |||\bar{u}_\varepsilon|||_T (1+t)^{-p} \\ + \varepsilon |||\bar{u}_\varepsilon|||_T \int_0^t \int_0^\tau E_\varepsilon(t,\tau) e^{-\varepsilon\gamma(\tau-s)}(1+s)^{-p} \mathrm{d}s\mathrm{d}\tau \\ + C_{\mathrm{quad}} |||\bar{u}_\varepsilon|||_T^2 \int_0^t E_\varepsilon(t,\tau)(1+t)^{-p}\mathrm{d}\tau.\end{aligned}$$

We see that we may apply Lemma 3.4.5 twice to the third term on the right-hand side and once to the final term to obtain

$$\begin{aligned}||\bar{u}_\varepsilon(t)||_\infty \leq C\delta(1+t)^{-p} + C\delta |||\bar{u}_\varepsilon|||_T (1+t)^{-p} \\ + \frac{C_p^2}{r\gamma} |||\bar{u}_\varepsilon|||_T (1+t)^{-p} + \frac{C_p C_{\mathrm{quad}}}{r} |||\bar{u}_\varepsilon|||_T^2 (1+t)^{-p}.\end{aligned}$$

Multiplying both sides of our inequality by $(1+t)^p$ and taking the supremum over all $t \leq T$, we obtain

$$\begin{aligned}|||\bar{u}_\varepsilon|||_T \leq C\delta + C\delta |||\bar{u}_\varepsilon|||_T \\ + \frac{C_p^2}{r\gamma} |||\bar{u}_\varepsilon|||_T + \frac{C_p C_{\mathrm{quad}}}{r} |||\bar{u}_\varepsilon|||_T^2.\end{aligned}$$

We take $\delta_0 \leq \frac{1}{6C}$, $\gamma_0 = \frac{6C_p^2}{r}$, and suppose that we have chosen the maximal T such that $|||\bar{u}_\varepsilon|||_T \le \frac{r}{6C_pC_{\text{quad}}}$. Rearranging our inequality, we find that

$$|||\bar{u}_\varepsilon|||_T \le 2C\delta.$$

If we also require that $\delta_0 \le \frac{r}{12CC_pC_{\text{quad}}}$, then $|||\bar{u}_\varepsilon|||_T \le \frac{r}{6C_pC_{\text{quad}}}$, so we must have that $T = \frac{\tau_{\max}}{\varepsilon}$.

Lastly, we must control the offset in the w-direction. We recall that this obeys the equation

$$\bar{w}_\varepsilon(t) = \varepsilon \int_0^t e^{-\varepsilon\gamma(t-\tau)}\bar{u}_\varepsilon(\tau)\mathrm{d}\tau.$$

Taking the L^∞-norm in space, we find that

$$\begin{aligned}(1+t)^p||\bar{w}_\varepsilon(t)||_\infty &\le \varepsilon|||\bar{u}_\varepsilon|||_{\frac{\tau_{\max}}{\varepsilon}}(1+t)^p\int_0^t \frac{e^{-\varepsilon\gamma(t-\tau)}}{(1+\tau)^p}\mathrm{d}\tau \\ &\le \frac{|||\bar{u}_\varepsilon|||_{\frac{\tau_{\max}}{\varepsilon}}}{\gamma}.\end{aligned}$$

Taking the supremum for all $t \le \frac{\tau_{\max}}{\varepsilon}$, we end up with

$$|||\bar{w}_\varepsilon|||_{\frac{\tau_{\max}}{\varepsilon}} \le \frac{|||\bar{u}_\varepsilon|||_{\frac{\tau_{\max}}{\varepsilon}}}{\gamma_0}.$$

This completes the proof. □

3.4.7 Proof of estimates near slow manifold

In each of the next subsections, we shall apply the bootstrap theorem to prove our intended estimates. Each proof simply consists of verifying the four conditions given in Theorem 3.4.6.

3.4.7.1 Proof of Theorem 3.4.1

We recall that in Theorem 3.4.1, we have assumed the following conditions:

1. $f'(u_\varepsilon^{\text{base}}(t)) \leq -r_1 < 0$ uniformly for $t \leq T_{\max} = \frac{\tau_{\max}}{\varepsilon}$.
2. $||u_\varepsilon^0(\cdot) - u^{\text{base}}(0)||_\infty + ||w_\varepsilon^0(\cdot) - w^{\text{base}}(0)||_\infty < \delta$

and we wish to demonstrate that

1. $||u_\varepsilon^{\text{ODE}}(t;\cdot) - u^{\text{base}}(t)||_\infty + ||w_\varepsilon^{\text{ODE}}(t;\cdot) - w^{\text{base}}(t)||_\infty < \delta e^{-r_2 t}$
2. $||\bar{u}_\varepsilon(t)||_\infty + ||\bar{w}_\varepsilon(t)||_\infty \leq C\delta(1+t)^{-p}$.

First, we note that the first of our conclusions is a consequence of standard Fenichel theory given our second assumption, up to slightly decreasing $\tau_{\max}$. We shall make use of this fact along with our bootstrapping result to reach the second conclusion.

The first condition of our assumptions immediately implies the first condition of 3.4.6, so we turn to the second. Via the smoothness of of our initial data, we may apply Theorem 8.10 of Folland (1999) to place the spatial derivatives on the heat kernel. We then invoke Lemma 3.4.4 on the decay of the derivatives of the heat kernel. Although our lemma only guarantees decay controlled by inverse powers of t, we may replace this by $1 + t$ without loss due to the smoothness of the function

$u_\varepsilon^{\mathrm{ODE}} - u_\varepsilon^{\mathrm{base}}$. In summary, we obtain

$$\begin{aligned}
&\int_0^t E_\varepsilon(t,\tau)||[\mathscr{N}(\cdot, t-\tau) * (u_\varepsilon^{\mathrm{ODE}} - u_\varepsilon^{\mathrm{base}})_{xx}]||_\infty \mathrm{d}\tau \\
&\quad = \int_0^t E_\varepsilon(t,\tau)||[\mathscr{N}_{xx}(\cdot, t-\tau) * (u_\varepsilon^{\mathrm{ODE}} - u_\varepsilon^{\mathrm{base}})]||_\infty \mathrm{d}\tau \\
&\quad \leq C_1 \int_0^t \frac{E_\varepsilon(t,\tau)}{(1+(t-\tau))}||u_\varepsilon^{\mathrm{ODE}} - u_\varepsilon^{\mathrm{base}}||_\infty \mathrm{d}\tau \\
&\quad \leq C_1 \int_0^t \frac{E_\varepsilon(t,\tau)}{(1+(t-\tau))^p}||u_\varepsilon^{\mathrm{ODE}} - u_\varepsilon^{\mathrm{base}}||_\infty \mathrm{d}\tau.
\end{aligned}$$

We invoke the first condition of Theorem 3.4.6 and its second conclusion (since we have verified both), which yields

$$\begin{aligned}
\int_0^t E_\varepsilon(t,\tau)||[\mathscr{N}(\cdot, t-\tau) * (u_\varepsilon^{\mathrm{ODE}} - u_\varepsilon^{\mathrm{base}})_{xx}]||_\infty \mathrm{d}\tau &\leq C_1\delta \int_0^t \frac{e^{-r_2\tau}}{(1+(t-\tau))^p}\mathrm{d}\tau \\
&\leq \frac{C_1 C_p \delta}{r_2}(1+t)^{-p}.
\end{aligned}$$

This establishes the second condition of Theorem 3.4.6. Regarding the third condition, we find that

$$\begin{aligned}
\int_0^t \frac{E_\varepsilon(t,\tau)}{(1+\tau)^p}||f'(u_\varepsilon^{\mathrm{ODE}}(\tau)) - f'(u_\varepsilon^{\mathrm{base}}(\tau))||_\infty \mathrm{d}\tau &\leq C_2\delta \int_0^t \frac{e^{-r_1(t-\tau)}}{(1+\tau)^p}\mathrm{d}\tau \\
&= \leq C_2\delta \int_0^t \frac{e^{-r_1\tau}}{(1+(t-\tau))^p}\mathrm{d}\tau \\
&\leq \frac{C_2 C_p \delta}{r_1}(1+t)^{-p}.
\end{aligned}$$

Thus, we have established the third condition. Finally, the fourth condition follows by the smoothness of the function $f(u) = u(u-a)(1-u)$ and the boundedness of $u_\varepsilon^{\mathrm{ODE}}$. We may therefore invoke our bootstrapping theorem, which yields the second conclusion of our decay result.

3.4.7.2 Choosing r_1: a neighborhood of the fold

In the proof of the bootstrapping theorem, the first assumption enforced uniform exponential decay on the function $E_\varepsilon(t,\tau)$. However, in order to meet this condition in our problem, one must choose a relatively small r_1. We recall that the definition of E_ε is

$$E_\varepsilon(t,\tau) := \exp\Big(\int_\tau^t f'(u_\varepsilon^{\text{base}}(s))ds\Big)$$

for a suitable base solution $(u_\varepsilon^{\text{base}}, w_\varepsilon^{\text{base}})$. As $(u_\varepsilon^{\text{base}}, w_\varepsilon^{\text{base}})$ approaches the fold point in Figure 3.1, $f'(u_\varepsilon^{\text{base}})$ tends to zero. One is naturally led to wonder what an appropriate choice of r_1 could be.

A partial answer can be found in the analysis of our kinetic system near the fold point. In order to understand the dynamics of a fast-slow system in this regime, Krupa and Szmolyan (2001) first transform the system to a standard form. The equations take the form

$$\begin{aligned}\frac{da}{dt} &= -b + a^2 + h(a,b,\varepsilon)\\ \frac{db}{dt} &= \varepsilon g(a,b,\varepsilon).\end{aligned} \tag{3.23}$$

In the equations above, we have that $h(a,b,\varepsilon) = \mathcal{O}(\varepsilon, ab, b^2, a^3)$ and $g(a,b,\varepsilon) = -1 + \mathcal{O}(a,b,\varepsilon)$. For a small $\rho > 0$ and an interval J, the authors then define two sections

$$\Delta_{\text{in}} = \{(a,\rho^2), a \in J\}$$

and

$$\Delta_{\text{out}} = \{(\rho,b), b \in \mathbb{R}\}.$$

Since in the form of (3.23) the critical manifold of our system is $b = a^2$, the geomet-

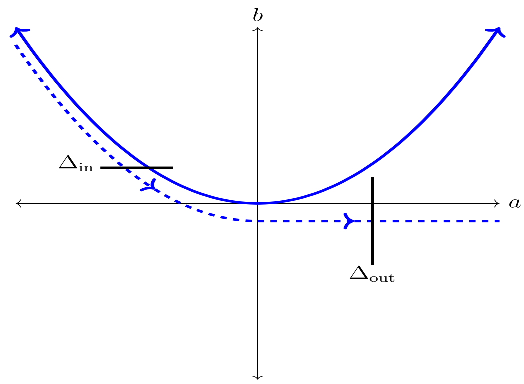

Figure 3.7: The setting for geometric blowup near the fold point in a system of fast-slow ODEs. A smaller ρ indicates a smaller region traversed by the solution to the system as it transitions from a slow drift to a fast jump.

rical setting for our problem is transformed to that of Figure 3.7. We see that one introduces a cutoff at a height of ρ^2 above the origin via the section Δ_{in}. The section meets the critical manifold at (ρ, ρ^2).

In our problem, the transformation to standard form will be shown to be linear. Therefore, introducing a similar cutoff in our problem to define the region around the fold implies that the terminal point of u_ε^{base} is $\mathcal{O}(\rho)$, and $|f'(u_\varepsilon^{base})| = \mathcal{O}(\rho)$ at the boundary of this neighborhood. Ultimately, this implies that we must take $r_1 = \mathcal{O}(\rho)$ to satisfy the conditions of our bootstrapping theorem. In the proof of the bootstrap theorem, we were also required to take γ larger than a constant that was $\mathcal{O}(\frac{1}{r})$. Thus, our proof requires γ to be large relative to its values in standard applications. One can take smaller values of γ if one does not track the kinetic solutions all the way to the transition to the fold.

3.4.7.3 Proof of Theorem 3.4.2

We once again recall our starting assumptions and desired conclusions. In the case of Theorem 3.4.2, these are

1. $f'(u_\varepsilon^{\text{base}}(t)) \leq -r_1 < 0$ uniformly for $t \leq T_{\max} = \frac{\tau_{\max}}{\varepsilon}$.

and

1. $||\bar{u}_\varepsilon||_\infty + ||\bar{w}_\varepsilon||_\infty \leq C\delta$

respectively. As in the previous section, the first condition of our bootstrapping result follows from the only condition of this theorem. Manipulating the first term of (3.20) in an analogous way to the previous section, we find that

$$\begin{aligned}\int_0^t E_\varepsilon(t,\tau)||[\mathscr{N}(\cdot,t-\tau) * (u_\varepsilon^{\text{ODE}} - u_\varepsilon^{\text{base}})_{xx}]||_\infty \mathrm{d}\tau &\leq C_1\delta \int_0^t \frac{e^{-r_1(t-\tau)}}{(1+(t-\tau))^p}\mathrm{d}\tau \\ &\leq C_1\delta \int_0^t e^{-r_1(t-\tau)}\mathrm{d}\tau \\ &\leq \frac{C_1\delta}{r_1},\end{aligned}$$

which is our second condition. Turning to the third condition, we find that

$$\begin{aligned}\int_0^t E_\varepsilon(t,\tau)||f'(u_\varepsilon^{\text{ODE}}(\tau)) - f'(u_\varepsilon^{\text{base}}(\tau))||_\infty \mathrm{d}\tau &\leq C_2\delta \int_0^t e^{-r_1(t-\tau)}\mathrm{d}\tau \\ &\leq \frac{C_2\delta}{r_1}.\end{aligned}$$

In proving both of the estimates above, we have used the fact that $||u_\varepsilon^{\text{ODE}} - u_\varepsilon^{\text{base}}||_\infty$ is non-increasing. This fact follows from the normal stability of the critical manifold. The fourth condition follows in the same manner as the previous section. Applying the bootstrap theorem completes the proof.

3.4.7.4 Proof of Theorem 3.4.3

Finally, we turn to the stability of the origin. We assume that $||u_\varepsilon^0||_\infty + ||w_\varepsilon^0||_\infty < \delta\varepsilon$ for $\delta > 0$ sufficiently small, uniformly in ε. First and foremost, we note that $f'(u^{\text{base}}(t)) = f'(0) = -a$, so we satisfy the first condition of our bootrstapping result with $r = a$ and $\tau_{\max} = \infty$.

In order to verify the next condition, we must establish decay for the solution to our kinetic system. To that end, we consider the linearization of (3.2) about the origin. If we define

$$F(u,w) = \begin{pmatrix} f(u) - w \\ \varepsilon(u - \gamma w) \end{pmatrix}$$

then

$$\begin{aligned} DF_{(u,w)}(0,0) &= \begin{pmatrix} f'(0) & -1 \\ \varepsilon & -\varepsilon\gamma \end{pmatrix} \\ &= \begin{pmatrix} -a & -1 \\ \varepsilon & -\varepsilon\gamma \end{pmatrix}. \end{aligned}$$

The eigenvalues of the linearization therefore solve

$$0 = (\lambda + a)(\lambda + \varepsilon\gamma) + \varepsilon$$

Computing these explicitly, we find that

$$\lambda = (-a - \varepsilon\gamma)\frac{1 \pm \sqrt{1 - \frac{4\varepsilon(1+a\gamma)}{(a+\varepsilon\gamma)^2}}}{2}.$$

Therefore, we see that for small ε, one eigenvalue is approximately equal to a, and the other is a negative number on the order of $\mathcal{O}(\varepsilon)$. We then see that for $\delta > 0$ small enough,

$$||u_\varepsilon^{\mathrm{ODE}}(t) - u_\varepsilon^{\mathrm{base}}(t)||_\infty = ||u_\varepsilon^{\mathrm{ODE}}(t)||_\infty \leq \delta\varepsilon e^{-\tilde{r}_2\varepsilon t}$$

for some $\tilde{r}_2 > 0$ by the stable manifold theorem. With these preliminaries in hand, we find that

$$\begin{aligned}
&\int_0^t E_\varepsilon(t,\tau)||[\mathscr{N}(\cdot, t-\tau) * (u_\varepsilon^{\mathrm{ODE}} - u_\varepsilon^{\mathrm{base}})_{xx}]||_\infty \mathrm{d}\tau \\
&\quad = \int_0^t E_\varepsilon(t,\tau)||[\mathscr{N}_{xx}(\cdot, t-\tau) * u_\varepsilon^{\mathrm{ODE}}]||_\infty \mathrm{d}\tau \\
&\quad \leq C_1 \int_0^t \frac{E_\varepsilon(t,\tau)}{(1+(t-\tau))}||u_\varepsilon^{\mathrm{ODE}}||_\infty \mathrm{d}\tau \\
&\quad \leq C_1 \int_0^t \frac{E_\varepsilon(t,\tau)}{(1+(t-\tau))^p}||u_\varepsilon^{\mathrm{ODE}}||_\infty \mathrm{d}\tau \\
&\quad \leq C_1\delta\varepsilon \int_0^t \frac{e^{-\tilde{r}_2\varepsilon\tau}}{(1+(t-\tau))^p} \mathrm{d}\tau \\
&\quad \leq \frac{C_1 C_p \delta}{\tilde{r_2}}
\end{aligned}$$

where in the final line we have applied Lemma 3.4.5. This establishes the second condition. Turning to the third condition, we find that

$$\begin{aligned}
\int_0^t \frac{E_\varepsilon(t,\tau)}{(1+t)^p}||f'(u_\varepsilon^{\mathrm{ODE}}(\tau)) - f'(u_\varepsilon^{\mathrm{base}}(\tau))||_\infty \mathrm{d}\tau &\leq C_2\delta\varepsilon \int_0^t \frac{e^{-a(t-\tau)}}{(1+\tau)^p} \mathrm{d}\tau \\
&\leq \frac{C_2 C_p \delta\varepsilon}{a}(1+t)^{-p}.
\end{aligned}$$

The fourth condition follows once again from the smoothness of f. This completes the proof.

Remark 8. It is important to note that Theorem 3.4.3 is the only one of our results to require that the initial data for (1.1) lies within $\mathcal{O}(\varepsilon)$ of a given point or fiber. However, it dispenses with any additional assumptions on f'. As we have shown above, this holds because $f'(u_\varepsilon^{\mathrm{base}}(t))$ is uniformly negative, but the decay of our spatially-inhomogeneous solutions to the base solution occurs on the slow timescale, weakening the result.

3.5 Behavior along fast jump

As in the previous section, we suppose that we have nearly spatially-homogeneous initial data $(u^0, w^0)(x)$. In particular, we suppose that there exists a point $(u^{\mathrm{base},0}, w^{\mathrm{base},0})$ such that

$$||u^0 - u^{\mathrm{base},0}||_\infty + ||w^0 - w^{\mathrm{base},0}||_\infty < \delta$$

for some $\delta > 0$ sufficiently small, in a manner to be made more precise later. We also suppose that $(u_\varepsilon^{\mathrm{base}}(t), w_\varepsilon^{\mathrm{base}}(t))$ is the solution of our kinetic equations with initial data $(u^{\mathrm{base},0}, w^{\mathrm{base},0})$ and is undergoing a fast jump.

We now seek to prove that if $(u_\varepsilon, w_\varepsilon)$ solve the Fitzhugh–Nagumo equation with initial data (u^0, w^0), then the offsets $\bar{u}_\varepsilon := u_\varepsilon - u_\varepsilon^{\mathrm{base}}$ and $\bar{w}_\varepsilon := w_\varepsilon - w_\varepsilon^{\mathrm{base}}$ remain bounded uniformly in ε for ε sufficiently small. We recall from the introduction that we do not aim for a result stronger than boundedness since the underlying system of ODEs is unstable when linearized about a fast jump solution.

Remark 9. In this section, we have altered the definition of the offsets from what was given near the slow manifold. We note that the new offsets satisfy

$$u_\varepsilon - u_\varepsilon^{\mathrm{base}} = (u_\varepsilon - u_\varepsilon^{\mathrm{ODE}}) + (u_\varepsilon^{\mathrm{ODE}} - u_\varepsilon^{\mathrm{base}}),$$

so the definitions are equivalent up to the addition of $u_\varepsilon^{\mathrm{ODE}} - u_\varepsilon^{\mathrm{base}}$. Since the behavior of this term is well-understood near the slow manifold, the previous definition allowed us to prove decay results. However, along the fast jump, we have no convenient results controlling its magnitude, so we dispense with the added complication.

Our offsets satisfy the equation

$$\begin{aligned}\frac{\partial \bar{u}_\varepsilon}{\partial t} &= \frac{\partial^2 \bar{u}_\varepsilon}{\partial x^2} + f'(u_\varepsilon^{\text{base}})\bar{u}_\varepsilon - \bar{w}_\varepsilon + N(\bar{u}_\varepsilon, u_\varepsilon^{\text{base}}) \\ \frac{\partial \bar{w}_\varepsilon}{\partial t} &= -\varepsilon\gamma w + \varepsilon u\end{aligned} \tag{3.24}$$

3.5.1 Variation of parameters

In a manner very similar to §3.4.1, we may solve (3.24). The main difference is that (3.24) does not contain any inhomogeneous source terms, at the cost of our offsets having nonzero initial data. The result is that

$$\begin{aligned}\bar{u}_\varepsilon(t) = E_\varepsilon(t,0)\mathscr{N}(\cdot,t) * \bar{u}^0 &- \int_0^t E_\varepsilon(t,\tau)e^{-\varepsilon\gamma\tau}\mathscr{N}(\cdot,t-\tau) * \bar{w}^0 \mathrm{d}\tau \\ &- \varepsilon \int_0^t \int_0^\tau E_\varepsilon(t,\tau)e^{-\varepsilon\gamma(\tau-s)}\big[\mathscr{N}(\cdot,t-\tau) * \bar{u}_\varepsilon(s)\big]\mathrm{d}s\mathrm{d}\tau \\ &+ \int_0^t E_\varepsilon(t,\tau)[\mathscr{N}(\cdot,t-\tau) * N(\bar{u}_\varepsilon, u_\varepsilon^{\text{base}})(\cdot,\tau)]\mathrm{d}\tau \\ \bar{w}_\varepsilon(t) = e^{-\varepsilon\gamma t}\bar{w}^0 + \varepsilon \int_0^t & e^{-\varepsilon\gamma(t-\tau)}\bar{u}_\varepsilon(\tau)\mathrm{d}\tau\end{aligned} \tag{3.25}$$

where $\bar{u}^0 = u^0 - u^{\text{base},0}$ and similarly for $\bar{w}^0$, and $E_\varepsilon(t,\tau)$ is defined as before by (3.19). We shall now compute estimates on this quantity.

3.5.2 Estimates on $E_\varepsilon(t,\tau)$

Near the slow manifold, we made the very simple estimate that $E_\varepsilon(t,\tau) \le e^{-r(t-\tau)}$ for some $r > 0$. Since we can no longer assume such exponential decay, we must find an alternative strategy to control this factor. The answer to this quandary comes from the fact that along a fast jump, the variable w is constant to lowest order in ε. This behavior is intuitively clear from taking the limit as $\varepsilon \to 0^+$ in (1.2).

Recalling the discussion in §1.2.3, we have that $w_\varepsilon^{\text{base}}(t) = w^{\text{base},0} + \varepsilon \hat{w}_\varepsilon^{\text{base}}(t)$ for $t \in [0, \bar{T}]$, where $\bar{T} = \mathcal{O}(1)$ with respect to ε. We then have that

$$\begin{aligned}
\int_\tau^t f'(u_\varepsilon^{\text{base}}(s))\mathrm{d}s &= \int_\tau^t \frac{f'(u_\varepsilon^{\text{base}}(s))}{\dot{u}_\varepsilon^{\text{base}}} \dot{u}_\varepsilon^{\text{base}} \mathrm{d}s \\
&= \int_\tau^t \frac{f'(u_\varepsilon^{\text{base}}(s))}{f(u_\varepsilon^{\text{base}}(s)) - w_\varepsilon^{\text{base}}(s)} \dot{u}_\varepsilon^{\text{base}} \mathrm{d}s \\
&= \int_{f(u_\varepsilon^{\text{base}}(\tau))}^{f(u_\varepsilon^{\text{base}}(t))} \frac{\mathrm{d}x}{x - w^{\text{base},0} - \varepsilon \hat{w}_\varepsilon^{\text{base}}(s(x))} \\
&= \int_{f(u_\varepsilon^{\text{base}}(\tau))}^{f(u_\varepsilon^{\text{base}}(t))} \frac{\mathrm{d}x}{x - w^{\text{base},0}} \mathrm{d}x \\
&\quad + \int_{f(u_\varepsilon^{\text{base}}(\tau))}^{f(u_\varepsilon^{\text{base}}(t))} \frac{1}{x - w^{\text{base},0} - \varepsilon \hat{w}_\varepsilon^{\text{base}}(s(x))} - \frac{1}{x - w^{\text{base},0}} \mathrm{d}x
\end{aligned}$$

where we have made the change of variables $x = f(u_\varepsilon^{\text{base}}(s))$. Turning to the second term, we have that

$$\begin{aligned}
\Big| \int_{f(u_\varepsilon^{\text{base}}(\tau))}^{f(u_\varepsilon^{\text{base}}(t))} & \frac{1}{x - w^{\text{base},0} - \varepsilon \hat{w}_\varepsilon^{\text{base}}(s(x))} - \frac{1}{x - w^{\text{base},0}} \mathrm{d}x \Big| \\
&\leq \varepsilon \int_{f(u_\varepsilon^{\text{base}}(\tau))}^{f(u_\varepsilon^{\text{base}}(t))} \Big| \frac{\hat{w}_\varepsilon^{\text{base}}(s(x))}{(x - w^{\text{base},0} - w_\varepsilon^*(x))^2} \Big| \mathrm{d}x \\
&= \varepsilon \Big| \frac{\hat{w}_\varepsilon^{\text{base}}(s(\tilde{x}))}{(\tilde{x} - w^{\text{base},0} - w_\varepsilon^*(\tilde{x}))^2} \Big| \big[f(u_\varepsilon^{\text{base}}(t)) - f(u_\varepsilon^{\text{base}}(\tau)) \big]
\end{aligned}$$

where $|w^*(x)| \leq \varepsilon \hat{w}_\varepsilon^{\text{base}}$ comes from applying the mean-value theorem to the integrand, and $\tilde{x} \in [f(u_\varepsilon^{\text{base}}(\tau)), f(u_\varepsilon^{\text{base}}(t))]$ comes from applying the mean-value theorem for integrals. Therefore, for $t, \tau \in [0, \bar{T}]$ we find that

$$\Big| \int_{f(u_\varepsilon^{\text{base}}(\tau))}^{f(u_\varepsilon^{\text{base}}(t))} \frac{1}{x - w^{\text{base},0} - \varepsilon \hat{w}_\varepsilon^{\text{base}}(s(x))} - \frac{1}{x - w^{\text{base},0}} \mathrm{d}x \Big| \leq C_{\text{jump}} \varepsilon$$

for some constant $C_{\text{jump}} > 0$. Returning to the first term, we can explicitly compute that

$$\begin{aligned}\int_{f(u_\varepsilon^{\text{base}}(\tau))}^{f(u_\varepsilon^{\text{base}}(t))} \frac{\mathrm{d}x}{x - w^{\text{base},0}} &= \ln|x - w^{\text{base},0}|\Big|_{f(u_\varepsilon^{\text{base}}(\tau))}^{f(u_\varepsilon^{\text{base}}(t))} \\ &= \ln \frac{|f(u_\varepsilon^{\text{base}}(t)) - w^{\text{base},0}|}{|f(u_\varepsilon^{\text{base}}(\tau)) - w^{\text{base},0}|}.\end{aligned}$$

We summarize these results in the following lemma.

Lemma 3.5.1. *If there exists a $\bar{T} > 0$ such that $w_\varepsilon^{\text{base}}(t) = w^{\text{base},0} + \varepsilon \hat{w}_\varepsilon^{\text{base}}(t)$ for $t \in [0, \bar{T}]$, then there exists a constant C_{jump} such that for all $\varepsilon > 0$ sufficiently small*

$$E_\varepsilon(t, \tau) \leq \frac{w^{\text{base},0} - f(u_\varepsilon^{\text{base}}(t))}{w^{\text{base},0} - f(u_\varepsilon^{\text{base}}(\tau))} e^{C_{\text{jump}}\varepsilon}$$

for all t, τ in $[0, \bar{T}]$.

We note that the quantity $w^{\text{base},0} - f(u_\varepsilon^{\text{base}}(t))$ that appears in this bound represents the distance that $w^{\text{base},0}$ lies above the projection of the fast jump onto the critical manifold. Per the discussion in §3.4.7.2, this quantity is strictly positive uniformly in ε after exiting the region near the fold. Therefore, we may extend this bound as follows.

Lemma 3.5.2. *If there exists a $\bar{T} > 0$ such that $w_\varepsilon^{\text{base}}(t) = w^{\text{base},0} + \varepsilon \hat{w}_\varepsilon^{\text{base}}(t)$ for $t \in [0, \bar{T}]$, then there exists a constant $\bar{E}$ such that for all $\varepsilon > 0$ sufficiently small*

$$E_\varepsilon(t, \tau) \leq \bar{E}$$

for all t, τ in $[0, \bar{T}]$.

3.5.3 Boundedness of offsets

Now that we have computed a variation-of-parameters solution to (3.24) and obtained a bound on $E_\varepsilon(t,\tau)$, we can prove that our offsets remain bounded as $\varepsilon \to 0^+$. The result is as follows.

Theorem 3.5.3. *There exists a $\gamma_0 > 0$, $C > 0$, $C_{\text{quad}} > 0$ $\bar{T} > 0$, and $\delta > 0$ such that for all $\gamma > \gamma_0$ the following is true for all $\varepsilon > 0$ sufficiently small. Select a basepoint $(u_\varepsilon^{\text{base},0}, u_\varepsilon^{\text{base},0})$. Furthermore, suppose $u_\varepsilon^0(x) \in C_b^2(\mathbb{R}) \cap \left(u_\varepsilon^{\text{base},0} + L^1(\mathbb{R})\right)$ and $w_\varepsilon^0(x) \in C_b^2(\mathbb{R}) \cap \left(w_\varepsilon^{\text{base},0} + L^1(\mathbb{R})\right)$, and that $||u_\varepsilon^0 - u^{\text{base},0}||_\infty + ||w_\varepsilon^0 - w^{\text{base},0}||_\infty < \delta$ for $\delta > 0$ sufficiently small, uniformly in ε. Let $(u_\varepsilon^{\text{base}}, w_\varepsilon^{\text{base}})$ and $(\bar{u}_\varepsilon, \bar{w}_\varepsilon)$ be defined as in the derivation of (3.25). If the following condition holds:*

1. *For all $t \in [0, \bar{T}]$, $(u_\varepsilon^{\text{base}}, w_\varepsilon^{\text{base}})$ is a fast jump solution: $w_\varepsilon^{\text{base}}(t) = w^{\text{base},0}(t) + \varepsilon \hat{w}_\varepsilon^{\text{base}}(t)$*

2. *$||N(u, u_\varepsilon^{\text{base}})||_\infty \leq C_{\text{quad}} ||u||_\infty^2$*

then for all $t \leq \bar{T}$

1. *$||\bar{u}_\varepsilon||_\infty + ||\bar{w}_\varepsilon||_\infty \leq C\delta$*

Proof. Taking the L^∞ norm of both sides of (3.25), we find that

$$
\begin{aligned}
||\bar{u}_\varepsilon(t)||_\infty \leq E_\varepsilon(t,0)||\bar{u}^0||_\infty + ||\bar{w}^0||_\infty \int_0^t E_\varepsilon(t,\tau) e^{-\varepsilon\gamma\tau} \mathrm{d}\tau \\
+ \varepsilon \int_0^t \int_0^\tau E_\varepsilon(t,\tau) e^{-\varepsilon\gamma(\tau - s)} ||\bar{u}_\varepsilon(s)||_\infty \mathrm{d}s\mathrm{d}\tau \\
+ \int_0^t E_\varepsilon(t,\tau) ||N(\bar{u}_\varepsilon, u_\varepsilon^{\text{base}})(\cdot,\tau)||_\infty \mathrm{d}\tau \\
\bar{w}_\varepsilon(t) = ||\bar{w}^0||_\infty + \varepsilon \int_0^t e^{-\varepsilon\gamma(t-\tau)} ||\bar{u}_\varepsilon(\tau)|_\infty \mathrm{d}\tau.
\end{aligned}
$$

For some $T \leq \bar{T}$, let us define the norm $|||u|||_T = \sup_{t \leq T} ||u(t)||_\infty$. Focusing on the first inequality, we apply this definition, Lemma 3.5.2, and our assumptions on the magnitude of our initial data to conclude that

$$||\bar{u}_\varepsilon(t)||_\infty \leq \bar{E}\delta + \bar{E}\bar{T}\delta + \frac{\varepsilon \bar{E}\bar{T}^2}{2}|||\bar{u}_\varepsilon|||_T + C_{\text{quad}}\bar{E}\bar{T}|||\bar{u}_\varepsilon|||_T^2.$$

We choose the maximal $T > 0$ such that $|||\bar{u}_\varepsilon|||_T \leq \frac{1}{4C_{\text{quad}}\bar{E}\bar{T}}$ and require that $\varepsilon \leq \frac{1}{2\bar{E}\bar{T}^2}$. After taking the supremum over $t \leq T$ and rearranging, we obtain

$$|||\bar{u}_\varepsilon(t)|||_T \leq 2\bar{E}\delta(1 + \bar{T}).$$

For $\delta \leq \frac{1}{8C_{\text{quad}}\bar{E}^2\bar{T}(1+\bar{T})}$, $|||\bar{u}_\varepsilon|||_T \leq \frac{1}{4C_{\text{quad}}\bar{E}\bar{T}}$ uniformly in T. Therefore, we conclude that $T = \bar{T}$.

In order to control $\bar{w}_\varepsilon$, we need only observe that

$$\begin{aligned} ||\bar{w}_\varepsilon||_\infty &\leq ||\bar{w}^0||_\infty + \varepsilon|||u|||_{\bar{T}} \int_0^t e^{-\varepsilon\gamma(t-\tau)} \mathrm{d}\tau \\ &\leq \delta + \frac{2\bar{E}\delta(1+\bar{T})}{\gamma} \end{aligned}$$

$\square$

Remark 10. We note that in this proof, we did not make use of any properties of the fundamental solution besides the fact that its L^1-norm is 1. This corresponds to the fact that the L^∞-norm of the heat semigroup is bounded, but not exponentially decaying. Therefore, this proof could be carried out purely in the language of semigroups. We have written it in this manner to emphasize the connection with previous work.

3.6 Behavior near the fold

By now, we have proved that when solutions to (1.1) begin on a stable fiber of the underlying kinetic system (3.2), the difference in magnitude between those solutions and the spatial ansatz defined by evolving the initial data according to the kinetic system decays algebraically on the fast timescale.

We have also shown that if we remove the restriction of starting on a fiber, our solutions remain within a neighborhood of the slow manifold. They likewise remain within a neighborhood of a fast jump solution to (3.2). However, we have not yet addressed the behavior of solutions to (1.1) with nearly spatially-homogeneous initial data when the associated spatially-homogeneous solution passes within a neighborhood of the fold.

As alluded to in §3.4.7.2, the analysis of solutions in this regime is complicated by the fact that the system neither exhibits uniform exponential decay along fibers, as in §3.4.7.1, nor spends only a short amount of time in this region as in §3.5.3. We will therefore require finer control of key quantities such as $E_\varepsilon(t,\tau)$.

In this section, we shall make use of the coordinates found in Krupa and Szmolyan (2001) to prove estimates on these quantities, while discussing why they are ultimately not sufficient to establish boundedness using the methodology found in §3.5.3.

3.6.1 A standard form for Fitzhugh–Nagumo

As discussed in §3.4.7.2, Krupa and Szmolyan (2001) transformed systems with a fold point into the standard form

$$\begin{aligned}\frac{da}{dt} &= -b + a^2 + h(a,b,\varepsilon)\\ \frac{db}{dt} &= \varepsilon g(a,b,\varepsilon).\end{aligned}$$

with $h(a,b,\varepsilon) = \mathcal{O}(\varepsilon, ab, b^2, a^3)$ and $g(a,b,\varepsilon) = -1 + \mathcal{O}(a,b,\varepsilon)$. We shall begin by putting our kinetic system into a similar form. We reproduce the system below for convenience.

$$\begin{aligned}\frac{du}{dt} &= f(u) - w\\ \frac{dw}{dt} &= \varepsilon(u - \gamma w)\end{aligned}$$

We recall that the location of our fold point (u_*, w_*) is given by $f'(u_*) = 0$ and $w_* = f(u_*)$. We also note that the function $f(u)$ is a third-order polynomial. Therefore, we may substitute the Taylor series expansion of $f(u)$ to obtain

$$\begin{aligned}\frac{d(u-u_*)}{dt} &= f(u_*) - w_* + f'(u_*)(u-u_*) + \frac{f''(u_*)}{2}(u-u_*)^2 + \frac{f'''(u_*)}{6}(u-u_*)^3 - (w-w_*)\\ \frac{d(w-w_*)}{dt} &= \varepsilon(u_* - \gamma w_*) + \varepsilon\big[(u-u_*) - \gamma(w-w_*)\big].\end{aligned} \tag{3.26}$$

By the defining conditions of our fold point, the first two terms in the first equation of (3.26) vanish. Furthermore, multiplying out $f(u) = u(u-a)(1-u)$ demonstrates that $f'''(u) = -6$ for all $u \in \mathbb{R}$. We now define $\tilde{u} = \frac{|f''(u_*)|}{2}(u-u_*)$ and $\tilde{w} = \frac{|f''(u_*)|}{2}(w-w_*)$.

Multiplying both sides of both equations by $\frac{|f''(u_*)|}{2}$, we find that

$$\begin{aligned}\frac{d\tilde{u}}{dt} &= -\tilde{u}^2 - \tilde{w} - \frac{4}{|f''(u_*)|^2}\tilde{u}^3\\ \frac{d\tilde{w}}{dt} &= \frac{\varepsilon|f''(u_*)|}{2}(u_* - \gamma w_*) + \varepsilon\big[\tilde{u} - \gamma\tilde{w}\big].\end{aligned}$$

Finally, if we define $\tilde{\varepsilon} := \frac{\varepsilon|f''(u_*)|}{2}(u_* - \gamma w_*)$, then we obtain

$$\begin{aligned}\frac{d\tilde{u}}{dt} &= -\tilde{u}^2 - \tilde{w} - \frac{4}{|f''(u_*)|^2}\tilde{u}^3\\ \frac{d\tilde{w}}{dt} &= \tilde{\varepsilon}\Big(1 + \frac{2}{|f''(u_*)|(u_* - \gamma w_*)}\big[\tilde{u} - \gamma\tilde{w}\big]\Big).\end{aligned} \tag{3.27}$$

We have therefore transformed our kinetic system to match the standard form, with the only difference being sign changes that reflect the orientation of the critical manifold. We may also apply the same change of variables to the full Fitzhugh–Nagumo model, which yields

$$\begin{aligned}\frac{\partial\tilde{u}}{\partial t} &= \frac{\partial^2\tilde{u}}{\partial x^2} - \tilde{u}^2 - \tilde{w} - \frac{4}{|f''(u_*)|^2}\tilde{u}^3\\ \frac{\partial\tilde{w}}{\partial t} &= \tilde{\varepsilon}\Big(1 + \frac{2}{|f''(u_*)|(u_* - \gamma w_*)}\big[\tilde{u} - \gamma\tilde{w}\big]\Big).\end{aligned} \tag{3.28}$$

Remark 11. In previous sections, we have enforced lower bounds on γ to prove estimates. However, γ is also part of our coordinate transformations, and as such one would need to be very careful not to make a circular assumption when attempting to prove similar results near the fold. We shall not make any such assumptions on the magnitude of γ in this section.

3.6.2 Offset definition and variation of parameters

In order to understand the relevance of the estimates to follow, let us suppose that we were attempting to prove that solutions to the transformed Fitzhugh–Nagumo model remain within a neighborhood of solutions to the kinetic system in standard form. Following the methodology of §3.5, we first define the offsets $\bar{u}_{\tilde{\varepsilon}} := \tilde{u}_{\tilde{\varepsilon}} - \tilde{u}_{\tilde{\varepsilon}}^{\mathrm{base}}$, where $\tilde{u}_{\tilde{\varepsilon}}$ solves (3.28) and $\tilde{u}_{\tilde{\varepsilon}}^{\mathrm{base}}$ solves (3.27). Defining $\bar{w}_{\varepsilon}$ similarly, it follows that

$$\begin{aligned}\frac{\partial \bar{u}_{\tilde{\varepsilon}}}{\partial t} &= \frac{\partial^2 \bar{u}_{\tilde{\varepsilon}}}{\partial x^2} - 2\tilde{u}_{\tilde{\varepsilon}}^{\mathrm{base}}\bar{u}_{\tilde{\varepsilon}} - \bar{w}_{\tilde{\varepsilon}} + N(\bar{u}_{\tilde{\varepsilon}}, \tilde{u}_{\tilde{\varepsilon}}^{\mathrm{base}}) \\ \frac{\partial \bar{w}_{\varepsilon}}{\partial t} &= \varepsilon(\bar{u}_{\tilde{\varepsilon}} - \gamma \bar{w}_{\tilde{\varepsilon}}).\end{aligned} \tag{3.29}$$

We note that the second equation only depends explicitly on ε, and not $\tilde{\varepsilon}$. The form of this equation is nearly an exact match for (3.24), and we may similarly solve it using variation of parameters to obtain

$$\begin{aligned}\bar{u}_{\tilde{\varepsilon}}(t) &= E_{\tilde{\varepsilon}}(t,0)\mathscr{N}(\cdot,t) * \bar{u}^0 - \int_0^t E_{\tilde{\varepsilon}}(t,\tau)e^{-\varepsilon\gamma\tau}\mathscr{N}(\cdot,t-\tau) * \bar{w}^0 \mathrm{d}\tau \\ &\quad - \varepsilon \int_0^t \int_0^\tau E_{\tilde{\varepsilon}}(t,\tau)e^{-\varepsilon\gamma(\tau-s)}\big[\mathscr{N}(\cdot,t-\tau) * \bar{u}_{\tilde{\varepsilon}}(s)\big]\mathrm{d}s\mathrm{d}\tau \\ &\quad + \int_0^t E_{\tilde{\varepsilon}}(t,\tau)[\mathscr{N}(\cdot,t-\tau) * N(\bar{u}_{\varepsilon}, u_{\varepsilon}^{\mathrm{base}})(\cdot,\tau)]\mathrm{d}\tau \\ \bar{w}_{\tilde{\varepsilon}}(t) &= e^{-\varepsilon\gamma t}\bar{w}^0 + \varepsilon\int_0^t e^{-\varepsilon\gamma(t-\tau)}\bar{u}_{\tilde{\varepsilon}}(\tau)\mathrm{d}\tau,\end{aligned} \tag{3.30}$$

where

$$E_{\tilde{\varepsilon}}(t,\tau) := \exp\Big(-2\int_\tau^t u_{\tilde{\varepsilon}}^{\mathrm{base}}(s)\mathrm{d}s\Big).$$

3.6.3 Identifying relevant quantities to estimate

We now suppose that we are in the midst of a proof of boundedness for solutions to (3.30). Proceeding by analogy with the proof for fast jumps, we define a norm of the form

$$|||u|||_T = \sup_{t \leq T} ||u(t)||_\infty$$

for some suitable $T > 0$. Taking the L^∞-norm on both sides of (3.30), we find that

$$\begin{aligned}
||\bar{u}_{\tilde{\varepsilon}}(t)||_\infty \leq{}& E_{\tilde{\varepsilon}(t,0)}||\bar{u}^0||_\infty + ||\bar{w}^0||_\infty \int_0^t E_{\tilde{\varepsilon}}(t,\tau)e^{-\varepsilon\gamma\tau}\mathrm{d}\tau \\
&+ \varepsilon|||\bar{u}_{\tilde{\varepsilon}}|||_T \int_0^t \int_0^\tau E_{\tilde{\varepsilon}}(t,\tau)e^{-\varepsilon\gamma(\tau-s)}\mathrm{d}s\mathrm{d}\tau \\
&+ C_{\text{quad}}|||\bar{u}_{\tilde{\varepsilon}}|||_T^2 \int_0^t E_{\tilde{\varepsilon}}(t,\tau)\mathrm{d}\tau \\
||\bar{w}_{\tilde{\varepsilon}}(t)||_\infty \leq{}& ||\bar{w}^0||_\infty + \varepsilon|||\bar{u}_{\tilde{\varepsilon}}|||_T \int_0^t e^{-\varepsilon\gamma(t-\tau)}\mathrm{d}\tau,
\end{aligned}$$

which can be simplified to

$$\begin{aligned}
||\bar{u}_{\tilde{\varepsilon}}(t)||_\infty \leq{}& E_{\tilde{\varepsilon}}(t,0)||\bar{u}^0||_\infty + ||\bar{w}^0||_\infty \int_0^t E_{\tilde{\varepsilon}}(t,\tau)e^{-\varepsilon\gamma\tau}\mathrm{d}\tau \\
&+ \frac{|||\bar{u}_{\tilde{\varepsilon}}|||_T}{\gamma} \int_0^t E_{\tilde{\varepsilon}}(t,\tau)\mathrm{d}\tau \\
&+ C_{\text{quad}}|||\bar{u}_{\tilde{\varepsilon}}|||_T^2 \int_0^t E_{\tilde{\varepsilon}}(t,\tau)\mathrm{d}\tau \\
||\bar{w}_{\tilde{\varepsilon}}(t)||_\infty \leq{}& ||\bar{w}^0||_\infty + \frac{|||\bar{u}_{\tilde{\varepsilon}}|||_T}{\gamma}.
\end{aligned}$$

In the section on fast jumps, we controlled each of the terms in blue by observing that both the integrands and the bounds of integration were uniformly bounded in ε. This strategy will no longer suffice, since neither supposition holds true near the fold. We shall present computations to estimate all of the highlighted quantities in the next section.

3.6.4 Computing $E_{\tilde{\varepsilon}}(t,\tau)$

We recall that

$$E_{\tilde{\varepsilon}}(t,\tau) := \exp\Big(-2\int_\tau^t u_{\tilde{\varepsilon}}^{\text{base}}(s)\mathrm{d}s\Big).$$

As discussed in §1.2.2, the authors of Krupa and Szmolyan (2001) separated the neighborhood around the fold point into three regions D_1, D_2, and D_3 parametrized by the coordinate charts K_1, K_2, and K_3. The situation is depicted in Figure 3.8. Let us define T_i to be the time when $u_{\tilde{\varepsilon}}^{\text{base}}(t)$ exits the region defined by the coordinate chart K_i. Turning our attention to the integral in the definition of $E_{\tilde{\varepsilon}}(t,\tau)$, we see that

$$\int_\tau^t u_{\tilde{\varepsilon}}^{\text{base}}(s)\mathrm{d}s = \int_\tau^{T_1} u_{\tilde{\varepsilon}}^{\text{base}}(s)\mathrm{d}s + \int_{T_1}^{T_2} u_{\tilde{\varepsilon}}^{\text{base}}(s)\mathrm{d}s + \int_{T_2}^{t} u_{\tilde{\varepsilon}}^{\text{base}}(s)\mathrm{d}s.$$

This implies that

$$E_{\tilde{\varepsilon}}(t,\tau) = E_{\tilde{\varepsilon}}(T_1,\tau)E_{\tilde{\varepsilon}}(T_2,T_1)E_{\tilde{\varepsilon}}(t,T_2) \tag{3.31}$$

Therefore, it is possible to compute $E_{\tilde{\varepsilon}}(t,\tau)$ by assuming that our base solution lies entirely in a region covered by one of the coordinate charts K_i and computing each of these results separately. We turn to this task in the subsections to follow. For convenience and readability, we drop the superscript base and the subscript $\tilde{\varepsilon}$ from $u_{\tilde{\varepsilon}}^{\text{base}}$ when carrying out these computations. We also assume without loss that $t \geq T_2$, since one can simply drop terms from (3.31) if this is not the case.

3.6.4.1 $E_{\tilde{\varepsilon}}(t,\tau)$ in the K_1 chart

The region D_1 allows us to match solutions coming from the vicinity of the slow manifold into a neighborhood of the fold. Therefore, we expect that our exponential should be decaying in time, since the solutions are still near the normally attracting

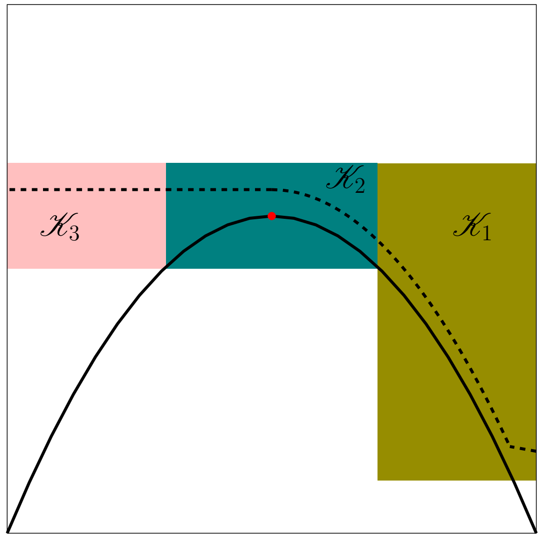

Figure 3.8: In the region D_1, to the right in green, the solution lies near the slow manifold. In the D_2 region, teal in the middle, the solution spends $\mathcal{O}(\tilde{\varepsilon}^{-\frac{1}{3}})$-time within a neighborhood of size $\mathcal{O}(\tilde{\varepsilon}^{\frac{1}{3}})$ of the fold point, shown in red. Finally, the solution makes a fast jump in D_3, pink on the left. Each region is labeled by the name of its coordinate chart.

slow manifold. We make the change of variables

$$\tilde{u} = -r_1 u_1, \quad \tilde{w} = -r_1^2, \quad \tilde{\varepsilon} = r_1^3 \varepsilon_1$$

System (3.27) then becomes

$$\begin{aligned} \frac{du_1}{dt_1} &= -1 + u_1^2 + \varepsilon_1 u_1 + \mathcal{O}(r_1) \\ \frac{dr_1}{dt_1} &= \frac{1}{2} r_1 \varepsilon_1 (-1 + \mathcal{O}(r_1)) \\ \frac{d\varepsilon_1}{dt_1} &= \frac{3}{2} \varepsilon_1^2 (1 + \mathcal{O}(r_1)) \end{aligned} \tag{3.32}$$

where $\frac{d}{dt_1} = \frac{1}{r_1}\frac{d}{dt}$ is the desingularized time coordinate in the K_1 chart. Following the authors of Krupa and Szmolyan (2001), we are interested in analyzing solutions to these equations in the region

$$D_1 := \{(u_1, r_1, \varepsilon_1) : u_1 \in \mathbb{R}, 0 \leq r_1 \leq \rho, 0 \leq \varepsilon_1 \leq \delta\}$$

where $\rho, \delta > 0$ are small constants. We suppose that our base solution enters this region through the section

$$\Sigma_1^{\text{in}} = \{(u_1, r_1, \varepsilon_1) \in D_1 : r_1 = \rho\}$$

and exits via

$$\Sigma_1^{\text{out}} = \{(u_1, r_1, \varepsilon_1) \in D_1 : \varepsilon_1 = \delta\}.$$

With these preliminaries in hand, we attempt to rewrite $\int_\tau^t u_{\tilde{\varepsilon}}^{\text{base}}(s)\mathrm{d}s$ in terms of the quantities defined in this new coordinate chart. We find that

$$-2\int_\tau^t u_{\tilde{\varepsilon}}^{\text{base}}(s)\mathrm{d}s = 2\int_\tau^t r_1(s)u_1(s)\mathrm{d}s$$

Per Proposition 2.6 of Krupa and Szmolyan's work, we have that there exists an attracting center manifold of (3.32) given by the graph $u_1 = h_1(r_1, \varepsilon_1)$, where

$$-\frac{3}{2} < h_1(r_1, \varepsilon_1) < -\frac{1}{2}$$

As in Carter and Sandstede (2015), if we make the change of variables $v_1 = u_1 - h_1(r_1, \varepsilon_1)$, our system of equations becomes

$$\begin{aligned}
\frac{dv_1}{dt_1} &= v_1(-2 + v_1 + \mathcal{O}(r_1, \varepsilon_1)) \\
\frac{dr_1}{dt_1} &= \frac{1}{2}r_1\varepsilon_1(-1 + \mathcal{O}(r_1)) \\
\frac{d\varepsilon_1}{dt_1} &= \frac{3}{2}\varepsilon_1^2(1 + \mathcal{O}(r_1))
\end{aligned} \tag{3.33}$$

Rewriting our integral in terms of these new variables, we find that

$$\begin{aligned}
-2\int_\tau^t u_{\tilde{\varepsilon}}^{\mathrm{base}}(s)\mathrm{d}s &= 2\int_\tau^t r_1(s)v_1(s)\mathrm{d}s + 2\int_\tau^t r_1(s)h_1(r_1(s),\varepsilon_1(s))\mathrm{d}s \\
&\leq 2\int_\tau^t r_1(s)v_1(s)\mathrm{d}s - \int_\tau^t r_1(s)\mathrm{d}s \\
&= 2\int_\tau^t \frac{1}{-2+v_1(s)+\mathcal{O}(r_1,\varepsilon_1)}\frac{dv_1}{ds}\mathrm{d}s - \int_\tau^t r_1(s)\mathrm{d}s \\
&= 2\int_{v_1(\tau)}^{v_1(t)} \frac{\mathrm{d}v}{-2+v+\mathcal{O}(r_1,\varepsilon_1)}\mathrm{d}v - \int_\tau^t r_1(s)\mathrm{d}s
\end{aligned}$$

where we have used the first equation in (3.33) in the third line. Since we know that $r_1 \leq \rho$ and $\varepsilon_1 \leq \delta$ in D_1, we may apply similar mean-value theorem arguments as we did when bounding integrals in §3.5.2 to conclude that

$$\begin{aligned}
2\int_{v_1(\tau)}^{v_1(t)} \frac{\mathrm{d}v}{-2+v+\mathcal{O}(r_1,\varepsilon_1)}\mathrm{d}v &= 2\int_{v_1(\tau)}^{v_1(t)} \frac{\mathrm{d}v}{-2+v}\mathrm{d}v + \mathcal{O}(\rho,\delta) \\
&= 2\ln\Big(\frac{2-v_1(t)}{2-v_1(\tau)}\Big) + \mathcal{O}(\rho,\delta).
\end{aligned}$$

Turning to our final term, we see that for $\rho > 0$ small enough,

$$\begin{aligned}
\int_\tau^t r_1(s)\mathrm{d}s &= \int_\tau^t \frac{2}{3\varepsilon_1^2(1+\mathcal{O}(r_1))}\frac{d\varepsilon_1}{ds}\mathrm{d}s \\
&\geq \frac{4}{3}\int_\tau^t \frac{1}{\varepsilon_1^2}\frac{d\varepsilon_1}{ds}\mathrm{d}s \\
&= \frac{4}{3}\int_{\varepsilon_1(\tau)}^{\varepsilon_1(t)} \frac{\mathrm{d}v}{v^2} \\
&= \frac{4}{3}\Big(\frac{1}{\varepsilon_1(\tau)} - \frac{1}{\varepsilon_1(t)}\Big).
\end{aligned}$$

We summarize these results in the following lemma.

Lemma 3.6.1. *For $\rho > 0$ and $\delta > 0$ sufficiently small, the following is true for all $\tilde{\varepsilon} > 0$ and t, τ such that $u_{\tilde{\varepsilon}}^{\mathrm{base}}$ is in D_1.*

$$-2\int_\tau^t u_{\tilde{\varepsilon}}^{\mathrm{base}}(s)\mathrm{d}s \leq -\frac{4}{3}\Big(\frac{1}{\varepsilon_1(\tau)} - \frac{1}{\varepsilon_1(t)}\Big) + 2\ln\Big(\frac{2-v_1(t)}{2-v_1(\tau)}\Big) + \mathcal{O}(\rho,\delta)$$

which implies that

$$E_{\tilde{\varepsilon}}(t,\tau) \le (1+\mathcal{O}(\rho,\delta))\Big(\frac{2-v_1(t)}{2-v_1(\tau)}\Big)^2 \exp\Big(\frac{4}{3\varepsilon_1(t)} - \frac{4}{3\varepsilon_1(\tau)}\Big)$$

The dominant term in this bound is the exponential, since in D_1 we have that $|v_1| = \mathcal{O}(\rho^3\delta)$. If we take $t = T_1$ and $\tau = 0$, we note that from the definition of Δ_1^{in} and Δ_1^{out} that $\varepsilon_1(T_1) = \delta$ and $r_1(0) = \rho$. Since $\varepsilon_1(0)r_1^3(0) = \tilde{\varepsilon}$, we find that

$$E_{\tilde{\varepsilon}}(T_1,0) \le (1+\mathcal{O}(\rho,\delta)) \exp\Big(\frac{4}{3\delta} - \frac{4\rho^3}{3\tilde{\varepsilon}}\Big)$$

Therefore, $E_{\tilde{\varepsilon}}(T_1,0)$ is exponentially small in $\tilde{\varepsilon}$.

3.6.4.2 $E_{\tilde{\varepsilon}}(t,\tau)$ in the K_2 chart

Relative to the computation in the K_1 chart, our bound in the K_2 chart is extremely simple. We recall from §1.2.2 that in this chart we make the change of variables

$$\tilde{u} = -r_2 u_2, \quad \tilde{w} = -r_2^2 w_2, \quad \varepsilon = r_2^3.$$

Our system becomes

$$\begin{aligned} \frac{du_2}{dt_2} &= -w_2 + u_2^2 + \mathcal{O}(r_2) \\ \frac{dw_2}{dt_2} &= -1 + \mathcal{O}(r_2) \\ \frac{dr_2}{dt_2} &= 0 \end{aligned} \tag{3.34}$$

where $t_2 = r_2 t$. The integral we must bound is

$$-2\int_{\tau}^{t} u_{\tilde{\varepsilon}}^{\text{base}}(s)\mathrm{d}s = -2\int_{\tau}^{t} r_2 u_2(s)\mathrm{d}s.$$

We now note that in D_2, u_2 is bounded. Therefore, we find that

$$\begin{aligned}\left| -2\int_{\tau}^{t} u_{\tilde{\varepsilon}}^{\text{base}}(s)\mathrm{d}s\right| &\leq 2C_{\rho,\delta} r_2(t-\tau)\\ &\leq \tilde{C}_{\rho,\delta}\end{aligned}$$

since $r_2 t$ and $r_2 \tau$ are the desingularized times in the chart K_2, which are bounded. We summarize this result in the following lemma.

Lemma 3.6.2. *For $\rho > 0$ and $\delta > 0$ sufficiently small, the following is true for all $\tilde{\varepsilon} > 0$ and t, τ such that $u_{\tilde{\varepsilon}}^{\text{base}}$ is in D_2.*

$$-2\int_{\tau}^{t} u_{\tilde{\varepsilon}}^{\text{base}}(s)\mathrm{d}s \leq \tilde{C}_{\rho,\delta}$$

which implies that

$$E_{\tilde{\varepsilon}}(t,\tau) \leq e^{\tilde{C}_{\rho,\delta}}$$

Therefore, we have neither growth nor decay in $\tilde{\varepsilon}$ in this chart.

3.6.4.3 $E_{\tilde{\varepsilon}}(t,\tau)$ in the K_3 chart

Finally, we turn to the chart K_3 in order to match our solutions in K_2 to the outgoing fast jumps. Here, we make the change of variables

$$\tilde{u} = -r_3, \quad \tilde{w} = -r_3^2 w_3, \quad \varepsilon = r_3^3 \varepsilon_3.$$

In this chart, our system of equations becomes

$$\begin{aligned}\frac{dr_3}{dt} &= r_3^2 F_3(r_3, w_3, \varepsilon_3)\\ \frac{dw_3}{dt} &= r_3[(-1+\mathcal{O}(r_3)) - 2w_3 F_3(r_3, w_3, \varepsilon_3)]\\ \frac{d\varepsilon_3}{dt} &= -3r_3\varepsilon_3 F_3(r_3, w_3, \varepsilon_3)\end{aligned} \tag{3.35}$$

where $F_3(r_3, w_3, \varepsilon_3) = 1 - w_3 + \mathcal{O}(r_3)$. In this chart, we consider solutions which enter via the section

$$\Delta_3^{\text{in}} := \{(r_3, w_3, \varepsilon_3) \in D_3 : 0 < r_3 < \rho, \quad w_3 \in [-\beta, \beta], \quad \varepsilon_3 = \delta\}.$$

for some small $\beta > 0$. Solutions exit the region via the section

$$\Delta_3^{\text{out}} := \{(r_3, w_3, \varepsilon_3) \in D_3 : r_3 = \rho, \quad w_3 \in [-\beta, \beta], \quad 0 < \varepsilon_3 < \delta\}.$$

In our region of interest, we will thus consider solutions such that $|w_3| < \beta$, which implies that for small enough β and ρ, $F(r_3, w_3, \varepsilon_3) > \frac{1}{1+\alpha}$ for some $\alpha > 0$. With these preliminaries in hand, we see that

$$\begin{aligned}-2\int_\tau^t u_{\bar{\varepsilon}}^{\text{base}}(s)\mathrm{d}s &= 2\int_\tau^t r_3(s)\mathrm{d}s\\ &= 2\int_\tau^t \frac{1}{r_3(s)F(r_3(s), w_3(s), \varepsilon_3(s))}\frac{dr_3}{ds}\mathrm{d}s\\ &\le 2(1+\alpha)\int_{r_3(\tau)}^{r_3(t)} \frac{\mathrm{d}v}{v}\\ &= 2(1+\alpha)\ln\left(\frac{r_3(t)}{r_3(\tau)}\right).\end{aligned}$$

We summarize this result in the following lemma.

Lemma 3.6.3. *For any $\alpha > 0$, for $\rho > 0$, $\delta > 0$, and β sufficiently small,*

$$-2\int_{\tau}^{t} u_{\tilde{\varepsilon}}^{\text{base}}(s)\mathrm{d}s \leq 2(1+\alpha)\ln\left(\frac{r_3(t)}{r_3(\tau)}\right)$$

for all $\tilde{\varepsilon} > 0$ and t, τ such that $u_{\tilde{\varepsilon}}^{\text{base}}$ is in D_3, which implies that

$$E_{\tilde{\varepsilon}}(t,\tau) \leq \left(\frac{r_3(t)}{r_3(\tau)}\right)^{2(1+\alpha)}$$

3.6.5 Bounding $\int_0^t E_{\tilde{\varepsilon}}(t,\tau)\mathrm{d}\tau$

We wish to bound two more of our highlighted quantities, namely $\int_0^t E_{\tilde{\varepsilon}}(t,\tau)\mathrm{d}\tau$ and $\int_0^t E_{\tilde{\varepsilon}}(t,\tau)e^{-\varepsilon\gamma\tau}\mathrm{d}\tau$. The latter is less than or equal to the former, so we will focus on the first quantity. We note that

$$\begin{aligned}\int_0^t E_{\tilde{\varepsilon}}(t,\tau)\mathrm{d}\tau &= \int_0^{T_1} E_{\tilde{\varepsilon}}(t,\tau)\mathrm{d}\tau + \int_{T_1}^{T_2} E_{\tilde{\varepsilon}}(t,\tau)\mathrm{d}\tau + \int_{T_2}^{t} E_{\tilde{\varepsilon}}(t,\tau)\mathrm{d}\tau \\ &= E_{\tilde{\varepsilon}}(t,T_2)E_{\tilde{\varepsilon}}(T_2,T_1)\int_0^{T_1} E_{\tilde{\varepsilon}}(T_1,\tau)\mathrm{d}\tau + E_{\tilde{\varepsilon}}(t,T_2)\int_{T_1}^{T_2} E_{\tilde{\varepsilon}}(T_2,\tau)\mathrm{d}\tau + \int_{T_2}^{t} E_{\tilde{\varepsilon}}(t,\tau)\mathrm{d}\tau.\end{aligned} \tag{3.36}$$

Therefore, we once again need only focus on computing our quantity of interest within a single region D_i, as the results can be computed separately and combined together. Ultimately, we will prove the following.

Lemma 3.6.4. *For any $\alpha > 0$, if $\rho > 0$, $\delta > 0$, and $\beta > 0$ are sufficiently small, then*

$$\int_0^t E_{\tilde{\varepsilon}}(t,\tau)\mathrm{d}\tau \leq \frac{\kappa}{\tilde{\varepsilon}^{1+\alpha}}$$

for all $\tilde{\varepsilon} > 0$ and a $\kappa > 0$.

3.6.5.1 Bounding $\int_0^{T_1} E_{\tilde{\varepsilon}}(T_1,\tau)\mathrm{d}\tau$

Making use of our results from §3.6.4.1, we have that for small enough ρ and δ

$$\int_0^{T_1} E_{\tilde{\varepsilon}}(T_1,\tau)\mathrm{d}\tau \leq 2\int_0^{T_1} \exp\Big(\frac{4}{3\varepsilon_1(T_1)} - \frac{4}{3\varepsilon_1(\tau)}\Big)\mathrm{d}\tau.$$

We recall that $r_1^3\varepsilon_1 = \tilde{\varepsilon}$. Combined with the mean-value theorem, we obtain

$$\begin{aligned}
\frac{4}{3\varepsilon_1(T_1)} - \frac{4}{3\varepsilon_1(\tau)} &= \frac{4r_1^3(T_1)}{3\tilde{\varepsilon}} - \frac{4r_1^3(\tau)}{3\tilde{\varepsilon}} \\
&= \frac{4}{\tilde{\varepsilon}} r_1^2 \frac{dr_1}{dt}\Big|_{t=\tau^*}(T_1-\tau) \\
&\leq -\frac{1}{\tilde{\varepsilon}} r_1^4\varepsilon_1\Big|_{t=\tau^*}(T_1-\tau) \\
&= -r_1(\tau^*)(T_1-\tau)
\end{aligned}$$

where in the final line we have made use of the fact that, for ρ small enough

$$\frac{dr_1}{dt} = \frac{1}{2}r_1^2\varepsilon_1(-1+\mathcal{O}(r_1)) \leq -\frac{1}{4}r_1^2\varepsilon_1.$$

Finally, we observe that

$$r_1^3(\tau^*) = \frac{\tilde{\varepsilon}}{\varepsilon_1(\tau^*)} \geq \frac{\tilde{\varepsilon}}{\delta}.$$

We can therefore conclude that for ρ and δ small enough,

$$\begin{aligned}
\int_0^{T_1} E_{\tilde{\varepsilon}}(T_1,\tau)\mathrm{d}\tau &\leq 2\int_0^{T_1} \exp\Big(-\frac{\tilde{\varepsilon}^{\frac{1}{3}}}{\delta^{-\frac{1}{3}}}(T_1-\tau)\Big)\Big)\mathrm{d}\tau \\
&\leq \frac{2\delta^{\frac{1}{3}}}{\tilde{\varepsilon}^{\frac{1}{3}}}
\end{aligned}$$

Summarizing our results in a lemma, we obtain

Lemma 3.6.5. *For $\rho > 0$ and $\delta > 0$ sufficiently small, for all $\tilde{\varepsilon} > 0$*

$$\int_0^{T_1} E_{\tilde{\varepsilon}}(T_1, \tau)\mathrm{d}\tau \leq \frac{2\delta^{\frac{1}{3}}}{\tilde{\varepsilon}^{\frac{1}{3}}}.$$

Remark 12. We may repeat this argument without excluding the term $e^{-\varepsilon\gamma\tau}$. The result is then $\mathcal{O}(\varepsilon^{-\frac{1}{3}}e^{-\varepsilon\gamma t})$, in line with Remark 7.

3.6.5.2 Bounding $\int_{T_1}^{T_2} E_{\tilde{\varepsilon}}(T_2, \tau)\mathrm{d}\tau$

As was the case when computing $E_{\tilde{\varepsilon}}(t, \tau)$ in this chart, our bound is relatively simple. We note that

$$\begin{aligned} \int_{T_1}^{T_2} E_{\tilde{\varepsilon}}(T_2, \tau)\mathrm{d}\tau &\leq E_{\tilde{\varepsilon}}(T_2, T_1)(T_2 - T_1) \\ &\leq K\tilde{\varepsilon}^{-\frac{1}{3}} \end{aligned}$$

for some constant $K > 0$. Despite the simplicity of the approach taken here, we note that this bound is asymptotically identical to the result detailed in Lemma 3.6.5. We summarize it as a lemma as well.

Lemma 3.6.6. *For $\rho > 0$ and $\delta > 0$ sufficiently small, for all $\tilde{\varepsilon} > 0$*

$$\int_{T_1}^{T_2} E_{\tilde{\varepsilon}}(T_2, \tau)\mathrm{d}\tau \leq K\tilde{\varepsilon}^{-\frac{1}{3}}.$$

3.6.5.3 Bounding $\int_{T_2}^{t} E_{\tilde{\varepsilon}}(t,\tau)\mathrm{d}\tau$ in the K_3 chart

Finally, we turn to the K_3 chart. Via Lemma 3.6.3, we have that for ρ and δ small enough

$$\begin{aligned}
\int_{T_2}^{t} E_{\tilde{\varepsilon}}(t,\tau)\mathrm{d}\tau &\leq \int_{T_2}^{t} \Big(\frac{r_3(t)}{r_3(\tau)}\Big)^{2(1+\alpha)}\mathrm{d}\tau \\
&= [r_3(t)]^{2(1+\alpha)} \int_{T_2}^{t} [r_3(\tau)]^{-2(1+\alpha)}\mathrm{d}\tau \\
&= [r_3(t)]^{2(1+\alpha)} \int_{T_2}^{t} \frac{[r_3(\tau)]^{-2(1+\alpha)}}{r_3^2(\tau)F_3(r_3(\tau), w_3(\tau), \varepsilon_3(\tau))} \frac{dr_3}{d\tau}\mathrm{d}\tau \\
&\leq 2(1+\alpha)[r_3(t)]^{2(1+\alpha)} \int_{T_2}^{t} [r_3(\tau)]^{-4-2\alpha}\frac{dr_3}{d\tau}\mathrm{d}\tau \\
&= 2(1+\alpha)[r_3(t)]^{2(1+\alpha)} \int_{r_3(T_2)}^{r_3(t)} v^{-4-2\alpha}\mathrm{d}v \\
&= \frac{2(1+\alpha)}{3+2\alpha}[r_3(t)]^{2(1+\alpha)}\Big([r_3(T_2)]^{-3-2\alpha} - [r_3(t)]^{-3-2\alpha}\Big)
\end{aligned}$$

We summarize this result in the following lemma.

Lemma 3.6.7. *For any $\alpha > 0$ and for $\rho > 0$, $\delta > 0$, and $\beta > 0$ sufficiently small,*

$$\int_{T_3}^{T_2} E_{\tilde{\varepsilon}}(T_2,\tau)\mathrm{d}\tau \leq \Big(\frac{2+2\alpha}{3+2\alpha}\Big)\frac{[r_3(T_3)]^{2+2\alpha}}{[r_3(T_2)]^{3+2\alpha}}$$

We note that since $\tilde{\varepsilon} = r_3^3\varepsilon_3$ and $\varepsilon_3(T_2) = \delta$, the right-hand side of our inequality is $\mathcal{O}(\tilde{\varepsilon}^{-(1+\frac{2}{3}\alpha)})$.

3.6.6 Inadequacy of estimates

We see that we can prove Lemma 3.6.4 by substituting the estimates of the last two sections into (3.36). We can take $t = T_3$ without loss, since $E_{\tilde{\varepsilon}}(t,\tau) \geq 0$.

Ultimately, it is clear that Lemma 3.6.4 is not strong enough to establish estimates on the norm of the offset. As we saw in the proofs for the boundedness of offsets along fast jumps and in all three proofs for results near the slow manifold, if a term on the right-hand side of an inequality such as

$$\begin{aligned} ||\bar{u}_{\tilde{\varepsilon}}(t)||_\infty \leq E_{\tilde{\varepsilon}(t,0)}||\bar{u}^0||_\infty + ||\bar{w}^0||_\infty \int_0^t E_{\tilde{\varepsilon}}(t,\tau)e^{-\varepsilon\gamma\tau}\mathrm{d}\tau \\ + \frac{|||\bar{u}_{\tilde{\varepsilon}}|||_T}{\gamma}\int_0^t E_{\tilde{\varepsilon}}(t,\tau)\mathrm{d}\tau \\ + C_{\text{quad}}|||\bar{u}_{\tilde{\varepsilon}}|||_T^2 \int_0^t E_{\tilde{\varepsilon}}(t,\tau)\mathrm{d}\tau \end{aligned}$$

highlighted in blue cannot be bounded above by 1, then the bootstrapping argument we have used to collect like terms on the left-hand side does not close. As our lemma shows that this term is inversely proportional to a power of $\tilde{\varepsilon}$, we are unable to establish any bounds on our offsets near the fold.

3.7 Discussion

We have examined the behavior of solutions to the Fitzhugh–Nagumo equation with nearly spatially-homogeneous initial data in three regions: when a basepoint solution defined for comparison drifts along the slow manifold, near a fold point, along fast jumps, and near a fold point.

In the first situation, we have seen that the offset $u_\varepsilon - u_\varepsilon^{\text{ODE}}$ decays algebraically if the initial data for our problem is arranged along the fast fibers that arise from considering the underlying kinetic system (3.2). In the kinetic system, deviations along the fiber decay exponentially on the fast timescale while tracking a basepoint that slowly drifts along the slow manifold. In the PDE case, we track a solution to the kinetic system while deviations decay algebraically along the fast timescale. While the analogy between the two situations is not perfect, the theory in this regime bears a resemblance to its cousin in the ODE case.

In the second case, we saw that we could prove that solutions to the full Fizthugh-Nagumo model remained within a neighborhood of a fast jump solution to the kinetic system, and therefore made the transition to a different portion of the slow manifold as well. While it seems unlikely *a priori* that the solution to the Fitzhugh–Nagumo model would be arranged along a fast fiber after making this jump, we can at least show that the qualitative behavior of a jump persists.

Ultimately, we were not able to establish bounds on offsets in the vicinity of the fold point. While we were able to compute estimates for key quantities that appeared in proofs near the slow manifold and the fast jump, they were not strong enough to close a bootstrapping argument. Unlike near the slow manifold, the bounds on our exponential are large with respect to ε. One possible interpretation for this difference is that the neighborhood of the fold point acts as a takeoff zone to begin the fast jump. Therefore, if points parametrized by different values of x reach the takeoff zone at slightly different times, they rapidly diverge from each other. In order to understand the behavior of solutions in this regime, an alternative approach will be required.

Chapter Four

Localized Oscillations in a $\lambda - \omega$ Model

The following chapter will be published separately as *Localized synchronous patterns in weakly coupled bistable oscillators*, in collaboration with Björn Sandstede and Jason Bramburger (Concordia University).

4.1 Introduction

Coupled oscillators arise in many natural and engineering systems, and their dynamics has been the focus of much work, including Kuramoto (1984), Ermentrout and Kopell (1991, 1990), Brown et al. (2003), Heagy et al. (1994), Hoppensteadt and Izhikevich (1997). A typical scenario begins with identical oscillators that, when uncoupled, evolve to a stable periodic orbit of a dynamical system of the form $\dot{x} = F(x, \mu)$, which may depend on a parameter μ. When these oscillators are coupled, synchronous oscillations may arise where the phases of the different oscillators lock to generate a globally periodic motion. There are many ways to encode the coupling between oscillators: we consider the case of oscillators that are coupled through the graph Laplacian of an underlying network, which results in systems of the form

$$\dot{x}_n = F(x_n, \mu) + \varepsilon \sum_{m \in} A_{mn}(x_m - x_n), \quad n \in, \tag{4.1}$$

where $A_{mn} \in \{0, 1\}$ describes whether the oscillators at nodes m and n are coupled ($A_{mn} = 1$) or uncoupled ($A_{mn} = 0$), and where $\varepsilon > 0$ denotes the coupling strength. We are primarily interested in the case of weak coupling where $0 < \varepsilon \ll 1$ is small.

We focus on nonlinear systems $\dot{x} = F(x, \mu)$ for the uncoupled oscillators that exhibit bistable dynamics for $\mu \in (a, b)$. As illustrated in the sample bifurcation diagram shown in Figure 4.1, we assume that we have coexistence of a stable equilibrium, a stable periodic orbit, and an unstable periodic orbit inside the bistability region $\mu \in (a, b)$, where the unstable periodic orbit emerges from the equilibrium in a Hopf bifurcation at $\mu = a$, and the periodic orbits connect in a fold bifurcation at $\mu = b$. Our goal is to understand the existence and dependence on μ of solutions of (4.1) for initial data where some nodes are set to the periodic orbits, while the others remain at the equilibrium. This question is relevant for understanding localized breather solutions of discrete nonlinear Schrödinger equations, as in Shi and Zhang (2015), Parker et al. (2020), Flach and Willis (1998), Cuevas-Maraver and Kevrekidis (2019), Parker and Aceves (2021), and localized oscillations in chains of coupled mechanical oscillators as in Clerc et al. (2018), Fontanela et al. (2018), Niedergesäß et al. (2021), Papangelo et al. (2018), Vakakis et al. (2001), Shiroky et al. (2020), Chiu et al. (2001), Papangelo et al. (2017).

We begin by outlining why we cannot expect that the coupled system (4.1) will exhibit smooth branches of periodic solutions when some of the nodes follow the stable periodic orbit and others the unstable periodic orbit. To see this, suppose that a subset of M connected nodes are initialized at the periodic orbits, while the remaining nodes are initialized at the equilibrium. For $\varepsilon = 0$ and with μ inside the bistability region, the set of such initial data corresponds to a normally hyperbolic M-dimensional torus. The invariant manifold theorem of (Hale, 2009, Theorem VII.2.1) guarantees that this invariant torus persists for each $0 < \varepsilon \ll 1$. Synchrony occurs when the persisting M-dimensional torus contains a periodic orbit. The question is whether and for which values of $\mu \in (a, b)$ synchrony occurs and how the resulting periodic orbits connect in function space as μ varies. Restricting to $M = 2$, we assume that one node is initialized at the stable periodic orbit, while the second node is set to the unstable periodic orbit. The dynamics on the persisting two-dimensional torus can be represented by a Poincare map on the circle, and this map has fixed points (corresponding to synchronous oscillations for the full system) if and only if its rotation number is rational. For $\varepsilon = 0$, the rotation number is given by the ratio of the two periods, and we expect this number to change as μ is varied in (a, b). For $0 < \varepsilon \ll 1$, we expect that the resulting rotation number is locally constant at rational values, while it varies monotonically at irrational numbers (where synchronous states do not exist). In particular, we cannot expect synchrony to occur

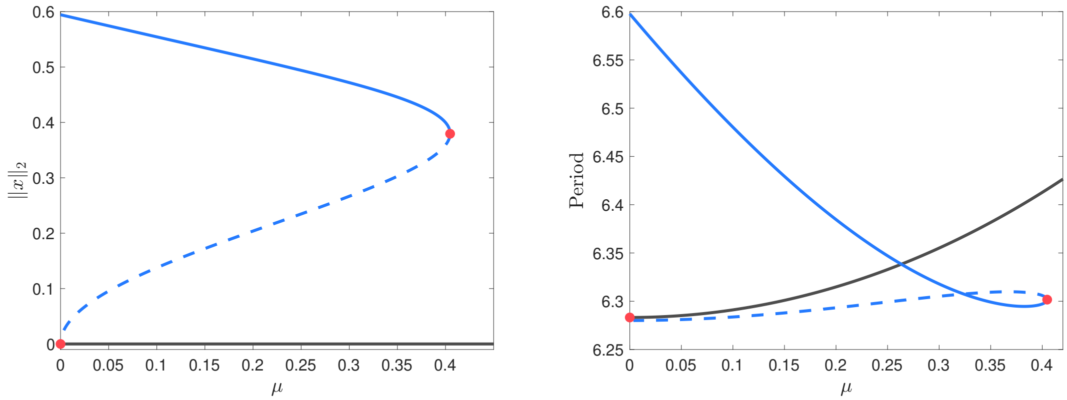

Figure 4.1: Left: Shown is the bifurcation diagram of system (4.2) for $\varepsilon = 0$. Periodic solutions are shown in blue, and the vertical axis is the L^2-norm of the solution over one period. Stable solutions are represented by solid curves, while unstable solutions use dashed curves. Right: The period (blue) of periodic solutions and the imaginary part of the eigenvalues of the linearization about $x = 0$ (black) are shown. Hopf and fold bifurcation points are indicated by red circles.

for all values of μ: instead, we expect to encounter synchrony for many small open intervals with fold bifurcations occurring at their end points. Thus, we expect to find phase-locked synchronized solutions only when the periods of the stable and unstable periodic orbits are close to each other throughout the bistability region $\mu \in (a, b)$.

However, these complicated synchrony patterns can indeed be observed in many systems. The authors of Papangelo et al. (2017), for instance, investigated localized oscillations in a parameter-dependent second-order mechanical system, which we re-cast here as the first order system

$$\begin{aligned} \dot{x}_n &= y_n \\ \dot{y}_n &= -\mu y_n + 2.4\pi^2 y_n^3 - 3.2\pi^4 y_n^5 + \varepsilon(x_{n+1} - x_n) + \varepsilon(x_{n-1} - x_n), \qquad n = 1, \ldots, N \end{aligned} \tag{4.2}$$

to match the setting of (4.1). Here, the N oscillators x_n are arranged around a ring with periodic coupling conditions $x_{N+1} = x_1$ and $x_0 = x_N$, and μ is the designated bifurcation parameter. Figure 4.1 shows that this system is bistable and exhibits

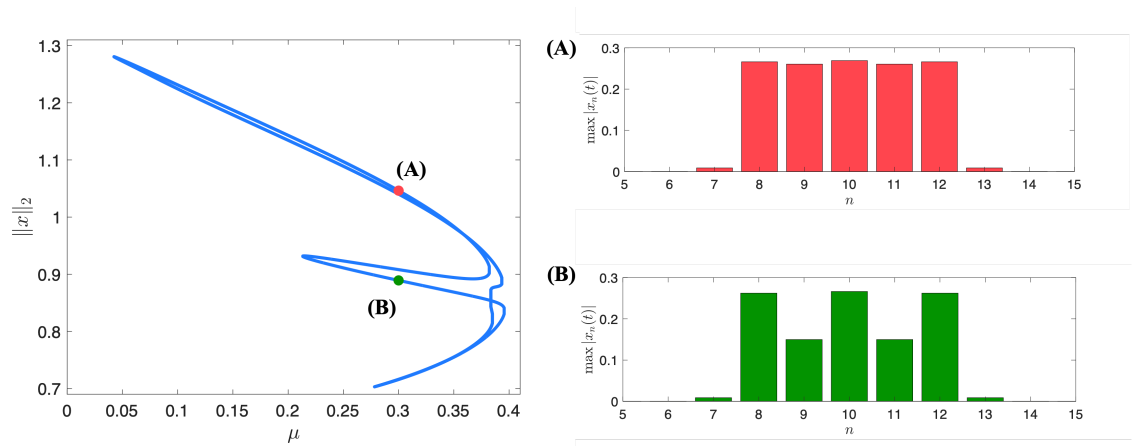

Figure 4.2: Left: An isola of localized oscillations to (4.2) with $N = 20$ and $\varepsilon = 0.01$ is shown. Right: Shown are the solution profiles for the points labeled (A) and (B) in the bifurcation curve at $\mu = 0.3$ (the maxima at those indices not plotted are zero to plotting accuracy).

the features we discussed above. As shown in Figure 4.2, periodic orbits of (4.2) for $\varepsilon > 0$ lie along closed bifurcation curves, which we will refer to as isolas. This is aligned with our discussion above, and in sharp contrast to the case of localized structures composed of equilibria which typically lie on curves with a simple figure-8 shape Bramburger (2021), Bramburger and Sandstede (2020) (see Figure 4.2.3 below for an example).

In this manuscript, we therefore consider systems of the form (4.1) under the assumptions of (i) weak coupling across nodes and (ii) weak dependence of the periods on the amplitude of the periodic orbits for the uncoupled oscillators. In addition, we focus on nonlinearities of Lambda-Omega or Ginzburg–Landau type. In this setting, we will prove that localized in-phase oscillatory patterns lie on smooth branches.

The remainder of the paper is organized as follows. In §4.2, we will introduce the specific system we study, along with all hypotheses and results. We leave the proofs to sections §4.3 and §4.4. We conclude with a discussion of the results and a comparison with numerical solutions in §4.5.

4.2 Snaking of localized phase-locked oscillators

4.2.1 Coupled Ginzburg–Landau oscillators

We will consider the generalized system

$$\dot{Z}_n = Z_n\lambda(|Z_n|,\mu) + iZ_n\omega(|Z_n|,\mu) + \varepsilon(Z_{n+1} + Z_{n-1} - 2Z_n), \qquad Z_n \in, \qquad |n| \leq N \tag{4.3}$$

of Ginzburg–Landau (or Lambda-Omega) oscillators, where we set $Z_{\pm(N+1)} = 0$ and assume that the functions λ, ω are real-valued. We make the following assumptions on the function λ which reflect the bifurcation diagram shown in the left panel of Figure 4.1, albeit with different axes.

Hypothesis 1. *The function* $\lambda\colon \mathbb{R}^2 \to \mathbb{R}, (r,\mu) \mapsto \lambda(r,\mu)$ *is smooth and satisfies the following:*

Symmetry: The function λ *is even in* r *so that* $\lambda(-r,\mu) = \lambda(r,\mu)$.

Equilibria: For each $\mu \in (0,1)$ *the function* $\lambda(r,\mu)$ *has exactly two nontrivial positive roots, denoted* $r = r_\pm(\mu)$, *with* $0 < r_-(\mu) < r_+(\mu)$.

Stability: For each $\mu \in (0,1)$ *we have* $\lambda(0,\mu), \lambda_r(r_+(\mu),\mu) < 0 < \lambda_r(r_-(\mu),\mu)$.

Pitchfork bifurcation: At $\mu = 0$, *the roots* $r = 0$ *and* $r = \pm r_-(\mu)$ *of the function* $r\lambda(r,\mu)$ *collide in a generic subcritical pitchfork bifurcation.*

Fold bifurcation: At $\mu = 1$, *the roots* $r = r_\pm(\mu)$ *collide in a generic saddle-node bifurcation at* $r = 1$.

As we argued in the introduction, localized periodic solutions involving both stable and unstable periodic orbits of individual oscillators should generally only occur when the frequencies of these periodic orbits are sufficiently close. We formulate this requirement as a hypothesis.

Hypothesis 2. *There exist smooth functions* $\Omega\colon \mathbb{R} \to \mathbb{R}$ *and* $g\colon \mathbb{R}^3 \to \mathbb{R}$ *so that* $\omega(r, \mu, \varepsilon) = \Omega(\mu) + \varepsilon^2 g(r, \mu, \varepsilon)$.

Similar assumptions on ω have been used to demonstrate the existence of spiral waves in Lambda-Omega systems, and we refer for instance to Aguareles et al. (2016), Paullet et al. (1994), Cohen et al. (1978), Troy (2022) for the spatially continuous setting and to Bramburger (2020), Paullet and Ermentrout (1998), Bramburger (2019) for systems posed on square lattices. We demonstrate that utilizing the weaker assumption $\omega(r, \mu, \varepsilon) = \Omega(\mu) + \varepsilon g(r, \mu, \varepsilon)$ is not sufficient to guarantee the existence of periodic solutions to (4.3) in Appendix B.

Common explicit choices for the functions λ and ω, which are motivated by the normal form of subcritical Hopf bifurcations, are

$$\lambda(r, \mu) = -\mu + 2r^2 - r^4 \tag{4.4}$$

$$\omega(r, \mu, \varepsilon) = \Omega(\mu) + q(\varepsilon) r^2. \tag{4.5}$$

The function λ in (4.4) satisfies Hypothesis 1, while the function ω in (4.5) satisfies Hypothesis 2 provided $|q(\varepsilon)| \leq C\varepsilon^2$.

4.2.2 Localized phase-locked oscillations

Next, we discuss periodic solutions of (4.3). This system is gauge invariant: if $(Z_n(t))_{|n| \leq N}$ is a solution to (4.3), so is $(e^{i\alpha} Z_n(t))_{|n| \leq N}$ for each fixed $\alpha \in \mathbb{R}$. Gauge invariance allows us to seek periodic solutions in the form of relative equilibria that are of the form

$$Z_n(t) = e^{i\bar{\omega}t} z_n, \qquad |n| \le N$$

for time-independent complex amplitudes z_n, where $\bar{\omega} \in \mathbb{R}$ is the temporal frequency of the periodic orbit. Hence, the complex amplitudes z_n can be found as a solution to

$$i\bar{\omega} z_n = z_n \lambda(|z_n|, \mu) + i z_n \omega(|z_n|, \mu) + \varepsilon(z_{n+1} + z_{n-1} - 2z_n), \quad |n| \le N \tag{4.6}$$

and $z_{\pm(N+1)} = 0$. Setting $\bar{\omega} = \Omega(\mu) + \epsilon\omega_0$ and using Hypothesis 2, we can write this equation as

$$0 = z_n \lambda(|z_n|, \mu) + i z_n \varepsilon(-\omega_0 + \varepsilon g(|z_n|, \mu, \varepsilon))\omega(|z_n|, \mu) + \varepsilon(z_{n+1} + z_{n-1} - 2z_n), \quad |n| \le N \tag{4.7}$$

with $z_{\pm(N+1)} = 0$. In the case of infinitely-many oscillators, our system (4.7) is posed on an integer lattice, and we can distinguish on-site and off-site solutions that are invariant under reflections across $n = 0$ and $n = -1/2$, respectively. We say that a solution $(z_n)_{|n| \le N}$ of (4.7) is an **on-site** solution if $z_n = z_{-n}$ for all n. A solution is said to be an **off-site** solution if $z_n = z_{-n-1}$ for all n.

It is convenient to write $z_n = r_n \mathrm{e}^{\mathrm{i}\theta_n}$ with $r_n, \theta_n \in \mathbb{R}$ for each n. We can then find analogues of on-site and off-site solutions by restricting the index n to $n \ge 0$ and including the boundary conditions $(r_1, \theta_1) = (r_{-1}, \theta_{-1})$ for on-site and $(r_0, \theta_0) = (r_{-1}, \theta_{-1})$ for off-site solutions. Gauge invariance implies that solutions depend only on the amplitudes r_n and the phase differences $\phi_n := \theta_{n+1} - \theta_n$ (rather than the individual phases θ_n). Exploiting this formulation turns (4.7) for the complex amplitudes z_n into the system

$$
\begin{aligned}
0 &= r_n\lambda(r_n,\mu) + \varepsilon\left(r_{n+1}\cos\phi_n + r_{n-1}\cos\phi_{n-1} - 2r_n\right), \qquad 0 \le n \le N\\
0 &= r_n(-\omega_0 + \varepsilon g(r_n,\mu,\varepsilon)) + r_{n+1}\sin(\phi_n) - r_{n-1}\sin(\phi_{n-1}), \quad 0 \le n \le N\\
(r_{N+1},\phi_N) &= (0,0)\\
(r_{-1},\phi_{-1}) &:= (r_1,-\phi_0) \qquad \text{for on-site solutions}\\
(r_{-1},\phi_{-1}) &:= (r_0,0) \qquad \text{for off-site solutions}
\end{aligned}
\tag{4.8}
$$

for the amplitudes $\boldsymbol{r} = (r_n)_{0\le n\le N}$ and the phase differences $\boldsymbol{\phi} = (\phi_n)_{0\le n\le N-1}$, so that the variables we have to solve for are given by

$$(\omega_0, \boldsymbol{r}, \boldsymbol{\phi}) = (\omega_0, (r_n)_{0\le n\le N}, (\phi_n)_{0\le n\le N-1}) \in X := \mathbb{R}\times\mathbb{R}^{N+1}\times\mathbb{R}^N.$$

We are interested in localized solutions of (4.8): we say that a solution is **localized** if there is an index $k \ge 0$ such that $r_n \approx r_\pm(\mu)$ for $n \le k$ and $|r_n| \ll 1$ for $n > k$. We can then further distinguish **in-phase** solutions, for which the relative phase differences $\phi_n \approx 0$ are close to zero for all $n \le k$ so that each oscillator is locked with the same phase as its neighbors, and **anti-phase** solutions, for which $\phi_n \approx \pi$ for $n \le k$ so that neighboring oscillators are out of phase with a phase difference of π. Note that in-phase solutions can be on- or off-site, since having identical phase respects both symmetries. Anti-phase solutions exist only as on-site solutions: the oscillator at $n = 1$ is π radians out of phase with the oscillator at $n = 0$, while the oscillator at $n = -2$ is in-phase with it. But the off-site condition would require the oscillators at $n = 1$ and $n = -2$ to be in-phase, which is a contradiction.

We end this section with two remarks. Firstly, if we remove the factor ε in front of the nonlinearity $g(r_n,\mu,\varepsilon)$ in (4.8), we see that it will be impossible to solve the phase equations unless we impose additional restrictions on g: this is the reason why we included the factor ε^2 in front of g in Hypothesis 2. For explicit computations, see §6.2.

Secondly. we note that when neighboring nodes have approximately equal amplitudes given by $\bar{r}$, the coupling term $r_{n+1}\cos\phi_n + r_{n-1}\cos\phi_{n-1} - 2r_n$ in the radial equation in (4.8) behaves very differently for in-phase and anti-phase solutions. For in-phase solutions with $\phi_n \approx 0$, this term is close to zero, while it is approximately equal to $-4\bar{r}$ for anti-phase solutions with $\phi_n \approx \pi$. As we will see below, this difference will cause in-phase solutions to snake, while preventing the study of anti-phase solutions without examining higher-order terms.

4.2.3 Results

To formulate our results, we first define the curves $\mu_*(s)$, $R_\pm(s)$, and $R_0(s)$ that trace out the parameter μ and the roots $r_\pm(\mu)$ of the function λ as a function of an arclength parameter s. We illustrate the parametrization for μ in Figure 4.3 and will use them below to describe branches of in-phase solutions. The parametrized curves are given by

$$\mu_*(s) \;:=\; \begin{cases} s & 0 \le s \le 1 \\ 2-s & 1 \le s \le 2 \\ \mu_*(s \bmod 2) & s \ge 2, \end{cases} \qquad R_0(s) \;:=\; \begin{cases} r_-(\mu_*(s)) & 0 \le s \le 1 \\ r_+(\mu_*(s)) & 1 \le s \le 2, \end{cases}$$

$$R_\pm(s) \;:=\; r_\pm(\mu_*(s)), \quad s \ge 0, \qquad \boldsymbol{e}_k \;:=\; \Big(\underbrace{1, \ldots, 1}_{0 \le n \le k}\Big) \in \mathbb{R}^{k+1}.$$

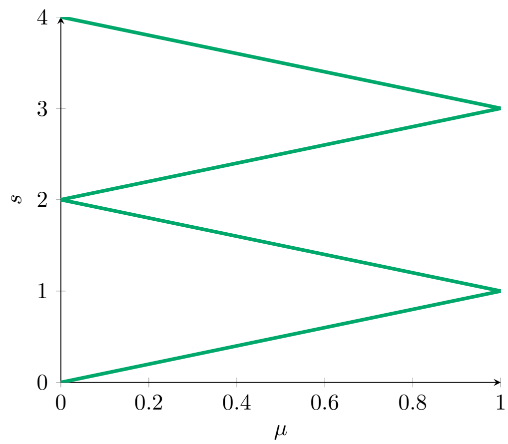

Figure 4.3: As s increases, we see that μ_* moves back and forth between 0 and 1.

As shown in Figure 4.3, the values of $\mu_*(s)$ move back and forth between $\mu = 0$ and $\mu = 1$ as s increases. At the same time, $R_+(s)$ and $R_-(s)$ stay, respectively, on the upper and lower branch of periodic orbits as s varies. Finally, $R_0(s)$ starts at $R_0(0) = 0$, traverses the full branch of periodic orbits from r_- to r_+ as s increases, and ends at $R_0(2) = r_+(0)$.

For each integer k with $0 < k < N$, we define

$$\begin{aligned} \gamma_{\text{in}}(k) \quad := \quad & \{(\omega_0, \boldsymbol{r}, \boldsymbol{\phi}, \mu) \in X \times [0,1] : \ \omega_0 = 0, \ \mu = \mu_*(s), \ \boldsymbol{\phi}(s) = \boldsymbol{0}, \\ & \boldsymbol{r}(s) = (R_+(s)\boldsymbol{e}_{k-1}, R_0(s), 0, 0, \ldots) \text{ for } 0 \le s \le 2\} \subset X \times [0,1]. \end{aligned}$$

We now stack the branches $\gamma_{\text{in}}(k)$ to construct the full branch of in-phase solutions by taking the union over the index k:

$$\Gamma_{\text{in}}(N) := \bigcup_{k=1}^{N-1} \gamma_{\text{in}}(k). \tag{4.9}$$

As we traverse the set $\Gamma_{\text{in}}(N)$, the number of nodes in the in-phase solution that exhibit oscillations grows from $k = 1$ to $k = N - 1$: we refer to this phenomenon as "snaking". For each $\delta > 0$ and each subset $\mathcal{S} \subset X \times [0,1]$, we denote by $\mathcal{B}_\delta(\mathcal{S})$

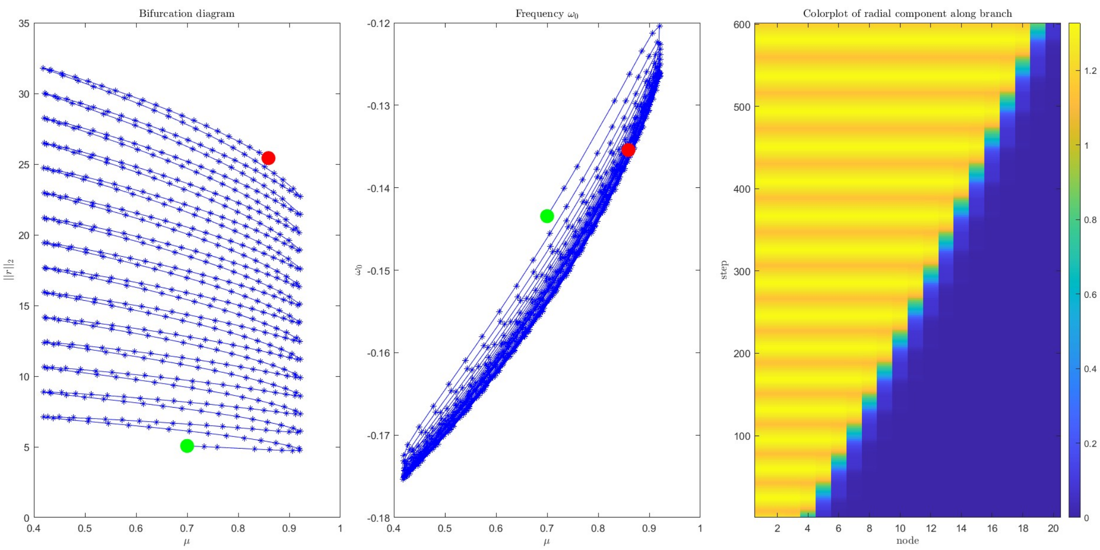

Figure 4.4: Shown is a snaking branch of localized solutions of (4.7) with λ and ω from (4.4) and (4.5), respectively, for $\varepsilon = 0.1$ and $q = \varepsilon^2$. The first figure is the bifurcation diagram of the continued solutions, the second shows the frequency ω_0, and the final plot shows the magnitude of each oscillator. The latter clearly demonstrates how new oscillators are recruited.

the δ-neighborhood of $\mathcal{S}$ in $X \times [0, 1]$. Our main result establishes the existence of in-phase solutions for weak coupling.

Theorem 4.2.1 (Snaking of in-phase solutions). *Assume that λ and ω satisfy Hypotheses 1 and 2, respectively. For each $\delta > 0$ there exist constants $\delta_*, \varepsilon_* > 0$ so that for $\varepsilon \in (0, \varepsilon_*)$ the set $\mathcal{B}_{\delta_*}(\Gamma_{\text{in}}(N)) \setminus \mathcal{B}_\delta(0, \mathbf{0}, \mathbf{0}, 0)$ contains two unique, nonempty, smooth branches $\Gamma_{\text{in}}^{\text{on}}(\varepsilon)$ and $\Gamma_{\text{in}}^{\text{off}}(\varepsilon)$ of, respectively, on-site and off-site periodic solutions of the Ginzburg–Landau equation (4.3). These branches depend smoothly on ε and converge to $\Gamma_{\text{in}}(N) \setminus \mathcal{B}_\delta(0, \mathbf{0}, \mathbf{0}, 0)$ in C^0 as $\varepsilon \to 0$.*

Our proof of Theorem 4.2.1 will sharpen the convergence assertions and, in particular, show that convergence is in C^m for each fixed $m \geq 1$ outside the set $\mathcal{B}_{\delta_*}(X \times \{0, 1\})$, while the branches inside $\mathcal{B}_{\delta_*}(X \times \{0, 1\})$ consist of generic fold bifurcations. Figure 4.2.3 illustrates the predictions for snaking of in-phase solutions.

4.3 Analysis inside the bistability region

We analyze (4.8) inside the hyperbolic bistability region, that is, for values of μ away from 0 and 1.

For each fixed $0 \leq k < N$, we will seek localized solutions of (4.8) in the form

$$r_n = \begin{cases} r_n^0(\mu) + \varepsilon\sigma_n, & 0 \leq n \leq k \\ \left[\frac{\varepsilon}{\lambda(0,\mu)}\right]^{n-k} r_k^0(\mu)\sigma_n, & k+1 \leq n \leq N, \end{cases} \tag{4.10}$$

where $r_n^0(\mu)$ lies in $\{r_-(\mu), r_+(\mu)\}$ for each $0 \leq n \leq k$. In particular, we decompose localized solutions into the **core** nodes for $0 \leq n \leq k$, where they attain the amplitudes of one of the two nonzero periodic orbits and the **far-field** nodes for $k < n$, where they are close to the equilibrium. Before substituting our ansatz into the Ginzburg–Landau system, we introduce the following definition.

Definition 4.3.1. Let $\Lambda \subset$ be an index set. We say that a family of functions $(f_n(\boldsymbol{\sigma}, \boldsymbol{\phi}, \varepsilon))_{n\in\Lambda}$ is **uniformly of order** ε if the following conditions are met.

- There exists a $k \in \mathbb{N}$ such that f_n depends at most on ε, $(\sigma_{n-k}, \sigma_{n-k+1}, \dots, \sigma_{n+k-1}, \sigma_{n+k})$, and $(\phi_{n-k}, \phi_{n-k+1}, \dots, \phi_{n+k-1}, \phi_{n+k})$ for each $n \in \Lambda$.
- For each $\delta > 0$ there exists a $C > 0$ such that $|f_n| + |D_{(\boldsymbol{\sigma},\boldsymbol{\phi})} f_n| \leq C\varepsilon$ for all $n \in \Lambda$ whenever $|\sigma| + |\Phi| \leq \delta$.

We shall denote a member of such a family of functions by the shorthand $\mathcal{O}^{\mathrm{u}}(\varepsilon)$.

With this definition in hand, substituting (4.10) into (4.8) yields the amplitude equations

$$
\begin{aligned}
0 &= (\lambda(r_n^0(\mu),\mu) + r_n^0(\mu)\lambda_r(r_n^0(\mu),\mu))\sigma_n \\
&\quad +[r_{n+1}^0(\mu)\cos(\phi_n) + r_{n-1}^0(\mu)\cos(\phi_{n-1}) - 2r_n^0(\mu)] + \mathcal{O}^{\mathrm{u}}(\varepsilon) && 0 \le n \le k-1 \\
0 &= (\lambda(r_k^0(\mu),\mu) + r_k^0(\mu)\lambda_r(r_k^0(\mu),\mu))\sigma_k + [r_{k-1}^0(\mu)\cos(\phi_{k-1}) - 2r_k^0(\mu)] + \mathcal{O}^{\mathrm{u}}(\varepsilon) && n = k \\
0 &= \sigma_{k+1} + \cos(\phi_k) + \mathcal{O}^{\mathrm{u}}(\varepsilon) && n = k+1 \\
0 &= \sigma_n + \sigma_{n-1}\cos(\phi_{n-1}) + \mathcal{O}^{\mathrm{u}}(\varepsilon) && k+2 \le n \le N
\end{aligned}
$$

after dividing by ε and the phase equations

$$
\begin{aligned}
0 &= -r_n^0(\mu)\omega_0 + r_{n+1}^0(\mu)\sin(\phi_n) - r_{n-1}^0(\mu)\sin(\phi_{n-1}) + \mathcal{O}^{\mathrm{u}}(\varepsilon) && 0 \le n \le k-1 \\
0 &= -r_k^0(\mu)\omega_0 - r_{k-1}^0(\mu)\sin(\phi_{k-1}) + \mathcal{O}^{\mathrm{u}}(\varepsilon) && n = k \\
0 &= -r_k^0\sin(\phi_k) + \mathcal{O}^{\mathrm{u}}(\varepsilon) && n = k+1 \\
0 &= -\sigma_{n-1}\sin(\phi_{n-1}) + \mathcal{O}^{\mathrm{u}}(\varepsilon) && k+2 \le n \le N.
\end{aligned}
$$

Next, instead of distinguishing amplitude and phase equation, we separate the core from the far-field nodes. The core system is then given by

$$
\begin{aligned}
0 &= (\lambda(r_n^0(\mu),\mu) + r_n^0(\mu)\lambda_r(r_n^0(\mu),\mu))\sigma_n \\
&\quad +[r_{n+1}^0(\mu)\cos(\phi_n) + r_{n-1}^0(\mu)\cos(\phi_{n-1}) - 2r_n^0(\mu)] + \mathcal{O}^{\mathrm{u}}(\varepsilon) && 0 \le n \le k-1 \\
0 &= (\lambda(r_k^0(\mu),\mu) + r_k^0(\mu)\lambda_r(r_k^0(\mu),\mu))\sigma_k + [r_{k-1}^0(\mu)\cos(\phi_{k-1}) - 2r_k^0(\mu)] + \mathcal{O}^{\mathrm{u}}(\varepsilon) && n = k \\
0 &= -r_n^0(\mu)\omega_0 + r_{n+1}^0(\mu)\sin(\phi_n) - r_{n-1}^0(\mu)\sin(\phi_{n-1}) + \mathcal{O}^{\mathrm{u}}(\varepsilon) && 0 \le n \le k-1 \\
0 &= -r_k^0(\mu)\omega_0 - r_{k-1}^0(\mu)\sin(\phi_{k-1}) + \mathcal{O}^{\mathrm{u}}(\varepsilon) && n = k,
\end{aligned}
\tag{4.11}
$$

while the far-field system becomes

$$
\begin{aligned}
0 &= \sigma_{k+1} + \cos(\phi_k) + \mathcal{O}^{\mathrm{u}}(\varepsilon) && n = k+1 \\
0 &= \sigma_n + \sigma_{n-1}\cos(\phi_{n-1}) + \mathcal{O}^{\mathrm{u}}(\varepsilon) && k+2 \le n \le N \\
0 &= -\sin(\phi_k) + \mathcal{O}^{\mathrm{u}}(\varepsilon) && n = k+1 \\
0 &= -\sigma_{n-1}\sin(\phi_{n-1}) + \mathcal{O}^{\mathrm{u}}(\varepsilon) && k+2 \le n \le N.
\end{aligned}
\tag{4.12}
$$

We introduce the core and far-field variables via

$$\boldsymbol{\sigma}^{\mathrm{c}} = (\sigma_n)_{0\le n\le k}, \qquad \boldsymbol{\phi}^{\mathrm{c}} = (\phi_n)_{0\le n\le k-1}, \qquad \boldsymbol{\sigma}^{\mathrm{f}} = (\sigma_n)_{k+1\le n\le N}, \qquad \boldsymbol{\phi}^{\mathrm{f}} = (\phi_n)_{k\le n\le N-1}.$$

Note that the far-field system depends on $a := (\sigma_k, \phi_{k-1})$ through the $\mathcal{O}^{\mathrm{u}}(\varepsilon)$ terms but not on any other variables from the core system. Similarly, the core system depends only on $b := (\sigma_{k+1}, \phi_k)$ from the far-field variables through the $\mathcal{O}^{\mathrm{u}}(\varepsilon)$ terms. We can therefore write the far-field equation (4.12) as $\mathscr{F}^{\mathrm{f}}(\boldsymbol{\sigma}^{\mathrm{f}}, \boldsymbol{\phi}^{\mathrm{f}}, a, \varepsilon) = 0$ and the core system as $\mathscr{F}^{\mathrm{c}}(\boldsymbol{\sigma}^{\mathrm{c}}, \boldsymbol{\phi}^{\mathrm{c}}, \omega_0, b, \varepsilon) = 0$.

4.3.0.1 Solving the far-field equations.

We shall prove the following lemma, which is based on the implicit function theorem and allows us to solve the far-field system (4.12) uniquely as a function of $a = (\sigma_k, \boldsymbol{\phi}_{k-1})$.

Lemma 4.3.2 (Far-field lemma)**.** *Consider the system*

$$\begin{aligned}
0 &= \gamma_1\sigma_{k+1} + \gamma_2\cos(\phi_k) + \mathcal{O}^{\mathrm{u}}(\varepsilon) && n = k+1\\
0 &= \gamma_3\sigma_n + \gamma_4\sigma_{n-1}\cos(\phi_{n-1}) + \mathcal{O}^{\mathrm{u}}(\varepsilon) && k+2 \le n \le N\\
0 &= \gamma_5\sin(\phi_k) + \mathcal{O}^{\mathrm{u}}(\varepsilon) && n = k+1\\
0 &= \gamma_6\sigma_{n-1}\sin(\phi_{n-1}) + \mathcal{O}^{\mathrm{u}}(\varepsilon) && k+2 \le n \le N
\end{aligned} \tag{4.13}$$

where $\boldsymbol{\gamma} = (\gamma_1, ..., \gamma_6)$ consists of nonzero constants, and the error terms of the equations for index $k+1$ may depend on $a = (\sigma_k, \phi_{k-1})$. For $\varepsilon = 0$, (4.13) has the solution $(\boldsymbol{\sigma}_0(\boldsymbol{\gamma}), \boldsymbol{\phi}_0, \varepsilon_0) = (\hat{\sigma}(\boldsymbol{\gamma}), \mathbf{0}, 0)$ for each value of a, where

$$\begin{aligned}
\hat{\sigma}_{k+1} &= -\tfrac{\gamma_2}{\gamma_1} && n = k+1\\
\hat{\sigma}_n &= -\tfrac{\gamma_2}{\gamma_1}(-\tfrac{\gamma_4}{\gamma_3})^{n-k-1} && k+2 \le n \le N
\end{aligned}$$

depends smoothly on $\boldsymbol{\gamma}$*. Given an open bounded set* A *in* $\mathbb{R}^2$*, there exists an* $\varepsilon_0 > 0$ *so that* (4.13) *has a unique solution* $(\boldsymbol{\sigma}, \boldsymbol{\phi})$ *near* $(\boldsymbol{\sigma}_0(\boldsymbol{\gamma}), \boldsymbol{\phi})$ *for each* $0 \leq \varepsilon < \varepsilon_0$*,* $a \in A$*, and* $\boldsymbol{\gamma}$*, and this solution depends smoothly on* $(\varepsilon, a, \boldsymbol{\gamma})$ *and is* $\mathcal{O}^{\mathrm{u}}(\varepsilon)$*-close to the solution* $(\boldsymbol{\sigma}_0(\boldsymbol{\gamma}), \mathbf{0})$*.*

Proof. To arrive at this result, we first note that by the definition of uniformly order ε terms, we need only differentiate the linear part of our operator to compute the Jacobian above. We find that

$$D\mathscr{F}_{(\boldsymbol{\sigma},\boldsymbol{\phi})}\big(\hat{\sigma}, \mathbf{0}, 0, a, \gamma\big) = \begin{pmatrix} \boldsymbol{A} & \mathbf{0} \\ \mathbf{0} & \mathbf{B} \end{pmatrix}$$

where $A_{11} = \gamma_1$, $A_{1,2} = \gamma_2$, and $A_{ii} = \gamma_3$, $A_{i,i+1} = \gamma_4$ for all $i \geq 2$ with all other elements equal to zero. Furthermore, $\mathbf{B} = \mathrm{diag}(\gamma_5, \gamma_6\tilde{\sigma}_{k+1}, \gamma_6\tilde{\sigma}_{k+2}, ..., \gamma_6\tilde{\sigma}_{N-1})$. The form of the operator $\boldsymbol{A}$ follows from differentiating the amplitude equations and observing that $\cos(0) = 1$. Likewise, when differentiating the amplitude equations with respect to the phase variables or vice-versa, we obtain only terms proportional to $\sin(\phi_m)$ for some m, which are equal to zero since $\phi_m = 0$. The diagonal nature of $\mathbf{B}$ follows from the form of the phase equations.

With this computation in hand, we see that all that is needed to apply the implicit function theorem is to check that both $\boldsymbol{A}$ and $\mathbf{B}$ are invertible. Our conditions on γ imply this fact immediately for $\mathbf{B}$, since it forces the elements on the diagonal to be nonzero. Since $\boldsymbol{A}$ is lower triangular, it is also invertible, and we may invoke the implicit function theorem to claim that for some $\varepsilon_0 > 0$, there exist functions such that $\boldsymbol{\sigma} = \boldsymbol{\sigma}(\varepsilon; a, \gamma)$ and $\boldsymbol{\phi} = \boldsymbol{\phi}(\varepsilon; a, \gamma)$ satisfying $\mathscr{F}^{\mathrm{f}}(s(\varepsilon; a, \gamma), \boldsymbol{\phi}(\varepsilon; a, \gamma), \varepsilon, a, \gamma) = \mathbf{0}$

for all $\varepsilon \in (0, \varepsilon_0)$. We note that by Taylor-expanding about $(0; a, \gamma)$

$$\begin{aligned}
\sigma_n(\varepsilon; a, \gamma) &= \sigma_n(0; a, \gamma) + \frac{\partial \sigma_n(\varepsilon_n^\sigma; a, \gamma)}{\partial \varepsilon}\varepsilon \\
&= \tilde{\sigma}_n + \frac{\partial \sigma_n(\varepsilon_n^\sigma; a, \gamma)}{\partial \varepsilon}\varepsilon \\
&= \tilde{\sigma}_n + \mathcal{O}(\varepsilon)
\end{aligned}$$

and

$$\begin{aligned}
\phi_n(\varepsilon; a, \gamma) &= \phi_n(0; a, \gamma) + \frac{\partial \phi_n(\varepsilon_n^\phi; a, \gamma)}{\partial \varepsilon}\varepsilon \\
&= \frac{\partial \phi_n(\varepsilon_n^\phi; a, \gamma)}{\partial \varepsilon}\varepsilon \\
&= \mathcal{O}(\varepsilon)
\end{aligned}$$

where $0 \leq \varepsilon_n^\sigma, \varepsilon_n^\phi \leq \varepsilon$. $\square$

Remark 13. We note that the inverse of the linearization of (4.13) around its root has norm of order N, which prevents us from extending this lemma, and thus our analysis, to an infinite number of oscillators.

We can apply Lemma 4.3.2 to solve (4.12) by taking $\gamma = (1, 1, 1, 1, -1, -1)$, which yields a unique solution $(\boldsymbol{\sigma}^{\mathrm{f}}, \boldsymbol{\phi}^{\mathrm{f}})$ as a smooth function of (a, ε) with

$$\sigma_n = (-1)^{n-k} + \mathcal{O}^{\mathrm{u}}(\varepsilon) \quad k+1 \leq n \leq N, \tag{4.14}$$

where all dependence on $(\sigma_k, \boldsymbol{\phi}_{k-1})$ is hidden in the uniformly small remainders. Substituting this solution into the core equation (4.11), we arrive at the system $\mathscr{F}^{\mathrm{c}}(\boldsymbol{\sigma}^{\mathrm{c}}, \boldsymbol{\phi}^{\mathrm{c}}, \omega_0, b(\sigma_k, \boldsymbol{\phi}_{k-1}, \varepsilon), \varepsilon) = 0$, where $b = (\sigma_{k+1}, \phi_k)$ is now a function of the core variables $a = (\sigma_k, \phi_{k-1})$. Since the term $b(\sigma_k, \boldsymbol{\phi}_{k-1}, \varepsilon)$ enters only through the $\mathcal{O}^{\mathrm{u}}(\varepsilon)$ terms, we will, with a slight abuse of notation, also write the resulting core system that incorporates the solution of the far-field system, as $\mathscr{F}^{\mathrm{c}}(\boldsymbol{\sigma}^{\mathrm{c}}, \boldsymbol{\phi}^{\mathrm{c}}, \omega_0, \varepsilon) = 0$.

We will solve this system next.

Remark 14. From the form of (4.14), it may appear that some of our amplitude variables are negative. However, the ansatz (4.10) contains another factor of $(-1)^{n-k}$ due to the presence of $\lambda(0, \mu)$, since this quantity is negative.

4.3.0.2 Solving the core system.

Turning to the core system (4.11), we obtain the following lemma.

Lemma 4.3.3. *We have that* $(\boldsymbol{\sigma}^{\mathrm{c}}, \omega_0, \boldsymbol{\phi}^{\mathrm{c}}, \varepsilon) = (\hat{\boldsymbol{\sigma}}, 0, \mathbf{0}, 0)$ *is a solution to* (4.11), *where*

$$\begin{aligned} \hat{\sigma}_n &= \frac{2r_n^0(\mu) - r_{n+1}^0(\mu) - r_{n-1}^0(\mu)}{\lambda(r_n^0(\mu), \mu) + r_n^0(\mu)\lambda_r(r_n^0(\mu), \mu)} \quad 0 \le n \le k-1 \\ \hat{\sigma}_k &= \frac{2r_k^0(\mu) - r_{k-1}^0(\mu)}{\lambda(r_k^0(\mu), \mu) + r_k^0(\mu)\lambda_r(r_k^0(\mu), \mu)} \end{aligned} \tag{4.15}$$

and we use the boundary conditions from (4.8) *separately for on- and off-site solution to determine the value of* (r_{-1}, ϕ_{-1}). *Furthermore, the linearization of* (4.11) *about this solution is invertible provided that* $r_n^0(\mu) \neq 0$ *for all* $1 \le n < k$, *and we can therefore continue it smoothly in* ε *to nonzero values of* ε.

Proof. The formula (4.15) can be derived from (4.11) upon setting phase lags ϕ_n, the frequency ω_0, and the parameter ε to zero. It remains to prove the claims about the linearization, which is of the form

$$D_{(\boldsymbol{\sigma}, \omega_0, \boldsymbol{\phi})}\mathscr{G}(\hat{\boldsymbol{\sigma}}, 0, \mathbf{0}, 0) = \begin{pmatrix} \mathbf{D}(\boldsymbol{r}^{\mathbf{0}}) & \mathbf{0} \\ \mathbf{0} & \boldsymbol{A}_{\mathrm{on/off}}(\boldsymbol{r}^{\mathbf{0}}) \end{pmatrix},$$

where $\mathbf{D}$ is an invertible diagonal matrix with nonzero diagonal entries given by $\mathbf{D}_{nn}(\boldsymbol{r}^{\mathbf{0}}) = \lambda(r_n^0(\mu), \mu) + r_n^0(\mu)\lambda_r(r_n^0(\mu), \mu)$, and the matrices $\boldsymbol{A}_{\mathrm{on/off}}$ for the phases encode the boundary conditions for, respectively, on- and off-site solutions through the $(1,2)$-th entry. We need to show that the matrices $\boldsymbol{A}_{\text{on/off}}$ are both invertible and we do this by computing its determinants via cofactor expansion and an induction argument, as follows. Focusing first on the off-site boundary condition case, we wish to compute

$$\det(\boldsymbol{A}_{\text{off}}(\boldsymbol{r^0})) = \begin{vmatrix} -r_0^0 & r_1^0 & 0 & 0 & 0 & \dots & 0 \\ -r_1^0 & -r_0^0 & r_2^0 & 0 & 0 & \dots & 0 \\ -r_2^0 & 0 & -r_1^0 & r_3^0 & 0 & \dots & 0 \\ \vdots & \vdots & & \ddots & \ddots & \ddots & \vdots \\ -r_{k-2}^0 & 0 & \dots & 0 & -r_{k-3}^0 & r_{k-1}^0 & 0 \\ -r_{k-1}^0 & 0 & \dots & \dots & 0 & -r_{k-2}^0 & r_k^0 \\ -r_k^0 & 0 & \dots & \dots & \dots & 0 & -r_{k-1}^0 \end{vmatrix}.$$

Via cofactor expansion, we find that

$$\det(\boldsymbol{A}_{\text{off}}) = -r_0^0 \det(\boldsymbol{A}_{\text{off}}(1|1)) - r_1^0 \det(\boldsymbol{A}_{\text{off}}(1|2)),$$

where

$$\boldsymbol{A}_{\text{off}}(1|1) = \begin{pmatrix} -r_0^0 & r_2^0 & 0 & 0 & \dots & 0 \\ 0 & -r_1^0 & r_3^0 & 0 & \dots & 0 \\ \vdots & & \ddots & \ddots & \ddots & \\ 0 & \dots & 0 & -r_{k-3}^0 & r_{k-1}^0 & 0 \\ 0 & \dots & \dots & 0 & -r_{k-2}^0 & r_k^0 \\ 0 & 0 & \dots & \dots & 0 & -r_{k-1}^0 \end{pmatrix}$$

and

$$\boldsymbol{A}_{\text{off}}(1|2) = \begin{pmatrix} -r_1^0 & r_2^0 & 0 & 0 & 0 & ... & 0 \\ -r_2^0 & -r_1^0 & r_3^0 & 0 & 0 & ... & 0 \\ -r_3^0 & 0 & -r_2^0 & r_4^0 & 0 & ... & 0 \\ \vdots & \vdots & & \ddots & \ddots & \ddots & \vdots \\ -r_{k-2}^0 & 0 & ... & 0 & -r_{k-3}^0 & r_{k-1}^0 & 0 \\ -r_{k-1}^0 & 0 & ... & ... & 0 & -r_{k-2}^0 & r_k^0 \\ -r_k^0 & 0 & ... & ... & ... & 0 & -r_{k-1}^0 \end{pmatrix}.$$

We observe that $\boldsymbol{A}_{\text{off}}(1|1)$ is simply an upper-triangular matrix, and thus we can easily compute its determinant. Furthermore, $\boldsymbol{A}_{\text{off}}(1|2)$ is of the same form as our original matrix, with the only change being that the element with the smallest index is r_1^0. Let us define the function

$$\psi(x_0, ..., x_k) \equiv \begin{vmatrix} -x_0 & x_1 & 0 & 0 & 0 & ... & 0 \\ -x_1 & -x_0 & x_2 & 0 & 0 & ... & 0 \\ -x_2 & 0 & -x_1 & x_3 & 0 & ... & 0 \\ \vdots & \vdots & & \ddots & \ddots & & \vdots \\ -x_{k-2} & ... & ... & ... & -x_{k-3} & x_{k-1} & 0 \\ -x_{k-1} & ... & ... & ... & ... & -x_{k-2} & x_k \\ -x_k & 0 & ... & ... & ... & ... & -x_{k-1} \end{vmatrix}.$$

Our cofactor expansion then shows that the determinant of interest satisfies the recurrence relation

$$\psi(r_0^0, r_1^0, ..., r_k^0) = (-1)^{k+1} r_0^0 \Big(\prod_{i=0}^{k-1} r_i^0 \Big) - r_1^0 \psi(r_1^0, r_2^0, ..., r_k^0).$$

Via a cofactor expansion very similar to what has already been performed, it is possibly to explicitly compute that

$$\psi(r^0_{k-3}, r^0_{k-2}, r^0_{k-1}, r^0_k) = \Big(\prod_{i=k-2}^{k-1} r^0_i \Big) \cdot \sum_{i=k-3}^{k} (r^0_i)^2.$$

We therefore assume that the solution to our recurrence relation is $\psi(r^0_0, ..., r^0_k) = (-1)^{k+1}\Big(\prod_{i=1}^{k-1} r^0_i \Big) \cdot \sum_{i=0}^{k} (r^0_i)^2$, which we verify by induction. Given the base case $\psi(r^0_{k-3}, r^0_{k-2}, r^0_{k-1}, r^0_k)$, we observe that

$$\begin{aligned}
\psi(r^0_0, r^0_1, ..., r^0_k) &= (-1)^{k+1} r^0_0 \Big(\prod_{i=0}^{k-1} r^0_i \Big) - r^0_1 \psi(r^0_1, r^0_2, ..., r^0_k) \\
&= (-1)^{k+1} r^0_0 \Big(\prod_{i=0}^{k-1} r^0_i \Big) - (-1)^k r^0_1 \Big(\prod_{i=2}^{k-1} r^0_i \Big) \cdot \sum_{i=1}^{k} (r^0_i)^2 \\
&= (-1)^{k+1} (r^0_0)^2 \Big(\prod_{i=1}^{k-1} r^0_i \Big) + (-1)^{k+1} \Big(\prod_{i=1}^{k-1} r^0_i \Big) \cdot \sum_{i=1}^{k} (r^0_i)^2 \\
&= (-1)^{k+1} \Big(\prod_{i=1}^{k-1} r^0_i \Big) [(r^0_0)^2 + \sum_{i=1}^{k} (r^0_i)^2] \\
&= (-1)^{k+1} \Big(\prod_{i=1}^{k-1} r^0_i \Big) \cdot \sum_{i=0}^{k} (r^0_i)^2.
\end{aligned}$$

as required. Thus, we find that our original determinant is

$$\det(\boldsymbol{A}_{\text{off}}(\boldsymbol{r^0})) = (-1)^{k+1} \Big(\prod_{i=1}^{k-1} r^0_i \Big) \cdot \sum_{i=0}^{k} (r^0_i)^2.$$

Turning now to the on-site phase block, we wish to compute

$$\det(\boldsymbol{A}_{\text{on}}(\boldsymbol{r^0})) = \begin{vmatrix} -r_0^0 & 2r_1^0 & 0 & 0 & 0 & \dots & 0 \\ -r_1^0 & -r_0^0 & r_2^0 & 0 & 0 & \dots & 0 \\ -r_2^0 & 0 & -r_1^0 & r_3^0 & 0 & \dots & 0 \\ \vdots & \vdots & & \ddots & \ddots & \ddots & \vdots \\ -r_{k-2}^0 & 0 & \dots & 0 & -r_{k-3}^0 & r_{k-1}^0 & 0 \\ -r_{k-1}^0 & 0 & \dots & \dots & 0 & -r_{k-2}^0 & r_k^0 \\ -r_k^0 & 0 & \dots & \dots & \dots & 0 & -r_{k-1}^0 \end{vmatrix}.$$

Proceeding via cofactor expansion once more, we find that

$$\begin{aligned} \det(\boldsymbol{A}_{\text{on}}) &= (-1)^{k+1} r_0^0 \prod_{i=0}^{k-1} r_i^0 - 2r_1^0 \psi(r_1^0, \dots, r_k^0) \\ &= (-1)^{k+1} r_0^0 \prod_{i=0}^{k-1} r_i^0 - (-1)^k 2 r_i^0 \Big(\prod_{i=2}^{k-1} r_i^0 \Big) \cdot \sum_{i=1}^{k} (r_i^0)^2 \\ &= (-1)^{k+1} \Big((r_0^0)^2 + 2 \sum_{i=1}^{k} (r_i^0)^2 \Big) \prod_{i=1}^{k-1} r_i^0, \end{aligned}$$

where we have used the results in the previous section. Summarizing these computations, we find that

$$\det(\boldsymbol{A}_{\text{off}}(\boldsymbol{r^0})) = (-1)^{k+1} \Big(\prod_{i=1}^{k-1} r_i^0 \Big) \cdot \sum_{i=0}^{k} (r_i^0)^2$$

and

$$\det(\boldsymbol{A}_{\text{on}}(\boldsymbol{r^0})) = (-1)^{k+1} \Big((r_0^0)^2 + 2 \sum_{i=1}^{k} (r_i^0)^2 \Big) \prod_{i=1}^{k-1} r_i^0.$$

Both determinants are nonzero given that $r_n^0(\mu) \neq 0$ for all $1 \leq n \leq k-1$, as required. $\square$

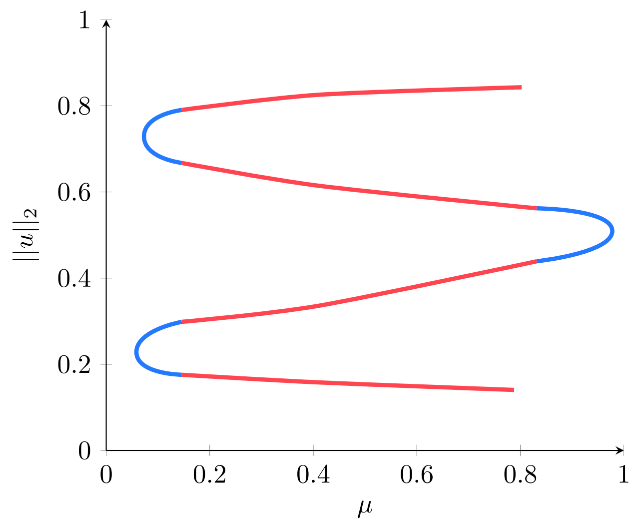

Figure 4.5: Constructing our snaking diagram. The portions of the curve coming from the bistability region are in red, and the regions where we rely on our blowup analysis are in blue.

4.4 In-phase solutions snake

We now discuss in-phase solutions to (4.8) near the boundaries $\mu = 0$ and $\mu = 1$ of the bistability region. We shall demonstrate that the system exhibits a Hopf bifurcation at $\mu = 0$ and a fold bifurcation of periodic orbits at $\mu = 1$. Our analysis is based on geometric blowup, which we carry out in two complementary coordinate charts. A diagram of our matching strategy can be found in Figure 4.5.

4.4.1 Fold bifurcation at $\mu = 1$

We begin with the fold bifurcation that occurs in the uncoupled amplitude equation for $(r, \mu) = (1, 1)$. We change coordinates near (r, μ) so that the uncoupled amplitude equation near $(r, \mu) = (1, 1)$ is put into the normal form

$$r\lambda(r, \mu) = (1 - \mu) - (1 - r)^2 + \mathcal{O}(|1 - \mu|^2, |1 - r|^3).$$

Motivated by this expansion, we introduce the ansatz

$$\varepsilon = \tilde{\varepsilon}\nu^2, \qquad \mu = 1 - \tilde{\mu}\nu^2, \qquad r_n = \begin{cases} 1 + \nu\sigma_n, & 0 \leq n \leq k \\ \left[\frac{\tilde{\varepsilon}\nu^2}{\lambda(0,1)}\right]^{n-k} \sigma_n, & k+1 \leq n \leq N. \end{cases} \tag{4.16}$$

Substituting these expressions into (4.8), dividing out by the highest power of ν and $\tilde{\varepsilon}$ in each equation, and rearranging the result into core and far-field modes, we obtain the core amplitude system

$$\begin{aligned} 0 &= \tilde{\mu} - \sigma_n^2 + \tilde{\varepsilon}[\cos(\phi_n) + \cos(\phi_{n-1}) - 2] + \mathcal{O}^{\mathrm{u}}(\nu) && 0 \leq n \leq k-1 \\ 0 &= \tilde{\mu} - \sigma_k^2 + \tilde{\varepsilon}[\cos(\phi_{k-1}) - 2] + \mathcal{O}^{\mathrm{u}}(\nu) && n = k, \end{aligned} \tag{4.17}$$

the core phase system

$$\begin{aligned} 0 &= -\omega_0 + \sin(\phi_n) - \sin(\phi_{n-1}) + \mathcal{O}^{\mathrm{u}}(\nu) && 0 \leq n \leq k-1 \\ 0 &= -\omega_0 - \sin(\phi_{k-1}) + \mathcal{O}^{\mathrm{u}}(\nu) && n = k, \end{aligned} \tag{4.18}$$

where $\phi_{-1} := -\phi_0$ for on-site and $\phi_{-1} := 0$ for off-site solutions, and the far-field system

$$\begin{aligned} 0 &= \sigma_{k+1} + \cos(\phi_k) + \mathcal{O}^{\mathrm{u}}(\nu) && n = k+1 \\ 0 &= \sigma_n + \sigma_{n-1}\cos(\phi_{n-1}) + \mathcal{O}^{\mathrm{u}}(\nu) && k+2 \leq n \leq N \\ 0 &= -\sin(\phi_k) + \mathcal{O}^{\mathrm{u}}(\nu) && n = k+1 \\ 0 &= -\sigma_{n-1}\sin(\phi_{n-1}) + \mathcal{O}^{\mathrm{u}}(\nu) && k+2 \leq n \leq N, \end{aligned} \tag{4.19}$$

where the $\mathcal{O}^{\mathrm{u}}(\nu)$ terms are uniform in $\tilde{\varepsilon} \geq 0$. The system (4.19) agrees with the far-field equation (4.12). Lemma 4.3.2 therefore guarantees that we can solve (4.19) uniquely for $(\sigma_n)_{k<n\leq N}$ and $(\phi_n)_{k\leq n<N}$ as smooth functions of $(\sigma_k, \phi_{k-1}, \tilde{\varepsilon}, \nu)$, and substituting this solution into (4.17)-(4.18) does not change the leading-order terms. Next, separately for on- and off-site solutions, we can solve the system (4.18) uniquely for $(\phi_n)_{0\leq n<k}$ and ω_0 near $(\phi, \omega_0) = 0$ as a smooth function of ν. The details are

identical to the bistability case. Substituting this solution into the remaining system (4.17) and using $(\phi_n)_{k\le n<N} = \mathcal{O}^{\mathrm{u}}(\nu)$, we finally arrive at the system

$$\begin{aligned} 0 &= \tilde{\mu} - \sigma_n^2 + \mathcal{O}^{\mathrm{u}}(\nu) && 0 \le n \le k-1 \\ 0 &= \tilde{\mu} - \sigma_k^2 - \tilde{\varepsilon} + \mathcal{O}^{\mathrm{u}}(\nu) && n = k \end{aligned} \tag{4.20}$$

for $(\sigma_n)_{0\le n\le k}$ and $(\tilde{\mu}, \tilde{\varepsilon}, \nu)$ with $0 \le \nu \ll 1$. We consider (4.20) separately in the coordinate charts $\tilde{\varepsilon} = 1$ and $\tilde{\mu} = 2$.

4.4.1.1 Solving in the chart $\tilde{\varepsilon} = 1$.

For $\tilde{\varepsilon} = 1$, the system (4.20) is given by

$$\begin{aligned} 0 &= \tilde{\mu} - \sigma_n^2 + \mathcal{O}^{\mathrm{u}}(\nu) && 0 \le n \le k-1 \\ 0 &= \tilde{\mu} - \sigma_k^2 - 1 + \mathcal{O}^{\mathrm{u}}(\nu) && n = k. \end{aligned} \tag{4.21}$$

For $\nu = 0$, its solutions are given by

$$\sigma_k := s, \qquad \tilde{\mu} = s^2 + 1, \qquad (\sigma_n)_{0\le n<k} = \sqrt{s^2+1} \qquad \text{where } |s| \le 1,$$

and we can solve (4.21) uniquely for $((\sigma_n)_{0\le n<k}, \tilde{\mu})$ as smooth functions of $\sigma_k = s \in [-1, 1]$ and $0 \le \nu \ll 1$. A slight extension of this argument shows that the family of solutions we just constructed exhibits a fold bifurcation for $(\tilde{\mu}, \sigma_k) = (\tilde{\mu}^{\mathrm{fold}}, \sigma_k^{\mathrm{fold}})(\nu) = (1 + \mathcal{O}^{\mathrm{u}}(\nu^2), \mathcal{O}^{\mathrm{u}}(\nu))$. We simply augment (4.21) by setting the derivative of the right-hand side of the latter equation with respect to σ_k to zero. This yields

$$\begin{aligned} 0 &= \tilde{\mu} - \sigma_n^2 + \mathcal{O}^{\mathrm{u}}(\nu) && 0 \le n \le k-1 \\ 0 &= \tilde{\mu} - \sigma_k^2 - 1 + \mathcal{O}^{\mathrm{u}}(\nu) && n = k \\ 0 &= -2\sigma_k + \mathcal{O}^{\mathrm{u}}(\nu) && n = k. \end{aligned} \tag{4.22}$$

Which has $((\sigma_n)_{0\leq n<k}, \tilde{\mu}, \sigma_k) = (\mathbf{0}, 1, 0)$ as a solution for $\nu = 0$. We can then solve (4.22) uniquely near this solution for $0 \leq \nu <\ll 1$.

Returning to our original coordinates, we showed that there is a $\delta > 0$ so that

$$\mu = 1-(1+s^2+\mathcal{O}(\sqrt{\varepsilon}))\varepsilon, \quad r_k = 1+s\sqrt{\varepsilon}+\mathcal{O}(\varepsilon), \quad (r_n)_{0\leq n<k} = 1+\sqrt{(1+s^2)\varepsilon}+\mathcal{O}(\varepsilon) \tag{4.23}$$

for $s \in [-1, 1]$ and $0 \leq \varepsilon \leq \delta$, which exhibits a fold bifurcation for $s = s^{\text{fold}}(\varepsilon) = \mathcal{O}(\sqrt{\varepsilon})$.

4.4.1.2 Solving in the chart $\tilde{\mu} = 2$.

Setting $\tilde{\mu} = 2$, the system (4.20) becomes

$$\begin{aligned} 0 &= 2 - \sigma_n^2 + \mathcal{O}^{\mathrm{u}}(\nu) && 0 \leq n \leq k-1 \\ 0 &= 2 - \sigma_k^2 - \tilde{\varepsilon} + \mathcal{O}^{\mathrm{u}}(\nu) && n = k. \end{aligned} \tag{4.24}$$

For $\nu = 0$, its solutions are given by

$$\sigma_k := s, \qquad \tilde{\varepsilon} = 2 - s^2, \qquad (\sigma_n)_{0\leq n<k} = 1 \qquad \text{where } |s| \leq 2,$$

and we can solve (4.24) uniquely for $((\sigma_n)_{0\leq n<k}, \tilde{\varepsilon}) = (1, 2 - s^2) + \mathcal{O}^{\mathrm{u}}(\nu)$ as smooth functions of $\sigma_k = s \in [-2, 2]$ and $0 \leq \nu \ll 1$. These results provide a description of the solution branch for each fixed $\mu = 1 - 2\nu^2$ as a function of $\varepsilon = \tilde{\varepsilon}\nu^2 = \tilde{\varepsilon}(1 - \frac{\mu}{2})$ where $\tilde{\varepsilon} = 2 - s^2$ for $|s| \leq 2$. These solutions intersect $\tilde{\varepsilon} = 0$ in exactly two unique points at which $s = \sigma_k = \pm\sqrt{2} + \mathcal{O}^{\mathrm{u}}(\nu)$. Thus, there is a $\delta > 0$ so that the original core amplitudes are given by

$$\begin{aligned} &\varepsilon = \frac{(2 - s^2 + \mathcal{O}(\sqrt{1-\mu}))(1-\mu)}{2}, \quad r_k = 1 + \frac{s\sqrt{2(1-\mu)}}{2} + \mathcal{O}(|1-\mu|), \\ &(r_n)_{0\le n<k} = 1 + \frac{\sqrt{2(1-\mu)}}{2} + \mathcal{O}(|1-\mu|) \end{aligned} \tag{4.25}$$

for $s \in [-2, 2]$ and $0 \le 1 - \mu \le \delta$, where $\varepsilon = 0$ precisely when $s = s^{\pm}(\mu) = \pm\sqrt{2} + \mathcal{O}(\sqrt{|1-\mu|})$.

4.4.1.3 Combining the results from the two coordinate charts.

Comparing the expressions in (4.23) and (4.25) completes the proof of Theorem 4.2.1 near $\mu = 1$. We depict how the solutions in the different blowup charts match with the solutions from the bistability region in Figure 4.6. More explicitly, we follow the solutions in the chart $\tilde{\mu} = 2$ for $s \approx -\sqrt{2}$ until $s \approx -1$, at which point we switch to the chart $\tilde{\varepsilon} = 1$ and unfold the saddle node bifurcation by varying s from approximately -1 to 1. We then return to the chart $\tilde{\mu} = 2$ to reconnect to the solutions computed in the bistable region, varying s from approximately $s = 1$ to $s = \sqrt{2}$.

Remark 15. The preceding derivation illustrates the difficulty of constructing anti-phase solutions with $\phi_n = \pi + \mathcal{O}^{\mathrm{u}}(\nu)$, since, instead of (4.20), we would have obtained the system

$$\begin{aligned} 0 &= \tilde{\mu} - \sigma_0^2 - 2\tilde{\varepsilon} + \mathcal{O}^{\mathrm{u}}(\nu) \quad && n = 0 \\ 0 &= \tilde{\mu} - \sigma_n^2 - 4\tilde{\varepsilon} + \mathcal{O}^{\mathrm{u}}(\nu) \quad && 0 < n < k \\ 0 &= \tilde{\mu} - \sigma_k^2 - 3\tilde{\varepsilon} + \mathcal{O}^{\mathrm{u}}(\nu) \quad && n = k, \end{aligned}$$

where the nodes for $0 < n < k$ exhibit a simultaneous fold bifurcation at $\sigma_n = 0$ for $\tilde{\mu} = 4\tilde{\varepsilon}$. It is not possible to unfold this nongeneric bifurcation without knowledge of the higher-order terms.

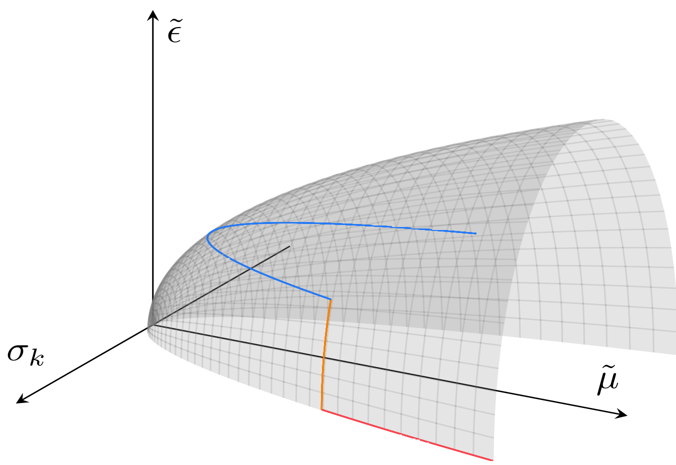

Figure 4.6: When $\tilde{\varepsilon} = 0$, we follow solutions from the bistable regime (red). We then connect to our solutions in the chart $\tilde{\varepsilon} = 1$ via those in the chart $\tilde{\mu} = 2$ (orange). Finally, we follow the solutions from our $\tilde{\varepsilon} = 1$ chart (blue) to unfold the saddle-node bifurcation. We follow the charts in the opposite direction to rejoin the bistable branch.

4.4.2 Hopf bifurcation at $\mu = 0$

To begin, we change coordinates so that the form of the uncoupled oscillator equation near $(r, \mu) = (0, 0)$ is in the normal form for a subcritical pitchfork bifurcation,

$$r\lambda(r, \mu) = -\mu r + r^3 + \mathcal{O}(r^2|\mu|, |r|\mu^2, r^4).$$

We shall assume that we have rescaled our variables so that $r_+(0) = 1$. We then propose

$$\varepsilon = \tilde{\varepsilon}\nu^3, \qquad \mu = \tilde{\mu}\nu^2, \qquad r_n = \begin{cases} 1 + \sigma_n, & 0 \leq n \leq k-1 \\ \nu\sigma_k & n = k \\ \left(\frac{\tilde{\varepsilon}}{\tilde{\mu}}\right)^{n-k} \nu^{n-k}\sigma_k\sigma_n, & k+1 \leq n \leq N \end{cases} \tag{4.26}$$

as a solution ansatz. Substituting into (4.8) and dividing out by the highest powers of ν, σ_k, $\tilde{\varepsilon}$, and $\tilde{\mu}^{-1}$ in each equation, we obtain the core amplitude equations

$$\begin{aligned} 0 &= (1+\sigma_n)\lambda_r(1,0)\sigma_n + \mathcal{O}^{\mathrm{u}}(\nu) && 0 \le n \le k-1 \\ 0 &= -\tilde{\mu}\sigma_k + \sigma_k^3 + \tilde{\varepsilon}(1+\sigma_{k-1})\cos(\phi_{k-1}) + \mathcal{O}^{\mathrm{u}}(\nu) && n = k, \end{aligned} \tag{4.27}$$

the core phase equations

$$\begin{aligned} 0 &= -\omega_0 + [\sin(\phi_n) - \sin(\phi_{n-1})] + \mathcal{O}^{\mathrm{u}}(\nu) && 0 \le n \le k-2 \\ 0 &= -\omega_0 - \sin(\phi_{k-2}) + \mathcal{O}^{\mathrm{u}}(\nu) && n = k-1 \\ 0 &= -\sin(\phi_{k-1}) + \mathcal{O}^{\mathrm{u}}(\nu) && n = k, \end{aligned} \tag{4.28}$$

and the far-field system

$$\begin{aligned} 0 &= -\sigma_{k+1} + \cos(\phi_k) + \mathcal{O}^{\mathrm{u}}(\nu) && n = k+1 \\ 0 &= -\sigma_n + \sigma_{n-1}\cos(\phi_{n-1}) + \mathcal{O}^{\mathrm{u}}(\nu) && k+2 \le n \le N \\ 0 &= -\sin(\phi_k) + \mathcal{O}^{\mathrm{u}}(\nu) && n = k+1 \\ 0 &= -\sigma_{n-1}\sin(\phi_{n-1}) + \mathcal{O}^{\mathrm{u}}(\nu) && k+2 \le n \le N. \end{aligned} \tag{4.29}$$

Via Lemma 4.3.2, we can solve system (4.29) in terms of $(\phi_{k-1}, \tilde{\varepsilon}, \tilde{\mu}, \nu)$ and substitute these results into our core systems, without altering them at leading order. Separately for on-site and off-site boundary conditions, we can then solve (4.28) near $(\phi, \omega_0) = \mathbf{0}$ as a smooth function of ν. Substituting into the core amplitude equations yields

$$\begin{aligned} 0 &= (1+\sigma_n)\lambda_r(1,0)\sigma_n + \mathcal{O}^{\mathrm{u}}(\nu) && 0 \le n \le k-1 \\ 0 &= -\tilde{\mu}\sigma_k + \sigma_k^3 + \tilde{\varepsilon}(1+\sigma_{k-1}) + \mathcal{O}^{\mathrm{u}}(\nu) && n = k. \end{aligned} \tag{4.30}$$

The equations for the modes $0 \le n \le k-1$ can then be solved near $(\sigma_n)_{0 \le n < k} = \mathbf{0}$. Therefore, $\sigma_{k-1} = \mathcal{O}^u(\nu)$ and we can focus our efforts on the equation

$$0 = -\tilde{\mu}\sigma_k + \sigma_k^3 + \tilde{\varepsilon} + \mathcal{O}^{\mathrm{u}}(\nu) \tag{4.31}$$

We shall now consider (4.31) separately in the charts $\tilde{\varepsilon} = 1$ and $\tilde{\mu} = 2$.

4.4.2.1 Solving in the chart $\tilde{\varepsilon} = 1$.

In this chart, we obtain

$$0 = -\tilde{\mu}\sigma_k + \sigma_k^3 + 1 + \mathcal{O}^{\mathrm{u}}(\nu) \tag{4.32}$$

Which has $(\sigma_k, \tilde{\mu}, \nu) = (s, \frac{1+s^3}{s}, 0)$ as a solution for any positive s. We can thus solve (4.32) uniquely for $\tilde{\mu}$ as a smooth function of s and $0 \leq \nu \ll 1$. An extension of this argument demonstrates that this family of solutions also exhibits a fold bifurcation, at

$$(\sigma_k, \tilde{\mu}) = (\tilde{\mu}^{\mathrm{fold}}, \sigma_k^{\mathrm{fold}})(\nu) = \left(\frac{1}{\sqrt[3]{2}}, \frac{3}{2}\sqrt[3]{2}\right) + \mathcal{O}^{\mathrm{u}}(\nu). \tag{4.33}$$

The methodology for computing this solution is precisely the same as the one found near $\mu = 1$. We augment (4.32) by setting the derivative of the right-hand side with respect to σ_k equal to zero, which yields

$$0 = -\tilde{\mu}\sigma_k + \sigma_k^3 + 1 + \mathcal{O}^{\mathrm{u}}(\nu) \tag{4.34}$$

$$0 = -\tilde{\mu} + 3\sigma_k^2 + \mathcal{O}^{\mathrm{u}}(\nu). \tag{4.35}$$

This equation has $(\sigma_k, \tilde{\mu}) = \left(\frac{1}{\sqrt[3]{2}}, \frac{3}{2}\sqrt[3]{2}\right)$ as a solution for $\nu = 0$, and we can solve it in a neighborhood of this point for $0 \leq \nu \ll 1$.

We also wish to show that the solutions computed in this chart connect with those computed in the chart $\tilde{\mu} = 2$. To that end, we must show that there exists two values of s such that $\tilde{\mu}(s, \nu) = 2$ for each $\nu \geq 0$ small. In other words, we seek two

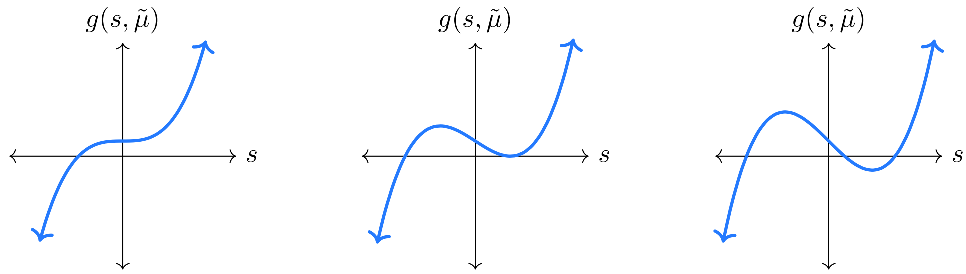

(a) $\tilde{\mu} < \tilde{\mu}_*$ (b) $\tilde{\mu} = \tilde{\mu}_*$ (c) $\tilde{\mu} > \tilde{\mu}_*$

Figure 4.7: As $\tilde{\mu}$ is increased, the cubic $f(\sigma_{k+1}) = -2\sigma_{k+1} + \sigma_{k+1}^3 + \tilde{\varepsilon}$ goes from having one real root to three.

roots of

$$0 = g(s, 2) + \mathcal{O}^{\mathrm{u}}(\nu) \tag{4.36}$$

where $g(s, \tilde{\mu}) := -\tilde{\mu} + s^3 + 1$. Explicit calculation shows that $g(s, 2)$ has two positive real roots,

$$s_- = \frac{\sqrt{5} - 1}{2}, \qquad s_+ = 1. \tag{4.37}$$

Furthermore, we note that

$$\frac{\partial g(s_\pm, 2)}{\partial s} = -2 + 3s_\pm^2 \neq 0,$$

which establishes the claim. We depict the situation geometrically in Figure 4.7. Returning to our original coordinates, we see that after shrinking the $\delta > 0$ from the previous section if necessary that

$$\mu = \Big(\frac{1 + s^3}{s} + \mathcal{O}(\sqrt[3]{\varepsilon})\Big)\varepsilon^{2/3}, \quad r_k = \Big(s + \mathcal{O}(\varepsilon^{1/3})\Big)\varepsilon^{1/3} \tag{4.38}$$

for $s \in [\frac{1}{2}, \frac{3}{2}]$ and $0 \leq \varepsilon \leq \delta$, with a fold bifurcation occuring at $s = s^{\mathrm{fold}} = \frac{1}{\sqrt[3]{2}} + \mathcal{O}(\varepsilon^{1/3})$.

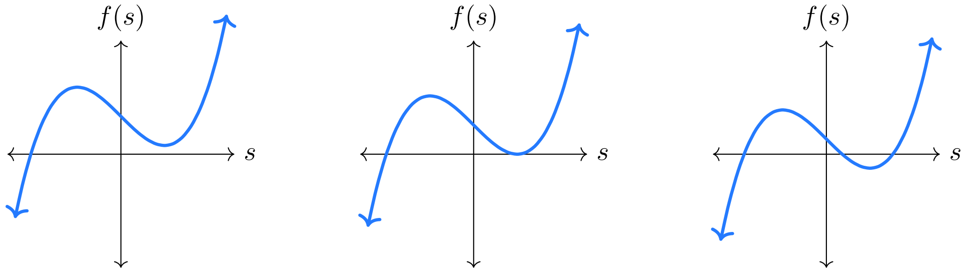

(a) $\tilde{\varepsilon} > \tilde{\varepsilon}_*$ (b) $\tilde{\varepsilon} = \tilde{\varepsilon}_*$ (c) $\tilde{\varepsilon} < \tilde{\varepsilon}_*$

Figure 4.8: For small enough $\tilde{\varepsilon}$, $f(s) = -2s + s^3 + \tilde{\varepsilon}$ has 2 positive real roots.

4.4.2.2 Solving in the chart $\tilde{\mu} = 2$.

We now set $\tilde{\mu} = 2$, so that (4.30) becomes

$$0 = -2\sigma_k + \sigma_k^3 + \tilde{\varepsilon} + \mathcal{O}^{\mathrm{u}}(\nu) \tag{4.39}$$

which has $(\sigma_k, \tilde{\varepsilon}, \nu) = (s, s(2-s^2), 0)$ as solutions. Thus, we can solve for $\tilde{\varepsilon}$ as a smooth function of s and $0 \le \nu \ll 1$. These results represent solutions with fixed $\mu = 2\nu^2$ as a function of $\varepsilon = \tilde{\varepsilon}\nu^3 = \frac{\tilde{\varepsilon}\mu^{3/2}}{2^{3/2}}$, and they intersect $\tilde{\varepsilon} = 0$ in two points: $\sigma_k = 0, \sqrt{2} + \mathcal{O}^{\mathrm{u}}(\nu)$. The situation is depicted geometrically in Figure 4.8.

Therefore, we see that after potentially shrinking the $\delta > 0$ found in the section near $\mu = 1$,

$$\varepsilon = \frac{\Big(s(2-s^2) + \mathcal{O}(\sqrt{\mu})\Big)\mu^{3/2}}{2^{3/2}}, \quad r_k = \frac{\Big(s + \mathcal{O}(\sqrt{\mu})\Big)\sqrt{2\mu}}{2} \tag{4.40}$$

for $s \in [-2, 2]$ and $0 \le \mu < \delta$. Finally, we have that $\varepsilon = 0$ when $s = 0, 1 + \mathcal{O}(\sqrt{\mu})$.

4.4.2.3 Combining the results from both charts.

In precisely the same manner as we did near $\mu = 1$, comparing (4.38) and (4.40) completes the proof of Theorem 4.2.1 near $\mu = 0$. As in §4.4.1.3, we follow the solutions in the chart $\tilde{\mu} = 2$ from $s \approx 0$ to $s \approx s_{-}$, unfold the bifurcation in the chart $\tilde{\varepsilon} = 1$ by varying s from approximately s_{-} to 1, then return to the chart $\tilde{\mu} = 2$ and vary s from approximately 1 to $\sqrt{2}$ to rejoin the bistable branch.

4.5 Discussion

In this chapter, we have rigorously demonstrated snaking behavior for weakly-coupled Ginzburg–Landau oscillators. However, a number of open problems remain. Primary among them is leveraging the analytical methods established herein to better understand the localized oscillations in the mechanical system (4.2). In particular, it would be important to establish what the phase-locking conditions are inside each of the Arnold tongues, similar to what was done in Section 4.3 for our coupled Ginzburg–Landau system. This would establish the relative phase discrepancies which could in turn help to explain the exotic isolas that solutions lie along, such as in Figure 4.1. We conjecture that it is bifurcations coming from these relative phase differences that drive the various saddle-node bifurcations inside the parameter regime where the original periodic orbits of the uncoupled system are hyperbolic.

There are many questions that remain open with our Ginzburg–Landau model as well. For example, with the motivating nonlinearities (4.4) and (4.5), is it possible to track the bifurcation curves from the small $|q|$ regime of Theorem 4.2.1 to the large $|q|$ parameter regime and establish that they are connected in phase space? Our preliminary numerics indicate that we should see qualitatively different behavior in this strong-coupling regime, such as phase-locking. At the intermediary ranges of $|q|$ we could better capture the varying periods of oscillation for the periodic orbits of the uncoupled system that are observed in the right panel of Figure 4.2 for the mechanical system (4.2). However, such a parameter regime would be difficult to explore analytically. Our preliminary numerics also seemed to indicate that anti-phase solutions may lie on isolas. Establishing this fact rigorously will require a more detailed analysis of higher-order terms than the in-phase case, as we have remarked. Yet another avenue for future investigation would be establishing the stability of the localized oscillations. We expect that analysis should proceed similarly to the proofs in Bramburger (2020) and yield exponential convergence to the amplitude components r_n and significantly slower algebraic convergence into the phase differences $\theta_n - \theta_{n-1}$. In summary, there are a number of directions that future investigations that can branch off from our novel analytical treatment of localized oscillations developed herein.

Chapter Five

Conclusion

5.1 Summary of contributions

The work in this thesis can be divided into three areas. First and foremost, we examined candidate toy models for the phenomenon of temporal pulse replication. We detailed the drawbacks and inadequacies of these models, in order to inform the search for improved models in the future.

Due to the difficulty of the temporal pulse replication problem, we also analyzed the simpler problem of the stability of spatially-homogeneous solutions to the Fitzhugh–Nagumo model. We demonstrated that as a base solution to the underlying kinetic equations drifts along the slow manifold, the deviation between the solution to the kinetic equations and the full Fitzhugh–Nagumo system decays algebraically. In doing so, we established the utility of pointwise methods in this context, since semigroup methods are insensitive to such decay rates. Ultimately, we were able to prove that the decay takes place on the fast timescale, so that solutions to the full PDEs and the kinetic equations become close even with a weaker rate of decay than in standard Fenichel theory. Morally speaking, we determine that although the presence of diffusion breaks the precise geometric picture needed to apply Fenichel theory, enough structure remains to salvage some decay near the slow manifold. We also presented proofs that the offsets between ODE and PDE solutions remain bounded during a fast jump, and derived bounds on quantities that must be controlled in order to conclude that solutions remain close in a neighborhood of the fold point as well.

Finally, we turned to the problem of analyzing weakly coupled bistable oscillators. We were able to demonstrate that in-phase solutions exhibit snaking behavior. The main challenge was the more general character of the function $\omega(r, \mu, \varepsilon)$ relative to previous work, which makes solving the phase equations more complicated. We demonstrated that the equations can nonetheless be solved, with the help of a core-far-field decomposition and a blowup to match hyperbolic solutions with those arising from a bifurcation.

5.2 Future directions

Each of these projects holds some possibilities for future study. The most obvious of these is the analysis of temporal pulse replication. In order to find a useful toy model for this phenomenon, it may be necessary to consider infinite-dimensional examples instead of attempting to project down to finitely-many dimensions.

In the study of the stability of spatially-homogeneous solutions to the Fitzhugh–Nagumo model, a full analysis near the fold point remains elusive. The bounds derived in this thesis are not strong enough to close a bootstrapping argument and show that solutions to the full PDE system remain close to the solutions to the kinetic system. As an additional note, in the analysis of the fold different assumptions about the size of the parameter γ were made than in the case of the fast jump or drift near the slow manifold. In order to completely characterize the solutions of the PDE in terms of the ODE, this discrepancy must be reconciled.

Lastly, we note that in addition to the directions mentioned in the discussion section of the chapter on coupled oscillators, we were forced to restrict ourselves to a finite number of modes. While the technical hurdles to extending the far-field lemma to infinitely-many oscillators without any changes to the underlying solution spaces are clear, it may still be possible to find some appropriately weighted space in which we can derive a stronger result. If a candidate space can be found, the proofs given here should extend fairly immediately to this more general setting.

Chapter Six

Appendices

6.1 Appendix A: Variational equations and coordinate transformations

In Chapter 2, we made use of Fenichel normal form to argue that our algebraic decay results were the best that one could expect to obtain as our ansatz $(u_\varepsilon^{\mathrm{ODE}}, w_\varepsilon^{\mathrm{ODE}})$ drifted near the slow manifold. In carrying out this analysis, we made use of the fact that the variational equations of a pair of ODEs linked by a coordinate transformation are also related in a very specific way. We summarize this connection in the following lemma.

Lemma 6.1.1. *Let us suppose that we are given a system of ODEs $\dot{u} = f(u)$, $f : \mathbb{R}^n \to \mathbb{R}^n$ and a diffeomorphism $g : \mathbb{R}^n \to \mathbb{R}^n$ with inverse $h : \mathbb{R}^n \to \mathbb{R}^n$. If we define $v(t) := g(u(t))$, then the following conclusions hold.*

1. *$\dot{v} = F(v)$, where $F(v) \equiv g_u(h(v))f(h(v))$*
2. *If $\tilde{u}$ solves the variational equation $\dot{\tilde{u}} = f_u(u)\tilde{u}$, then $g_u(u)\tilde{u}$ solves the variational equation for our transformed system, $\dot{\tilde{v}} = F_v(v)\tilde{v}$*

Proof. Both conclusions follow by direct calculation. Regarding the first, we have that

$$\begin{aligned}
\dot{v} &= g_u(u)\dot{u} \\
&= g_u(u)f(u) \\
&= g_u(h(v))f(h(v)) \\
&= F(v).
\end{aligned}$$

To prove the second conclusion, we will proceed in a component-wise fashion. To simplify the presentation, we shall also observe the **Einstein summation convention**: repeated indices are summed over. For example,

$$[g_u(u)\tilde{u}]_i = \frac{\partial g_i}{\partial u_j}\tilde{u}_j.$$

Since h and g are inverses, we have that $h(g(u)) = u$, and therefore that

$$\begin{aligned}
\delta_{ij} &= \frac{\partial u_i}{\partial u_j} \\
&= \frac{\partial}{\partial u_j}[h(g(u))]_i \\
&= \frac{\partial h_i}{\partial v_k}\frac{\partial g_k}{\partial u_j}
\end{aligned}$$

With this fact in hand, we now compute $\frac{d}{dt}[g_u(u)\tilde{u}]$ and $F_v(v)g_u(u)\tilde{u}$ and demonstrate that they are equal. Regarding the first of these quantities, we find that

$$\begin{aligned}
\frac{d}{dt}[g_u(u)\tilde{u}]_i &= \frac{\partial^2 g_i}{\partial u_j \partial u_k}\dot{u}_k\tilde{u}_j + \frac{\partial g_i}{\partial u_j}\dot{\tilde{u}}_j \\
&= \frac{\partial^2 g_i}{\partial u_j \partial u_k}\dot{u}_k\tilde{u}_j + \frac{\partial g_i}{\partial u_j}\frac{\partial f_j}{\partial u_k}\tilde{u}_k \\
&= \frac{\partial^2 g_i}{\partial u_j \partial u_k} f_k\tilde{u}_j + \frac{\partial g_i}{\partial u_j}\frac{\partial f_j}{\partial u_k}\tilde{u}_k.
\end{aligned}$$

Turning to the second, we have that

$$\frac{\partial F_i}{\partial v_j} = \frac{\partial^2 g_i}{\partial u_k \partial u_l}\frac{\partial u_l}{\partial v_j} f_k + \frac{\partial g_i}{\partial u_k}\frac{\partial f_k}{\partial u_l}\frac{\partial u_l}{\partial v_j}$$

Multiplying both sides by $[g_u(u)\tilde{u}]_j$, we find that

$$\begin{aligned}
\frac{\partial F_i}{\partial v_j}[g_u(u)\tilde{u}]_j &= \frac{\partial^2 g_i}{\partial u_k \partial u_l}\frac{\partial u_l}{\partial v_j} f_k [g_u(u)\tilde{u}]_j + \frac{\partial g_i}{\partial u_k}\frac{\partial f_k}{\partial u_l}\frac{\partial u_l}{\partial v_j}[g_u(u)\tilde{u}]_j \\
&= \frac{\partial^2 g_i}{\partial u_k \partial u_l}\frac{\partial u_l}{\partial v_j} f_k \frac{\partial g_j}{\partial u_m}\tilde{u}_m + \frac{\partial g_i}{\partial u_k}\frac{\partial f_k}{\partial u_l}\frac{\partial u_l}{\partial v_j}\frac{\partial g_j}{\partial u_m}\tilde{u}_m \\
&= \frac{\partial^2 g_i}{\partial u_k \partial u_l} f_k \tilde{u}_l + \frac{\partial g_i}{\partial u_k}\frac{\partial f_k}{\partial u_l}\tilde{u}_l
\end{aligned}$$

which is equal to our previous result up to a renaming of the indices. In the derivation above, we have used the fact that $\frac{\partial u_l}{\partial v_j} = \frac{\partial h_l}{\partial v_j}$. Combined with our result on the products of partial derivatives of h and g, we could then contract along l and m in the final line. $\square$

Lemma 6.1.1 is best understood in the context of differential geometry. The solutions to the ODEs $\dot{u} = f(u)$ and $\dot{v} = F(v)$ form curves embedded in n-dimensional space. The variational equation then describes how vectors in the tangent space evolve as one transports them along the curve. Written in terms of the directional derivative, the variational equations are

$$\dot{\tilde{u}} = \nabla_{\tilde{u}} f(u) \tag{6.1}$$

and

$$\dot{\tilde{v}} = \nabla_{\tilde{v}} F(v). \tag{6.2}$$

Understood in this context, our lemma says that if the solutions to two systems of ODEs are the images of each other under a diffeomorphism, then one can compute solutions to the variational equation of one by computing the **pushforward** of solutions to the other. Indeed, every instance of u and $\tilde{u}$ in (6.1) has been replaced by its pushforward in (6.2).

Given this geometric interpretation, one might imagine that the relationship between (6.1) and (6.2) might still hold even if a source term was added to the right-hand side of (6.1). The only modification would be that one would add the pushforward of this source term to the right-hand side of (6.1). We prove this statement in the following lemma.

Lemma 6.1.2. *Let us suppose that we are given a system of ODEs* $\dot{u} = f(u)$,

$f : \mathbb{R}^n \to \mathbb{R}^n$ and a diffeomorphism $g : \mathbb{R}^n \to \mathbb{R}^n$ with inverse $h : \mathbb{R}^n \to \mathbb{R}^n$. If $\tilde{u}$ solves

$$\dot{\tilde{u}} = \nabla_{\tilde{u}} f(u(t)) + z(t)$$

then $g_u(u)\tilde{u}$ satisfies

$$\dot{\tilde{v}} = \nabla_{\tilde{v}} F(v(t)) + g_u(h(v))z(t)$$

Proof. We have that

$$\begin{aligned}
\frac{d}{dt}[g_u(u)\tilde{u}]_i &= \frac{\partial^2 g_i}{\partial u_j \partial u_k}\dot{u}_k\tilde{u}_j + \frac{\partial g_i}{\partial u_j}\dot{\tilde{u}}_j \\
&= \frac{\partial^2 g_i}{\partial u_j \partial u_k}\dot{u}_k\tilde{u}_j + \frac{\partial g_i}{\partial u_j}\left[\frac{\partial f_j}{\partial u_k}\tilde{u}_k + z_j\right] \\
&= \left[\frac{\partial^2 g_i}{\partial u_j \partial u_k}\dot{u}_k\tilde{u}_j + \frac{\partial g_i}{\partial u_j}\frac{\partial f_j}{\partial u_k}\tilde{u}_k\right] + \frac{\partial g_i}{\partial u_j}z_j \\
&= \frac{\partial F_i}{\partial v_j}[g_u(u)\tilde{u}]_j + \frac{\partial g_i}{\partial u_j}z_j
\end{aligned}$$

where we have made use of the computations in the proof of Lemma 6.1.1 in the final line. □

6.2 Appendix B: The form of the phase coupling hypothesis

We discuss the necessity of taking $\omega(r,\mu,\varepsilon) = \Omega(\mu) + \mathcal{O}(\varepsilon^2)$ in Hypothesis 2, as opposed to the more intuitive $\omega(r,\mu,\varepsilon) = \Omega(\mu) + \mathcal{O}(\varepsilon)$. Let us suppose that we make the same substitutions as we have made above, with the exception that $\omega(r,\mu,\varepsilon) = \Omega(\mu) + \varepsilon g(r,\mu)$. Our phase equations in the core become

$$\begin{aligned} 0 &= r_n^0(g(r_n^0) - \omega_0) + r_{n+1}^0 \sin(\phi_n) - r_{n-1}^0 \sin(\phi_{n-1}) && 0 \le n \le k-1 \\ 0 &= r_k^0(g(r_n^0) - \omega_0) - r_{k-1}^0 \sin(\phi_{k-1}) && n = k. \end{aligned}$$

Thus, we see that our phase equations rely on g even at the lowest order. Suppose for the sake of exposition that we take $k = 3$ and use off-site boundary conditions, and that we wish to find solutions corresponding to $\Gamma_{\text{in}}(3)$. Our core system becomes

$$\begin{aligned} 0 &= r_+(g(r_+) - \omega_0) + r_+ \sin(\phi_0) && n = 0 \\ 0 &= r_+(g(r_+) - \omega_0) + r_+ \sin(\phi_1) - r_+ \sin(\phi_0) && n = 1 \\ 0 &= r_+(g(r_+) - \omega_0) + r_- \sin(\phi_2) - r_+ \sin(\phi_1) && n = 2 \\ 0 &= r_-(g(r_-) - \omega_0) - r_+ \sin(\phi_2) && n = 3. \end{aligned}$$

Summing up the first three equations yields

$$\begin{aligned} 0 &= 3r_+(g(r_+) - \omega_0) + r_- \sin(\phi_2) \\ 0 &= r_-(g(r_-) - \omega_0) - r_+ \sin(\phi_2). \end{aligned}$$

Multiplying the first of these equations by r_+ and the second by r_-, then adding the results yields

$$0 = 3r_+^2(g(r_+) - \omega_0) + r_-^2(g(r_-) - \omega_0).$$

Solving for ω_0 and substituting this result into the last of our equations yields

$$\sin(\phi_2) = \frac{r_-}{r_+}\Big[g(r_-) - \frac{3r_+^2 g(r_+) + r_-^2 g(r_-)}{3r_+^2 + r_-^2}\Big].$$

For this equation to hold the right-hand side must be constrained to lie in $[-1, 1]$, which is non-generic. As a result of these considerations, we adopt the scaling found in Hypothesis 2.

Bibliography

M. Aguareles, I. Baldomà, and T. M-Seara. On the asymptotic wavenumber of spiral waves in systems. *Nonlinearity*, 30(1):90, 2016.

P. Bates and C. K. Jones. Invariant Manifolds for Semilinear Partial Differential Equations. *Dynamics Reported*, 1989.

A. Bátkai and S. Piazzera. A Semigroup Method for Delay Equations with Relatively Bounded Operators in the Delay Term. *Semigroup Forum*, 2002.

M. Beck. *Topics in Stability Theory for Partial Differential Equations*. PhD thesis, Boston University, 2006.

M. Beck, B. Sandstede, and K. Zumbrun. Nonlinear Stability of Time-Periodic Viscous Shocks. *Archive for Rational Mechanics and Analysis*, 2010.

M. Beck, T. Nguyen, B. Sandstede, and K. Zumbrun. Towards nonlinear stability of sources via a modified Burgers equation. *Physica D*, 2011.

J. J. Bramburger. Rotating Wave Solutions to Lattice Dynamical Systems II: Persistence Results. *Journal of Dynamics and Differential Equations*, 31(1):499–536, 2019.

J. J. Bramburger. Stable periodic solutions to Lambda-Omega lattice dynamical systems. *Journal of Differential Equations*, 268(7):3201–3254, 2020.

J. J. Bramburger. Isolas of multi-pulse solutions to lattice dynamical systems. *Proceedings of the Royal Society of Edinburgh Section A: Mathematics*, 151(3):916–952, 2021.

J. J. Bramburger and B. Sandstede. Spatially localized structures in lattice dynamical systems. *Journal of Nonlinear Science*, 30(2):603–644, 2020.

E. Brown, P. Holmes, and J. Moehlis. Globally coupled oscillator networks. In *Perspectives and Problems in Nolinear Science*, pages 183–215. Springer, 2003.

P. Carter and B. Sandstede. Fast pulses with oscillatory tails in the Fitzhugh–Nagumo system. *SIAM Journal of Mathematical Analysis*, 2015.

P. Carter and B. Sandstede. Unpeeling a Homoclinic Bananain the Fitzhugh–Nagumo System. *SIAM Journal on Applied Dynamical Systems*, 2018.

P. Carter, B. Sandstede, and J. Rademacher. Pulse replication and the accumulation of eigenvalues. *SIAM Journal on Mathematical Analysis*, 2021.

P. Cartier. Perturbations singulieres des equations differentielles ordinaires et analyse non-standard,. *Séminaire Bourbaki 24*, 1981.

C.-H. Chiu, W.-W. Lin, and C.-S. Wang. Synchronization in lattices of coupled oscillators with various boundary conditions. *Nonlinear Analysis: Theory, Methods & Applications*, 46(2):213–229, 2001.

M. Clerc, S. Coulibaly, M. Ferré, and R. Rojas. Chimera states in a Duffing oscillators chain coupled to nearest neighbors. *Chaos: An Interdisciplinary Journal of Nonlinear Science*, 28(8):083126, 2018.

D. S. Cohen, J. C. Neu, and R. R. Rosales. Rotating spiral wave solutions of reaction-diffusion equations. *SIAM Journal on Applied Mathematics*, 35(3):536–547, 1978.

J. Cuevas-Maraver and P. G. Kevrekidis. Discrete Breathers in ϕ^4 and Related Models. In *A Dynamical Perspective on the ϕ^4 Model*, pages 137–162. Springer, 2019.

F. Dumortier. Singularities of vector fields on the plane. *Journal of Differential Equations*, 1977.

K.-J. Engel and R. Nagel. *One-Parameter Semigroups for Linear Evolution Equations*. 1999.

G. Ermentrout and N. Kopell. Oscillator death in systems of coupled neural oscillators. *SIAM Journal on Applied Mathematics*, 50(1):125–146, 1990.

G. B. Ermentrout and N. Kopell. Multiple pulse interactions and averaging in systems of coupled neural oscillators. *Journal of Mathematical Biology*, 29(3):195–217, 1991.

N. Fenichel. Geometric Singular Perturbation Theory for Ordinary Differential Equations. *Journal of Differential Equations*, 1979.

R. Fitzhugh. Impulses and Physiological States in Theoretical Models of Nerve Membrane. *Biophysical Journal*, 1961.

S. Flach and C. R. Willis. Discrete breathers. *Physics Reports*, 295(5):181–264, 1998.

G. Folland. *Real Analysis Modern Techniques and Their Applications*. John Wiley Sons, 1999.

F. Fontanela, A. Grolet, L. Salles, A. Chabchoub, and N. Hoffmann. Dark solitons, modulation instability and breathers in a chain of weakly nonlinear oscillators with cyclic symmetry. *Journal of Sound and Vibration*, 413:467–481, 2018.

J. Hale. *Ordinary Differential Equations*. Dover Books on Mathematics Series. Dover Publications, 2009. ISBN 9780486472119. URL https://books.google.ca/books?id=LdTZJ4HwCv4C.

J. Heagy, T. Carroll, and L. Pecora. Synchronous chaos in coupled oscillator systems. *Physical Review E*, 50(3):1874, 1994.

F. C. Hoppensteadt and E. M. Izhikevich. *Weakly connected neural networks*, volume 126. Springer Science & Business Media, 1997.

T. Kappitula. Stability of Weak Shocks in $\lambda - \omega$ Systems. *Indianna University Mathematics Journal*, 1991.

T. Kappitula. On the Stability of Traveling Waves in Weighted L^∞ Spaces. *Journal of Differential Equations*, 1992.

H. Kramers. Wellenmechanik und halbzahlige quantisierung. *Zeitschrift für Physik*, 1926.

M. Krupa and P. Szmolyan. Extending Geometric Singular Perturbation Theory To Nonhyperbolic Points-Fold and Canard Points In Two Dimensions. *SIAM Journal for Mathematical Analysis*, 2001.

Y. Kuramoto. Chemical turbulence. In *Chemical oscillations, waves, and turbulence*, pages 111–140. Springer, 1984.

R. Nagumo, S. Arimoto, and S. Yoshizawa. An Active Pulse Transmission Line Simulating Nerve Axon. *Proceedings of the IRE*, 1962.

B. Niedergesäß, A. Papangelo, A. Grolet, A. Vizzaccaro, F. Fontanela, L. Salles, A. Sievers, and N. Hoffmann. Experimental observations of nonlinear vibration localization in a cyclic chain of weakly coupled nonlinear oscillators. *Journal of Sound and Vibration*, 497:115952, 2021.

A. Papangelo, A. Grolet, L. Salles, N. Hoffmann, and M. Ciavarella. Snaking bifurcations in a self-excited oscillator chain with cyclic symmetry. *Communications in Nonlinear Science and Numerical Simulation*, 44:108–119, 2017.

A. Papangelo, N. Hoffmann, A. Grolet, M. Stender, and M. Ciavarella. Multiple spatially localized dynamical states in friction-excited oscillator chains. *Journal of Sound and Vibration*, 417:56–64, 2018.

R. Parker and A. Aceves. Standing-wave solutions in twisted multicore fibers. *Physical Review A*, 103(5):053505, 2021.

R. Parker, P. Kevrekidis, and B. Sandstede. Existence and spectral stability of multipulses in discrete Hamiltonian lattice systems. *Physica D: Nonlinear Phenomena*, 408:132414, 2020.

J. Paullet, B. Ermentrout, and W. Troy. The existence of spiral waves in an oscillatory reaction-diffusion system. *SIAM Journal on Applied Mathematics*, 54(5): 1386–1401, 1994.

J. E. Paullet and G. B. Ermentrout. Spiral waves in spatially discrete λ-ω systems. *International Journal of Bifurcation and Chaos*, 8(01):33–40, 1998.

S. Schecter. Persistent Unstable Equilibria and Closed Orbits of a Singularly Perturbed Equation. *Journal of Differential Equations*, 1985.

H. Shi and Y. Zhang. Existence of breathers for discrete nonlinear Schrödinger equations. *Applied Mathematics Letters*, 50:111–118, 2015.

I. Shiroky, A. Papangelo, N. Hoffmann, and O. Gendelman. Nucleation and propagation of excitation fronts in self-excited systems. *Physica D: Nonlinear Phenomena*, 401:132176, 2020.

W. C. Troy. Logarithmic spiral solutions of the Kopell–Howard lambda–omega reaction–diffusion equations. *Chaos: An Interdisciplinary Journal of Nonlinear Science*, 32(5):053104, 2022.

A. F. Vakakis, L. I. Manevitch, Y. V. Mikhlin, V. N. Pilipchuk, and A. A. Zevin. *Normal modes and localization in nonlinear systems*. Springer, 2001.

M. Wechselberger. *Geometric Singular Perturbation Theory Beyond the Standard Form*. 2020.